HOLOCENE SEDIMENTARY AND AQUATIC BIOGEOCHEMICAL RESPONSES REFLECTED IN ORDY POND, OAH'U, HAWAI'I

AND

CONTEMPORARY MODELING OF SUBMARINE GROUNDWATER DISCHARGE IN KAHANA BAY, OAH'U, HAWAI'I

A DISSERTATION SUBMITTED TO THE GRADUATE DIVISION OF THE UNIVERSITY OF HAWAI'I IN PARTIAL FULFILLMENT OF THE REQUIREMENTS FOR THE DEGREE OF

DOCTOR OF PHILOSOPHY

IN

GEOLOGY AND GEOPHYSICS

DECEMBER 2002

By

Geoffrey Hjorth Garrison

Dissertation Committee:

Craig Glenn, Chairman
Jane Schoonmaker
Brian Popp
Fred Mackenzie
Gary McMurtry

For my wife, who keeps me sane...

For my family, who got me here…

For my kids, who keep me smiling…

And for Rodger, an inspiration.

ABSTRACT

This dissertation explores aquatic geochemistry in two settings on O'ahu. Ordy Pond biogeochemistry responds rapidly to environmental changes, while Kahana Bay is influenced by significant groundwater and surface water influx and mixing with coastal ocean water. Thus, Ordy Pond is a better tool for studying Oahu's paleoenvironments, and Kahana Bay demonstrates the applicability of natural chemical tracers to quantify submarine groundwater discharge (SGD).

Work in Ordy Pond consisted of modern water column and particulate production time-series analyses, and sediment core study. Air temperature changes appeared to control the seasonal water chemistry. When the pond was thermally stratified in the spring/summer, epilimnion primary productivity increased dramatically as indicated by dissolved O_2, dissolved inorganic carbon, $\delta^{13}C_{DIC}$, and particulate production rates. Once the density gradient waned, the anoxic hypolimnion mixed with the epilimnion, organic matter productivity fell, and surface waters became suboxic to anoxic. Primary productivity is believed to have been controlled by the availability of sunlight; the longer daily photoperiod during stratification resulted in greater organic matter production, while greater mixing in winter reduced the photoperiod, increased phytoplankton respiration, and reduced organic matter production. The carbonate mineral flux increased during elevated primary productivity due to increased carbonate mineral saturation states. Modern particulate production closely reflected the water chemistry, and the biogeochemical processes in the modern pond were used to interpret the Holocene environmental history of the area through analysis of pond sediments. The sediments revealed three dramatic paleoenvironmental events: 1) the most recent post-glacial sea

level rise around O'ahu ~ 9.7 kya; 2) sea level fall ~1 kya following O'ahu's mid-Holocene sea level highstand; and 3) Western human contact with O'ahu and the introduction of plantation-scale agriculture.

Finally, in a separate study of the submarine ground water discharge to O'ahu's coastal waters, Kahana Bay was found to experience a much greater exchange with the surrounding environment than Ordy Pound. Total SGD in Kahana Bay is significant (90 x 10^6 L d^{-1}), providing 16% as much terrestrial water, five times as much phosphorus, and two times as much nitrogen as surface water runoff.

TABLE OF CONTENTS

LIST OF TABLES

LIST OF FIGURES

PREFACE

This work represents the culmination of six years of convoluted scientific exploration and discovery. These manuscripts are a testament to the fact that dissertation research is an attempt to find creative solutions to ill-defined problems. This preface attempts to give some background and explain how my work developed.

In 1996, my initial research effort at the University of Hawai'i involved studying controls on bioremediation of diesel fuel in a tidally influenced aquifer. However, after a year my interests turned back to sedimentology, particularly sediment chemistry. With the help of Craig Glenn and Francis Sansone, we tried twice to fund a project through the National Science Foundation to study carbonate diagenesis within a Holocene patch reef in Kaneohe Bay, O'ahu, Hawai'i. The work of Gordon Tribble and Francis Sansone had demonstrated that pore waters in Checker Reef were suboxic only a few meters below the reef surface. I had hoped to find what effect the development of anoxia was having on the physical and mineralogical structure of the reef interior, a place Craig Glenn had convinced me we might find modern dolomite. Alas, after our second unsuccessful round with NSF, I began to look for other projects. In 1998, I asked to be included on two proposals to the University of Hawai'i Sea Grant College Program. On the one hand, I helped Craig Glenn and Gary McMurtry submit a new proposal to study submarine groundwater discharge (SGD) in Kahana Bay on O'ahu's Windward Coast. On the other hand, I also asked Jane Schoonmaker to include me on her Sea Grant proposal to continue paleoenvironmental research on sediment cores from Ordy Pond on O'ahu's Leeward Coast. Both proposals were funded, and I found myself committed to two equally exciting research projects.

On the recommendations of my committee, most of research focused on Ordy Pond. However, I did not want to leave the Kahana Bay project because it was a great opportunity to study a process that is receiving growing interest and concern (i.e., SGD). Thus, I worked on both projects simultaneously, and this dissertation is presented as four chapters, each a separate manuscript intended for publication. Chapters I – III are from the work on Ordy Pond and Chapter IV is from the work on Kahana Bay. Each manuscript has been, or is intended to be, submitted to a scientific journal appropriate for its content. The title of each manuscript is presented on each chapter's cover page.

This dissertation studies the aquatic geochemistry of two different environments on O'ahu. The biogeochemical system in Ordy Pond responds rapidly to changes in the surrounding environment. The environmental sensitivity of the pond is due largely to the fact that the pond is a closed system with limited rainfall and limited groundwater seepage input. On an annual scale, changes in the pond's biogeochemical system are extrinsically forced by changes in air temperature and not by changes in external chemical inputs or outputs. In contrast, Kahana Bay is influenced by significant groundwater seepage, a large surface water influx, and mixing with coastal ocean water. The larger reservoir size and significant fluid exchange should buffer seasonal changes in the biogeochemistry of this bay. Therefore, any historical record of changes in the surrounding environment held within the waters and sediments of Kahana Bay have coarser temporal resolution than Ordy Pond waters and sediments. Thus, while the Ordy Pond study is a better tool for studying Oahu's past environmental history, the Kahana Bay study demonstrates the applicability of natural chemical tracers to quantify modern groundwater discharge into coastal marine waters.

In 1998, I began work on sediment cores from Ordy Pond. As samples were collected and analyzed, and I began to develop troubled theories about what the sediments represented, Craig pointed out that the sediments could be better understood by studying the modern chemistry and sediment production. In the summer of 1999, the work was assisted by Eric Grabowski from the University of Missouri. He came as part of NSF's Research Experience for Undergraduates (REU) program and participated with the first profile of the pond's water column. As often happens, this quick glimpse of the pond provided more questions than answers. Thus, in April of 2000, I began a one-year time-series analysis of the pond (Chapters I and II). Michael Dichner, a University of Hawai'i undergraduate, helped with bi-weekly profiles during the summer of 2000. In the fall of 2000 the sampling frequency was reduced to a bi-monthly program. I added sediment traps to the pond in June 2000 and collected particulates through the rest of the study. In the summer of 2001, the NSF REU program brought Lauren Rogers from Stanford University and Ellen Schulz from Harvard University. Lauren worked on particulate elemental and stable isotopic chemistry (Chapter II), while Ellen provided analyses of sedimentary phosphorus from the upper 8 m of the core (Chapter III). The paleoenvironmental interpretations made from of the sediment record (Chapter III) were made using the interpretations from the time-series analyses.

Chapter IV, "Measurement of submarine groundwater discharge in Kahana Bay, O'ahu, Hawai'i," was produced from my investigations of SGD in Kahana Bay on O'ahu's northern Windward Coast and has been accepted for publication in the journal *Limnology and Oceanography*. This work is unique it its effort to quantify the freshwater component of SGD from total submarine discharge. The work demonstrated how

important SGD is to a coastal Hawaiian environment, particularly with respect to dissolved nutrient input.

I would like to acknowledge all of the other tremendous support I have been fortunate to receive during my research at the University of Hawai'i. I owe great thanks to Jane Schoonmaker who not only supported me as Ordy Pond's Principal Investigator, but works still to preserve Ordy Pond as a precious scientific resource. Furthermore, both she and Brian Popp went far out of their way to improve the interpretations and clarity of these manuscripts. I would like to thank all of my committee members for there involvement, advice, contributions, and detailed critiques of this work. The Department of Geology and Geophysics at the University of Hawai'i has enabled me to extend my work not only through research and (many) teaching assistantship positions, but also through its generous William T. Coulbourn and Harold T. Stearns fellowship awards; I am grateful to have been part of such a fun and supportive department. I could not have understood the Ordy system at all without the help of the University of Hawai'i's Stable Isotope Biogeochemistry Laboratory, which is supervised by Brian Popp and managed by Terri Rust. I also thank Nicolas Cassar for his critiques and assistance in translating the organic chemistry of my "stinky little ocean." Lastly, I particularly wish to thank the entire School of Ocean and Earth Sciences and Technology at the University of Hawai'i. The multi-disciplined nature of the work presented here could not have been possible without a program as diversified as SOEST and yet whose every door, faculty or student, is always open for help. Finally, I would like to thank Craig Glenn who kept me on track through his tireless support and enthusiasm.

CHAPTER I.

Biogeochemical responses to seasonal stratification in a eutrophic saline pond and implications for interpreting O'ahu's environmental history

ABSTRACT

A time-series analysis was conducted of the aquatic geochemistry of Ordy Pond on O'ahu, Hawai'i, to evaluate whether pond sediments could hold a paleoenvironmental record. Measurements included temperature, conductivity, salinity, O_2, SO_4^{2-}, S^{2-}, NH_4^+, NO_3^-, NO_2^-, TDN, PO_4^{3-}, TDP, pH, total alkalinity, DIC, $\delta^{13}C_{DIC}$, Na^+, Ca^{2+}, Mg^{2+}, Sr^{2+}, Fe^{2+}, and Mn^{2+}. The only sources of water to Ordy Pond are rainfall and groundwater, and the chemistry of pond is sensitive to the surrounding environment. The pond was thermally stratified between May and September, and epilimnion primary productivity increased dramatically, as inferred from dissolved O_2 levels in excess of atmospheric saturation. Once the density gradient waned, the anoxic hypolimnion mixed with the epilimnion, primary productivity fell, and surface waters became suboxic to anoxic. Primary productivity is believed to have been controlled by the availability of sunlight. When phytoplankton were restricted to the surface waters during stratification, they had a longer daily photoperiod resulting in greater organic matter production. Without stratification, phytoplankton mixed below the euphotic zone, spent more time in the dark and respirative photosynthesis phase, and organic matter production decreased. In turn, primary productivity controlled the pond's carbonate mineral saturation state. The pond was always oversaturated with respect to low magnesium calcite and kutnahorite [$Ca(Mn_xMg_{1-x})(CaCO_3)_2$], and the dissolved saturation states of these minerals dropped significantly in the spring/summer epilimnion due to increased mineral precipitation.

1.1. INTRODUCTION

There is no question as to the importance of lakes and lake sediments as paleoenvironmental records. Lacustrine sediments can be superior to marine records for paleoenvironmental study because a lake's small reservoir can react more rapidly to changes in the surrounding environment than can the ocean system (Glenn and Kelts, 1991; Chivas et al., 1993). Many lakes are also seasonally or permanently stratified, and a suboxic to anoxic hypolimnion can develop through microbial remineralization of accumulating organic matter. Water column anoxia can enhance sediment preservation and thus add to a lake record's historical value because anoxic organic matter remineralization is normally much slower than aerobic organic matter remineralization (Atlas and Bartha, 1993). Furthermore, lacustrine systems typically have higher rates of both autochthonous and allocthonous sedimentation than open marine environments, and thus their sediment records can have a higher temporal resolution. Moreover, many lakes have been impacted by recent human activities which are both well known and dated. In such cases, a lake's sediment record can be calibrated against these known events to make a more refined interpretation of prehistoric sedimentary perturbations.

This paper presents a time-series analysis of the aquatic biogeochemistry of Ordy Pond on O'ahu, Hawai'i. Pond sediments are characterized by alternating green organic-rich laminae and tan inorganic carbonate mineral-rich laminae; radiocarbon dating and laminae counting suggest that laminae couplets may be varves (Tribble et al., 1999; Chapter III). We propose that the light laminae are spring/summer deposits produced during periods of higher primary productivity, while the dark organic laminae formed during cooler and wetter winter months. A one-year time-series analysis was made to test

this hypothesis and to evaluate whether pond sediments could hold a paleoenvironmental record of O'ahu.

The pond fills a 20+ m deep karst sinkhole 800 m from the shoreline in the Kalaeloa region (also known as Barbers Point) of 'Ewa Plain, an elevated Pleistocene carbonate reef complex (Fig. 1.1). The area around the pond formed during O'ahu's interglacial Waimanalo sea level stand (oxygen isotope Stage 5e), which lasted between 135-120 kya and was ~ 8 m higher than today (Ku et al., 1974; Stearns, 1974; Muhs and Szabo, 1991; Sherman et al., 1993; Szabo et al., 1994). The most recent post-glacial sea level rise inundated the sinkhole with groundwater, and today the pond is 0.5 ha in area and 5m deep. The pond is surrounded by a ring of American mangrove (*Rhizophora mangle)* within a forest of kiawe trees (*Prosopis pallida*) and sourbush (*Pluchea symphytifolia*), which shelter the pond and prevent wind-driven vertical mixing. The pond has neither surface inflow nor outflow. The only sources of water to the pond are rainfall and groundwater, and the pond is poorly connected with the surrounding aquifer. The water level in Ordy Pond is perpetually lower than the surrounding groundwater table, except after high rainfall events when the pond level exceeds the local groundwater elevation (Ogden, 1999). Furthermore, a 0.53 m tidal shift in the local sea level induces a 0.12 m change in the water table around the pond, yet the level of the pond itself remains unchanged (Ogden, 1999).

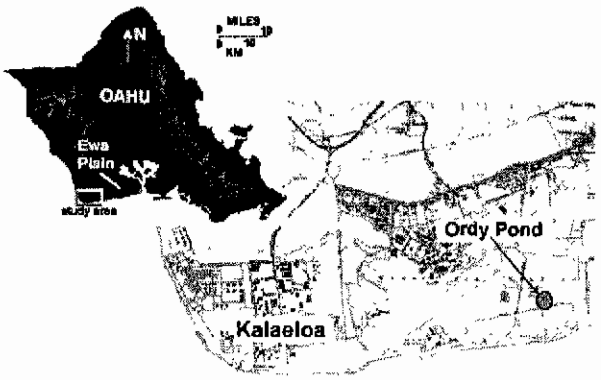

Figure 1.1. Location map of Ordy Pond in the Kalaeloa (formerly Barbers Point) area of 'Ewa Plain, O'ahu, Hawai'i.

1.2. METHODS

Local meteorological conditions around Ordy Pond were summarized daily from hourly measurements made at the NOAA weather station at the Barbers Point Naval Air Station airfield in Kalaeloa, approximately 2 km west of the pond (Fig. 1.1). These data were provided by the Hawai'i State Climate Office of NOAA's National Climatic Data Center, Dr. Pao-Shin Chu, Department of Meteorology, University of Hawai'i at Mānoa.

Water samples were collected not only from Ordy Pond, but also from a groundwater monitoring well located 10 m east of the pond's edge and extending 4 m below the water table. Prior to sampling the well, a water volume equivalent to three times the well casing volume was purged to obtain a representative groundwater sample. Within the pond, hydrocasts were made from a 2-person inflatable raft every 7 to 50 days from 4 April 2000 through 4 April 2001. At the start of each sampling period, a Horiba® model U-21 digital water quality meter, calibrated prior to each use, was used to measure temperature, pH, conductivity (and salinity), and turbidity at every 0.3 m depth. Hydrocasts were always made at the same central location over the area where the

sediment cores were collected. Sediment traps were also deployed during the time-series, and those results are reported in Chapter II.

A horizontal Van Doren-type bottle was used to collect discrete water samples at depths of 0, 0.3, 0.9, 1.5, 2.1, 3.4, and 4.3 m. Dissolved O_2 and S^{2-} were measured on subsamples from the same 265 ml ground glass vials. The S^{2-} in each sample was first precipitated as Zn_2S, and the supernatant was removed to a separate 65 ml ground glass vial for O_2 analysis. The Winkler method was used to measure O_2 (Grasshoff et al., 1983), and the O_2 saturation state of the solution was calculated with respect to the atmosphere according to the formulae of Weiss (1970). The Zn_2S was quantified titrimetrically with sodium thiosulfate (NaS_2O_3) according to the technique of Grasshoff (1983). Replicate S^{2-} sample analyses had a σ (standard deviation) of 0.3 μmol L^{-1} (n = 16), and replicate O_2 samples had a σ of 2 μmol L^{-1} (n = 18).

Nutrient and salinity samples were filtered with HCl-cleaned Whatman GF/C filters, collected in HCl-cleaned 125 ml HPDE bottles, frozen, and sent for analysis to either SOEST Analytical Services, University of Hawai'i, or to the Marine Laboratory Facilities at the University of Washington. Nutrient measurements were made using a standard spectrophotometric flowthrough autoanalysis unit (WOCE, 1994); average σ from replicate sample analyses: PO_4^{3-} – 0.19 μmol L^{-1} (n = 9); NO_2^- – 0.09 μmol $^{L-1}$ (n = 13); NO_3^- – 0.04 μmol $^{L-1}$ (n = 12); NH_4^+ – 2.80 μmol $^{L-1}$ (n = 10); Si – 11.9 μmol L^{-1} (n = 8). Salinity, reported in parts per thousand (ppt), was measured with a Guideline Instruments "Autosal" model 8400 salinometer, and replicated samples had a σ of 0.04 ppt (n = 13).

Dissolved cation concentrations were determined by inductively coupled plasma-optical emission spectroscopy (ICP-OES) using a Leeman Labs model PS-1 (Plasma Spec) eschelle grating spectrometer (e.g. De Carlo, 1992; De Carlo and Kramer, 2000). Commercial spectroscopic standards were used for calibration before and during each analytical run, and standard seawater from the International Association for the Physical Sciences of the Oceans (IAPSO) was used to confirm analytical accuracy; average σ for replicated sample analyses (n = 9): Mn^{2+}, Fe^{2+} – 0.14 μmol L^{-1}; Ca^{2+} – 0.16 μmol L^{-1}; Mg^{2+} – 0.52 μmol L^{-1}.

Total alkalinity (TA) was determined by Gran titration on a Brinkmann Metrohm 655 Dosimat autotitrator with a solution of 0.09553 mol HCl per kg of 600 mmol L^{-1} NaCl solution; average σ for replicate sample analyses was 0.10 meq kg^{-1} (n = 40). Dissolved inorganic carbon (DIC) and $\delta^{13}C_{DIC}$ were measured using a system based on the design of Kroopnick (1974); samples (0.73 ml) were acidified with an excess of 30% phosphoric acid, stripped with N_2 gas, and the evolved CO_2 trapped cryogenically. Inorganic carbon concentrations were determined by measuring CO_2 vapor pressure in a calibrated volume at a known temperature. Replicated DIC samples had σ of 0.074 mmol L^{-1} (n = 7) . The isotopic ratios of the CO_2 were analyzed on a Finnigan MAT 252 isotope-ratio-monitoring (IRM) mass spectrometer at the SOEST Stable Isotope Biogeochemistry Laboratory at the University of Hawai'i. Isotopic ratios are reported in standard delta notation, and $\delta^{13}C$ is reported relative to Vienna-PDB (V-PDB). Replicated sample analyses of $\delta^{13}C_{DIC}$ had a σ of 0.2‰ (n = 12), while analytical precision was ±0.05‰ based on routine analysis of internal laboratory reference materials. Laboratory standards were calibrated against NBS-19 ($\delta^{18}O$ = -2.2‰, $\delta^{13}C$ =

+1.95‰, V-PDB) and normalized to NBS-18 ($\delta^{18}O$ = -23.05‰, $\delta^{13}C$ = -5.04‰, V-PDB) in accordance with International Atomic Energy Agency (IAEA) guidelines.

Those chemical parameters not measured analytically, as listed in Table 1.3, were calculated mathematically. Ionic activities, dissolved gas concentrations, and dissolved mineral saturation states [Ω = (mineral ionic activity product – IAP)/(mineral solubility coefficient – $K_{mineral}$)] were calculated with EQ3NR version 7.2c (Wolery, 1992). The ".cmp" thermodynamic data file was used in an extended Debye-Hückel formalism with the ionic activity equation of Davies (1962):

$$\log \gamma_i = -Az_i^2 (\sqrt{I}/(1+\sqrt{I}) + 0.2I) \qquad (1)$$

where γ_i is the ionic activity coefficient of the *i*-th aqueous solution species, A is the temperature dependent Debye-Hückel constant (0.5115 @ 25° C, 0.5161 @ 30° C), z_i is the ionic charge balance of the *i*-th species, and I is the ionic strength of the solution.

Nutrient enrichment bioassay experiments were conducted in July and September 2001 to qualitatively assess what nutrients limit phytoplankton photosynthesis in the pond's aquatic flora (Uchikawa, 2002). Level-II enrichment experiments (Hecky and Kilham, 1988) were conducted using 500 ml polycarbonate culture bottles. Two duplicates were made with each treatment, including untreated control bottles. Each bottle was filled with filtered or centrifuged pond water, various nutrient combinations (Tables 1.1 & 1.2), and inoculated with 5 ml of untreated surface water. Bottles were covered with parafilm to allow gas exchange and at left at room temperature in front of a fluorescent light bank lit 24 hr d^{-1}. Chlorophyll was analyzed each day for 7 days on 6 ml aliquots filtered with glass fiber filters and extracted with HPLC-grade acetone. Samples were shaken prior to analysis to dislodge algae adhering to bottle walls. In July,

chlorophyll-a concentrations were measured with a Turner 1-11 fluorometer. Chlorophyll-a, -b, and -c were measured in September using a combination of Turner 10-AU and TD-700 fluorometers (Uchikawa, 2002)..

TABLE 1.1. Nutrient enrichment treatment types.

Treatment	P	N	Metals	Vitamins
1) Control	-	-	-	-
2) P	+	-	-	+
3) N	-	+	-	+
4) Trace metals	-	-	+	+
5) Everything	+	+	+	+
6) Ev'thing – P	-	+	+	+
7) Ev'thing – N	+	-	+	+
8) Ev'thing – metals	+	+	-	+

+ nutrient added - nutrient absent

TABLE 1.2. Constituents and concentrations used for nutrient enrichments

Nutrient	Ingredients	Concentration ($\mu mol\ L^{-1}$)
P	$NaPO_4$	0.02
N	$NaNO_3$	0.44
Trace metals	$CuSO_4$	3×10^{-5}
	$ZnSO_4$	4×10^{-5}
	$CoCl_2$	2×10^{-5}
	$MnCl_2$	4.5×10^{-4}
	Na_2MoO_4	2×10^{-5}
	$FeCl_3$	5×10^{-3}
	EDTA	
Vitamins	Vitamin B_{12}	2.5×10^{-8}
	Biotin	5×10^{-7}
	Thiamine	7.5×10^{-5}

Finally, rates of net organic carbon production were measured over a 24-hour period using *in situ* incubations inoculated with ^{13}C-labeled HCO_3^-. Clear, 250 ml, polycarbonate bottles were filled from, and moored at, depths of 0, 0.3, 1.5, 2.1, 3.4, and 4.3 m. Control bottles were killed with $HgCl_2$ and placed on the line at depths of 0.3, 2.1,

and 4.3 m. The tracer consisted of 1.000 g of ^{13}C-labeled $NaHCO_3^-$ (99% $NaH^{13}CO_3^-$, $\delta^{13}C$ = +8.7100 x 10^4‰ vs. V-PDB) in a 250 ml solution producing a tracer DIC concentration of 47.06 mmol L^{-1}. Based on previous DIC measurements, 2.5 ml of the tracer solution was added to each bottle. This 1:100 tracer-to-sample ratio added less carbon than 2% of the natural DIC pool at each depth, yet would produce an isotopic signal of +20‰ at a doubling rate of only 0.1. The water column was profiled at the beginning of the incubation, including measurements of particulate organic carbon (POC) and $\delta^{13}C_{POC}$. The bottles were placed on the line at 1030 (HST) on 4 April 2001 and recovered at 1030 (HST) on 5 April 2001 (24.0 hours). In order to avoid contaminating the samples with artificially high levels of sunlight (particularly the deeper samples), the collection, sample, and incubation bottles were kept in the dark while being manipulated at the pond's surface. The outside of the Van Doren sample bottle was covered with duct tape to keep waters dark while they were being retrieved. Once the incubation bottles were recovered, they were killed with 1 ml saturated $HgCl_2$ and analyzed for pH, TA, DIC, $\delta^{13}{}_{DIC}$, POC, and $\delta^{13}C_{POC}$. Particulate organic carbon (POC) and $\delta^{13}C_{POC}$ samples were collected on pre-combusted Whatman GF/F glass fiber filters. After filtration, the samples were acidified with 6% sulfurous acid (H_2SO_3) in silver sample boats to remove inorganic carbon. Samples were analyzed on a Carlo Erba 2500NC Elemental Analyzer coupled to a Finnigan MAT Delta Plus IRM mass spectrometer via a CONFLO II interface. Analytical precision of the organic $\delta^{13}C$ was ±0.15‰ based on routine analysis of internal laboratory reference materials, and replicated sample analyses had a σ of 0.7‰. The net organic carbon production rates (PR) were calculated as described by Hama et al. (1987; 1993):

$$PR = [\Delta POC(t)] \cdot t^{-1} = (a_f - a_i) \cdot (a_{ic} - a_i)^{-1} \cdot [POC(t)] \cdot t^{-1} \quad (2)$$

where:

a = ^{13}C:^{12}C ratio, $_i$ = initial, $_f$ = final, t = incubation time
a_{ic} = ^{13}C:^{12}C ratio of the incubation DIC (after tracer was added)
[POC(t)] = POC concentration at time t
[ΔPOC(t)] = increase in POC concentration during time t

1.3. RESULTS AND DISCUSSION

1.3.1. Local weather

The modern climate of Kalaeloa is characterized by long stretches of aridity punctuated by two or three significant yearly rainfall events. There are two seasons, hot and dry versus warm and wet (Fig. 1.2). During the dry season, between 1 April and 30 September 2000, surface air temperatures averaged 26° C and peaked at 33° C on 16 August 2000. During the wet season, between early October 2000 and late March 2001, air temperatures averaged 24° C and peaked at 32° C on 16 October 2000. Average annual rainfall between 1949 and 2001 was 508 mm, 381 mm of which fell in between October and March. During this study, however, only 151 mm of rain fell – 65.6 mm in spring/summer (52% of the 50-year average) and 85.8 mm in the fall/winter (23% of the 50-year average). Thus, it should be noted that the period of this study was one of the driest on record. Though the water column may have had a chemical composition more concentrated than average, the biogeochemical seasonality of the pond appears to have been a function more of changes in air temperature than of rainfall. Thus, the cycle of events observed are believed to be representative of a typical annual cycle.

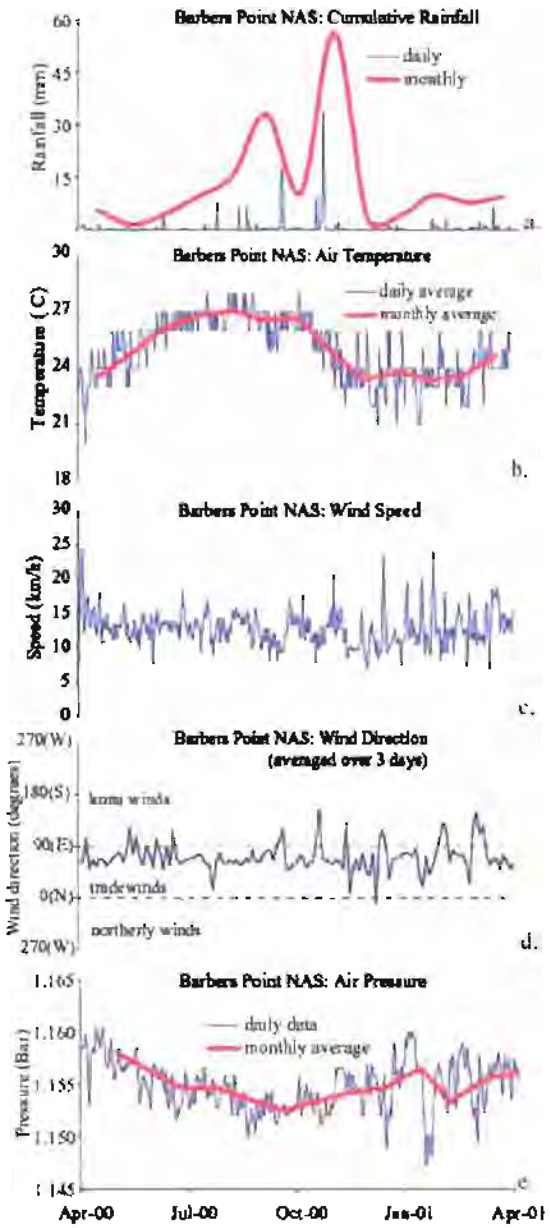

Figure 1.2. Weather conditions in Kalaeloa between April 2000 and April 2001.

1.3.2. Summary of pond chemistry

Pond and groundwater chemistry were significantly different (Table 1.3). Except for NO_3^- and NO_2^-, chemical constituents were 1-2 orders of magnitude more concentrated in the pond.

TABLE 1.3. Averaged time series measurements for Ordy Pond

	A vs. C*	SPRING/SUMMER SEASON		FALL/WINTER SEASON			Pond/	Ave	Pond/
		Epilimnion	Hypolimnion	Epilimnion	Hypolimnion	Groundwater	Groundwater	Sea water**	Sea water
Temp. (° C)	A	27.10	24.33	24.14	23.00	24.10	**24.10**		
Salinity (ppt)	A	23.11	23.02	22.99	23.00	1.8	**13**	35	**0.66**
Density (g cm^{-3})	C	1.006	1.009	1.009	1.010	0.998			
O_2 (µmol L^{-1})	A	190	8	63	5	20			
% O_2 saturation†	C	87%	3%	27%	2%	91%			
DIC (mmol L^{-1})	A	16.83	18.09	16.90	17.73	7.22	**2.4**	2.7	**8.7**
Ph	A	8.41	8.30	8.36	8.22	7.19			
TA (meq L^{-1})††	A	21.40	21.72	20.03	20.70	6.40	**3.3**	1.97	**11**
CO_3^{2-} (mmol $^{L-1}$)	C	4.461	3.414	3.232	3.058	0.021	**673.2**		
HCO_3^- (mmol L^{-1})	C	10.6	11.6	11.7	12.2	6.10	**1.89**	2	**5.8**
$CO_{2(aq)}$ (µmol L^{-1})	C	64.2	99.5	86.3	12.6	80.4	**0.117**		
NO_3^- (µmol $^{L-1}$)	A	0.39	0.49	0.09	0.04	117.06	**0.0022**		
NO_2^- (µmol $^{L-1}$)	A	0.22	0.16	0.36	0.41	10.38	**0.028**		
NH_4^+ (µmol $^{L-1}$)	A	26.56	118.33	85.38	185.35	0.44	**240**		
PO_4 (µmol $^{L-1}$)	A	0.72	1.89	1.82	5.79	1.08	**2.4**		
SO_4^{2-} (µmol $^{L-1}$)	A	7.37	7.31	7.35	7.42	1.45	**5.08**		
S^{2-} (µmol $^{L-1}$)	A	0.03	0.32	0.05	0.48	0.00			
Na^{2+} (mmol $^{L-1}$)	A	304.0	300.1	304.3	310.0	3.7	**82**	480	**0.63**
Ca^{2+} (mmol L^{-1})	A	2.31	2.30	3.24	3.01	0.726	**3.7**	10	**0.27**
Mg^{2+} (mmol $^{L-1}$)	A	46.49	46.30	46.42	46.48	0.19	**248**	52	**0.89**
Mg/Ca	C	20.1	20.1	14.3	15.44	0.26		5.2	
Mn^{2+} (µmol $^{L-1}$)	A	0.72	0.69	0.81	0.72	0.09	**8.1**	0.0005	**1500**
Fe^{2+} (µmol L^{-1})	A	3.72	3.91	3.75	3.77	0.008	**473**	0.00003	**126000**
B^{2+} (mmol L^{-1})	A	5.43	5.33	5.69	5.57	0.015	**374**	4.5	**1.4**

* A = analytical measurement; C = calculated measurement

** average seawater values are taken from (Nozaki, 2001)\

† O_2 saturation relative to the atmospheric saturation, calculated according to (Grasshoff et al., 1983), after (Weiss, 1970)

†† TA = Total Alkalinity

1.3.3. Thermal stratification

Between early May and late September, warm air temperatures heated the upper meter of the pond and thermally stratified the water column (Fig. 1.3a). During this period, the upper 0.9 m of the pond became 0.006 g cm^{-3} less dense than the rest of the water column and is considered the epilimnion. Density was calculated based on temperature, salinity and the equation of state for seawater of Millero and Poisson (1981). The temperature and salinity profiles (Figs. 1.3a & 1.3b) showed that stratification was primarily thermal; increased spring/summer salinity only slightly countered the stratification effect of higher temperatures. Furthermore, the pond had begun to become stratified again by the end of the time series in March 2001. Surface air temperatures became warmer earlier in 2001 than in 2000; average daily surface air temperature was 23° C in April 2000 but 25° C in April 2001 (Fig. 1.2b). Thus, the pond began to stratify sooner in 2001 than 2000.

1.3.4. Oxygen

Oxygen concentrations exceeded atmospheric saturation at the same time that the water column became thermally stratified (19 May 2000, Fig. 1.4a). After May, epilimnion O_2 concentrations continued to rise until their peak on 13 July 2000 when dissolved O_2 was 183% of atmospheric saturation ($O_{2(aq)}$ = 381 μmol L^{-1}, T = 29.60° C, salinity = 23.50ppt); the hypolimnion was always suboxic to anoxic. Once the density gradient broke down after October and vertical mixing increased, surface waters became undersaturated with O_2 and at times the epilimnion became anoxic. The variations in the O_2 profile would have been more extreme if not for the moderating effect of gas diffusion across the air-water interface. Assuming an average wind speed of 3.5 m s^{-1} (Fig.1.2c),

the O_2 flux averaged 3.3 x 10^4 mol m^{-2} d^{-1} out of the pond between May and September, but 1.8 x 10^4 mol m^{-2} d^{-1} into the pond between October and April (per Wanninkhof, 1992). Thus, without diffusion, O_2 levels would have been higher in summer and lower in winter.

Dissolved O_2 concentrations are considered to be a function of the balance between aerobic photosynthetic productivity (biologic reduction of inorganic carbon, Eq. (3)) versus biologic respiration (Eq. (3) to the left) and/or oxidation of reduced chemical species, Eq. (4).

$$CO_2 + H_2O = CH_2O + \cancel{O_2} \qquad (3)$$

$$\cancel{O_2} + 2Me^{2+} = 2MeO \qquad (4)$$

$$CO_2 + H_2O + 2Me^{2+} = CH_2O + 2MeO \qquad (5)$$

Equation (5) shows that we can expect an oxygenated Ordy Pond to have high levels of particulate organic matter (CH_2O) and low dissolved divalent metal concentrations, while the opposite would indicate a more anoxic system.

Thus, the spring/summer appears to have been a time of elevated photosynthetic productivity in the epilimnion. In the fall/winter, however, when stratification waned, the reduction in dissolved epilimnion O_2 levels was the combined effect of reduced productivity and mixing with reduced hypolimnion waters. Oxygen levels picked up again in March 2001 as the water column began to stratify with the next Spring/Summer season. The increase in O_2 levels from 0% to 44% of atmospheric saturation between January and March 2001 appears to have marked the beginning of the next phytoplankton bloom.

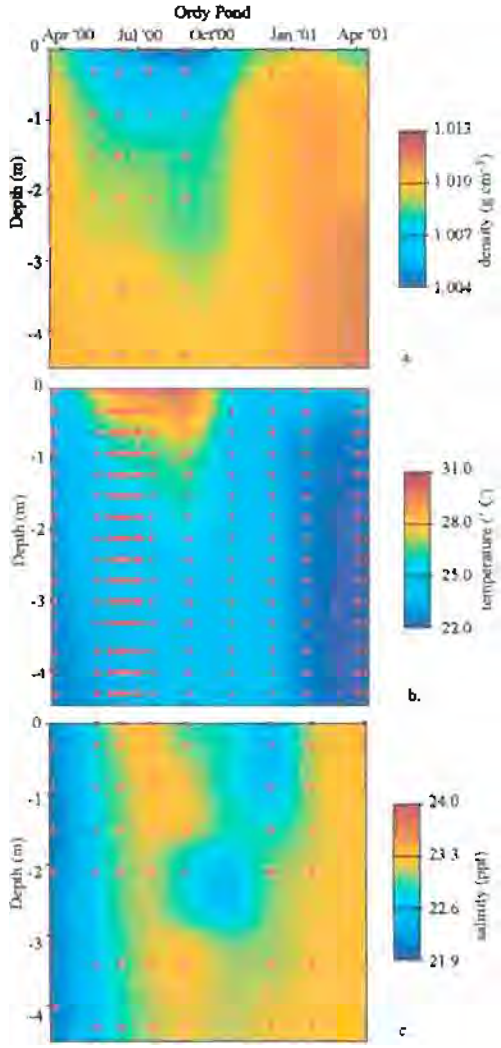

Figure 1.3. Profiles of density (1.3a.), temperature (1.3b.), and salinity (1.3c.). Each sample is represented in depth and time by ▪.

1.3.5. Inorganic Carbon

Dissolved inorganic carbon profiles were also affected by the seasonal changes in the biology of the pond. The $CO_{2(aq)}$ inventory (chemical concentration integrated along water column depth, reported in mol m^{-2}) dropped between April and May coeval with stratification onset and increased dissolved O_2 (Figs. 1.4b & 1.5a). The loss of $CO_{2(aq)}$ is further evidence that this was a period of increased phytoplankton productivity according

to the equation for organic carbon production via photosynthesis, Eq. (6). After May, the $CO_{2(aq)}$ inventory increased steadily through July as organic matter remineralization increased in response to the elevated organic production. The hypolimnion $CO_{2(aq)}$ inventory increased sharply in December and dropped dramatically in January. The December rise in $CO_{2(aq)}$ followed the increase in other reduced chemical species, as described below, as a result of intensified deep water anaerobic organic matter oxidation. The January drop in hypolimnion $CO_{2(aq)}$ followed a decrease in the other reduced chemical species as a result of vertical mixing and increased oxidation of the hypolimnion waters. Finally, the increase in $CO_{2(aq)}$ at the end of the study could have resulted from organic matter oxidation following the start of a new phytoplankton bloom between January and March 2001, as suggested by increased O_2 (Fig. 1.4a). Although the $CO_{2(aq)}$ inventory may indicate the start of a new phytoplankton bloom at the end of the time-series, the actual concentration levels at the start and end of the time-series are not the same; overall the pond's $CO_{2(aq)}$ inventory increased over the course of the study. It is probable that the levels of dissolved chemical components in the pond vary over time cycles greater than just one year.

The negative correlation of the CO_3^{2-} to $CO_{2(aq)}$ inventories (Fig. 1.5c) reveals how the processes which consume and produce $CO_{2(aq)}$ affected CO_3^{2-} levels by controlling pH. Equation (8) describes the conversion of bicarbonate to carbonate with the production of organic matter (CH_2O):

$$\cancel{CO_2} + \cancel{H_2O} = CH_2O + O_2 \qquad (6)$$

$$2HCO_3^- = \cancel{CO_2} + \cancel{H_2O} + CO_3^{2-} \qquad (7)$$

$$2HCO_3^- = CH_2O + O_2 + CO_3^{2-} \qquad (8)$$

Thus, the decrease of $CO_{2(aq)}$ between April and May reduced pond water acidity and the carbon species equilibrium shifted in favor of CO_3^{2-}. Likewise, the CO_3^{2-} inventory shrank as more $CO_{2(aq)}$ was remineralized from particulate organic matter. The total CO_3^{2-} inventory was also reduced by LMC and kutnahorite [$Ca(Mn_xMg_{1-x})(CaCO_3)_2$] precipitation which occurred throughout the time-series and will be detailed in Chapter II.

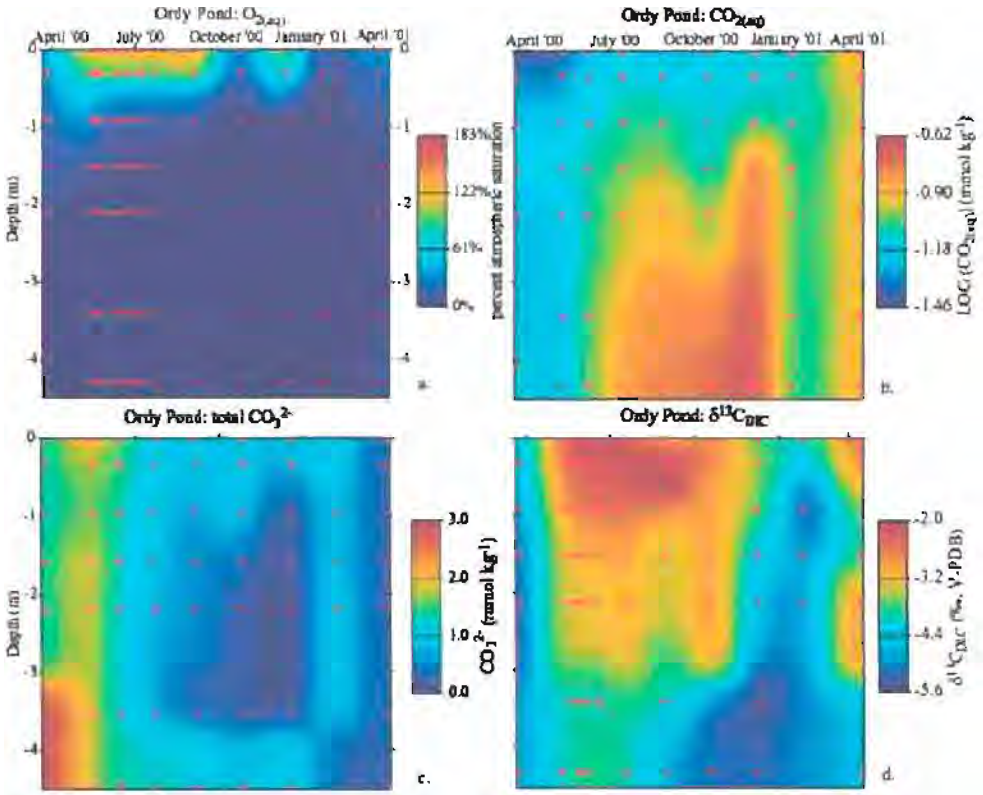

Figure 1.4. Profiles of dissolved O_2 (1.4a), total $CO_{2(aq)}$ (1.4b), CO_3^- (1.4c), and $\delta^{13}C_{DIC}$ (1.4d). Each sample is represented in depth and time by ▪.

The $\delta^{13}C_{DIC}$ data further support the interpretation that spring/summer was a period of increased phytoplankton productivity at the surface. Epilimnion $\delta^{13}C_{DIC}$ rose from -5.0 to -2.6‰ (V-PDB; Fig. 1.4d) between April and May 2000 as the water column became stratified. The epilimnion $\delta^{13}C_{DIC}$ continued to rise, though less steeply, until

July when it peaked at -1.8‰ (V-PDB). Once stratification waned, the epilimnion $\delta^{13}C_{DIC}$ fell to -4.6‰ (V-PDB) as remineralized inorganic carbon diffused up from the hypolimnion. Hypolimnion $\delta^{13}C_{DIC}$ fell between May and December revealing increased organic matter oxidation in the bottom of the pond following the phytoplankton bloom. Once the pond became more vertically mixed, the hypolimnion $\delta^{13}C_{DIC}$ rose and approached pre-stratification values. Finally, $\delta^{13}C_{DIC}$ rose again at the end of the time series, further evidence that another phytoplankton bloom may have begun.

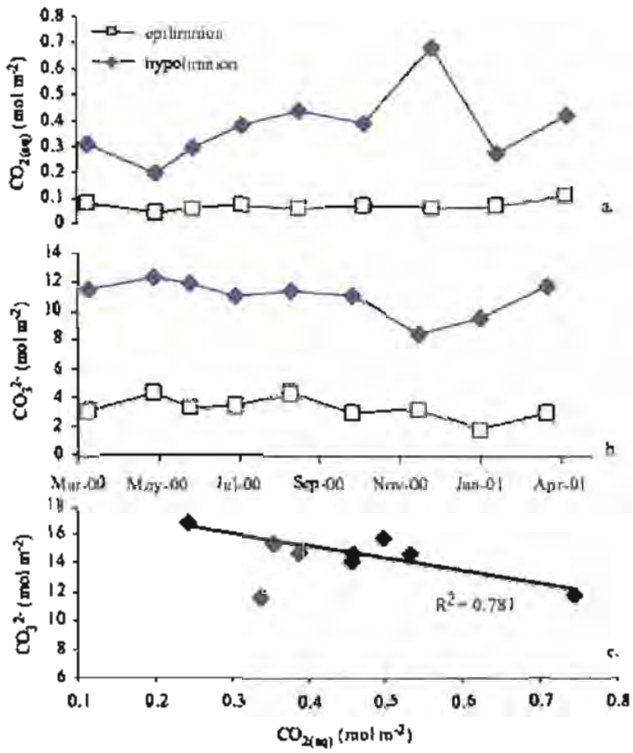

Figure 1.5. (1.5a) $CO_{2(aq)}$ and (1.5b) CO_3^{2-} inventories (concentration integrated along depth); note the different ordinate axes for the hypolimnion and epilimnion. (1.5c) Total CO_3^{2-} inventory plotted vs. $CO_{2(aq)}$ inventory.

1.3.6. Nitrogen and phosphorus

Nitrogen speciation in the pond is primarily controlled by the water's redox state. Except for the summer epilimnion, the pond remained in a chemically reduced state

throughout the study, and NH_4^+ made up on average 97% of the total inorganic nitrogen pool (Fig. 1.6). Nitrate disappeared in December coincident with a rise in $[NO_2^-]$ (Figs. 1.6a & 1.6b), which indicated an exhaustion of the NO_3^- pool by anaerobic microbial organic carbon oxidation via denitrification (9):

$$CH_2O + NO_3^- = CO_2 + NO_2^- + 2H^+ \qquad (9)$$

Also in December, there were significant increases of NH_4^+ and PO_4^{3-} in the hypolimnion produced by organic matter remineralization (Figs. 1.6c & d). Once the density gradient diminished in January, the remineralized N and P concentrated within the hypolimnion mixed across the water column. It also appears that some of the NH_4^+ that mixed upwards had oxidized to NO_2^- by the end of the time-series (Fig. 1.6b).

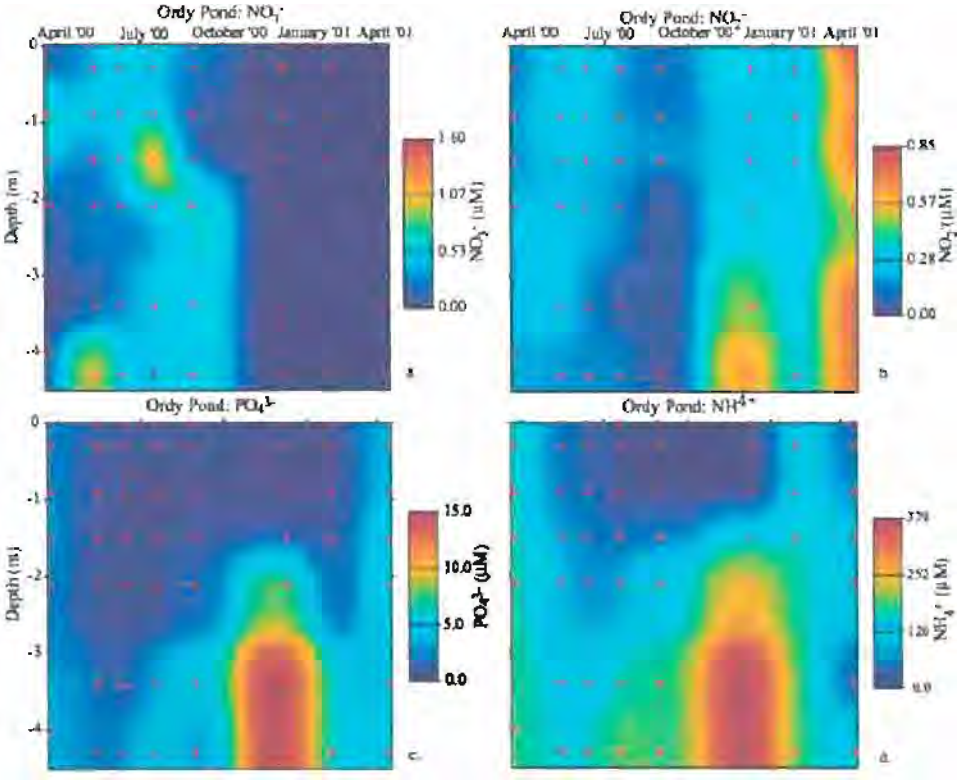

Figure 1.6. Profiles of NO_3^- (1.6a), NO_2^- (1.6b), PO_4^{3-} (1.6c), and NH_4^+ (1.6d). Each sample is represented in depth and time by ○.

1.3.7. Nutrient enrichment experiments

In the nutrient enrichment experiments, only P treatments resulted in significant additional phytoplankton growth (Fig. 1.7)., indicating that P is the most limiting nutrient to phytoplankton growth. Furthermore, the chlorophyll-a:chlorophyll-b ratio was ~3:1, indicating that the modern planktonic biota is dominated by green algae.

1.3.8. Mn & Fe

Dissolved Mn^{2+} and Fe^{2+} concentrations are controlled by the redox state of the solution (Chester, 1990), and the Mn^{2+} and Fe^{2+} profiles (Figs. 1.8a. & 1.8b.) reflect the redox state of Ordy Pond during the time-series. Theoretically, once anaerobic microbial oxidation of organic matter has exhausted NO_3^- as an electron acceptor, bacteria will next reduce manganese (10) and then iron (11) (Chester, 1990):

manganese(IV) reduction: $CH_2O + 2MnO_2 + 4H^+ = CO_2 + 2Mn^{2+} + 3H_2O$ (10)

iron(II) reduction: $CH_2O + 4Fe(OH)_3 + 8H^+ = CO_2 + 4Fe^{2+} + 11H_2O$ (11)

In Ordy Pond, total Mn^{2+} and Fe^{2+} concentrations increased across the water column in October after the NO_3^- pool was depleted. The increased Mn^{2+} and Fe^{2+} concentrations are not associated with increased supply since groundwater exchange with the pond is poor and there were no significant storms or wind events at these times. The rise in reduced metal concentrations are therefore believed to have resulted from intensified anaerobic microbial respiration. Furthermore, the October and December profiles revealed a three-fold rise in the hypolimnion S^{2-} concentration, which is believed to have been produced by microbial sulfate reduction of organic matter. Sulfate reduction requires more energy than iron, manganese, or nitrate reduction (Chester, 1990), and thus December is interpreted as the period when the pond was the most chemically reduced.

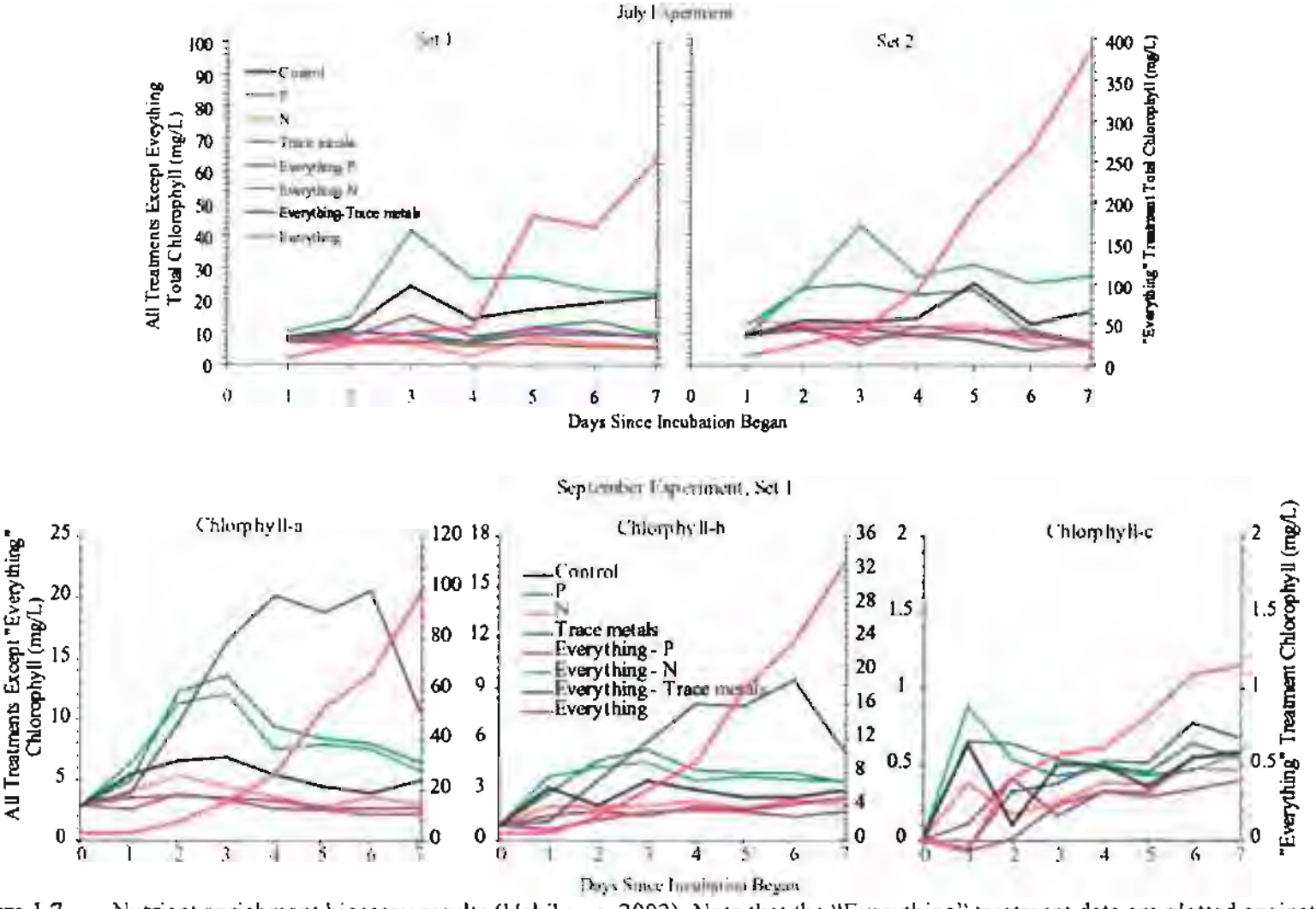

Figure 1.7. Nutrient enrichment bioassay results (Uchikawa, 2002). Note that the "Everything" treatment data are plotted against the right axes and all other data are plotted against the left axes. The upper panels show data from the duplicate sets of the July 2001 experiments which measured total chlorophyll. The lower panels show the separate chlorophyll-a, -b, and –c data for one set of the September treatments.

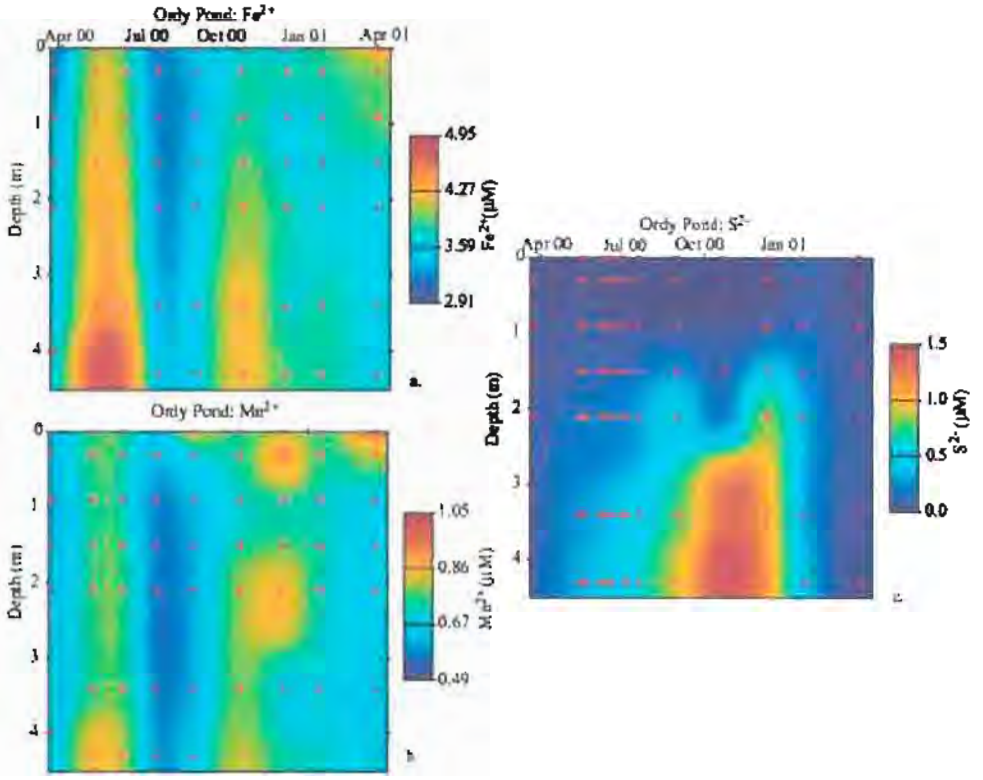

Figure 1.8. Profiles of Fe^{2+} (1.8a), Mn^{2+}(1.8b), and sulfide (1.8c). Each sample is represented in depth and time by ▪.

1.3.9. Carbonate mineral saturation states

The pond was perpetually oversaturated with respect to low magnesium calcite (LMC) and kutnahorite [$Ca(Mn_xMg_{1-x})(CaCO_3)_2$] (Fig. 1.9) owing to high CO_3^{2-} concentrations. Average North Pacific surface seawater, which is oversaturated with respect to LMC, has 20 times less CO_3^{2-} than Ordy Pond [ave. Ordy CO_3^{2-} = 3.54 mmol L^{-1}, Table 1.3; ave. N Pacific = 0.18 mmol L^{-1}, (Nozaki, 2001)], but 4 times as much Ca^{2+} [ave. Ordy Ca^{2+} = 2.7 mmol L^{-1}, Table 1.3; ave. N Pac. = 10 mmol L^{-1}, (Nozaki, 2001)]. Changes in the LMC and kutnahorite mineral saturation states [Ω = (mineral ionic activity product – IAP)/(mineral solubility coefficient – Ksp)] were reflective of changes in phytoplankton primary productivity (Fig. 1.9). The drop in LMC

and kutnahorite Ω values in July and September resulted from increased inorganic mineral precipitation promoted by increased CO_2 consumption by phytoplankton and higher pH in the epilimnion. The drop in the LMC and kutnahorite Ω's in the hypolimnion resulted from decreased $[CO_3^{2-}]$ due to increased microbial $CO_{2(aq)}$ production (Figs. 1.4b, 1.5a).

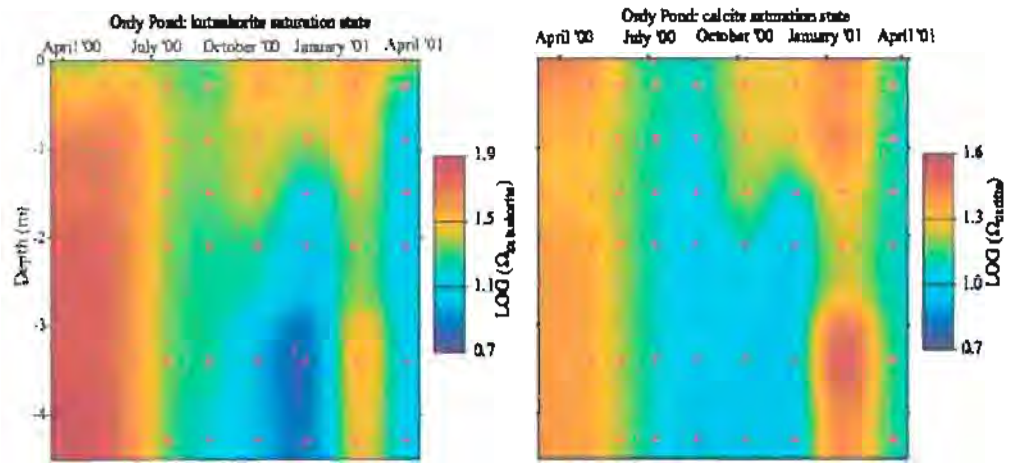

Figure 1.9. The saturation state of the water in Ordy Pond with respect to pure calcite and kutnahorite and as calculated with EQ3NR. Each sample is represented in depth and time by ▫.

1.3.10. Organic carbon production rates

Eighty-five percent of the organic carbon production measured occurred within the upper half meter of the water column (Table 1.4). For the most part, these organic carbon production rates reflect the rate of net primary productivity in the water column, i.e., the rate of autrotrophically fixed organic carbon in excess of autotrophic respiration (Schlesinger, 1995). Dark unpoisoned control bottles were not included in the experiment, so these rates include net daily organic carbon produced both photosynthetically and chemosynthetically, i.e. both light and dark inorganic carbon uptake. Furthermore, the ΔPOC(t) in Eq. (2) may also include carbon flow from

phytoplankton to zooplankton (Hama et al., 1993). The depth integrated net production rate was 472 mg C m^{-2} d^{-1}, or 172 g C yr^{-1}. This rate is comparable to rates been measured in the North Atlantic which are integrated over a mixing depth of 100 – 200 m (Maranon et al., 2000). Though organic carbon production rates vary between seasons, the pond was in a transition period between seasons during this experiment. Therefore, these data are believed to reflect a first order annual mean production rate. Finally, measurement of organic carbon production in the dim and anoxic hypolimnion (>0.9m) is evidence that anaerobic photo- and/or chemoautotrophic bacteria are present.

TABLE 1.4. Data from 24 hour incubation with ^{13}C-labelled HCO_3^{2-}

Depth (m)	Initial DIC (mmol L^{-1})	Initial $\delta^{13}C_{DIC}$ ‰,V-PDB	Medium $\delta^{13}C_{DIC}$ ‰,V-PDB*	Initial $\delta^{13}C_{POC}$ ‰,V-PDB	Final POC (mg/L)	Final $\delta^{13}C_{POC}$ ‰,V-PDB	PR** (mg C m^{-3} hr^{-1})
0.0	17.38	-2.2	2293.9	-31.7	15.38	+79.9	30.14
0.3	18.05	-3.0	2210.2	-31.7	14.65	+45.5	20.06
0.9	15.51	-3.5	2560.9	-30.3	10.01	-14.9	2.43
1.5	17.15	-4.0	2323.0	-30.3	8.44	-21.4	1.30
2.1	16.84	-3.4	2364.5	-30.1	7.20	-20.9	1.13
3.4	16.54	-2.8	2407.5	-31.8	11.74	-22.3	1.86
4.3	17.57	-4.7	2268.0	-30.0	7.26	-21.3	1.12

* $\delta^{13}C_{DIC}$ of the water in the incubation bottles once the ^{13}C tracer was added
** PR = production rate, calculated with Eq. (2)

1.4. CONCLUSIONS

Ordy Pond can be considered a two-phase system. In early May, 2001, the epilimnion warmed and became 0.006 g cm^{-3} less dense than the hypolimnion which stratified the water column; the pond remained thermally stratified until early October, 2000. In the spring/summer phase, surface warming, O_2 enrichment, CO_2 drawdown, and increased particulate production indicated a phytoplankton bloom triggered by stratification and a longer photoperiod. The drop in Ω_{LMC} and $\Omega_{kutnahorite}$ during the spring/summer was due partly to increased mineral precipitation contemporaneous with

elevated productivity. When the pond was not stratified in the fall/winter, phytoplankton spent more time in the darker depths of the water column and in the respirative photosynthesis dark phase, thus reducing production of organic matter. In this phase the pond was characterized by increased concentrations of reduced carbon, sulfur, nitrogen, phosphorus, and metal ions produced by remineralization of settling particulate organic matter and sediments beneath the pond.

It is not uncommon in aquatic systems for light availability to control primary production. Sverdrup (1953) described a simple model to explain how the depth of the mixed layer was responsible for the onset of spring blooms in the North Atlantic. Once the bottom of the mixed layer moves above the point at which net production equals community loss, i.e., the critical depth, the standing crop will increase and a bloom will begin. Sverdrup argued that if the mixed layer extends below the critical depth, photoautotrophs do not see enough sunlight to drive rates of primary production above that of community loss, and a bloom will not occur. Other examples where increased photosynthesis is coeval with thermal stratification include parts of the Bay of Biscay (Varela, 1996), the Chilean coast (Guzman and Campodonico, 1978), and the Baltic Sea (Kaiser and Schulz, 1976). Lacustrine examples include Lakes Constance and Zürich in Switzerland (Bleiker and Schanz, 1997; Gaedke et al., 1998), Lake Erken in Sweden (Pierson et al., 1992), and Lake Kinneret in Israel (Klein and Koren, 1998).

However, light is not the only control on photosynthetic productivity in Ordy Pond. The nutrient enrichment experiments indicated that phosphorus appears to limit phytoplankton growth. However, aerobic photosynthesis was not the only process for organic carbon fixation in the pond. The 24-hour ^{13}C-incubation measurements found low

but significant organic carbon fixation at light-poor depths without any O_2 production. This suggests that a community of anaerobic photoautotrophic and/or chemoautotrophic bacteria resides in the pond. Indeed, sediment trap samples collected during the study had physically observable concentrations of green and purple organic matter which were presumably photoautotrophic green and purple sulfur and purple non-sulfur bacteria (Atlas and Bartha, 1993).

At the end of the time-series in April 2001, conditions in the pond were similar to conditions in May of 2000. This seemed to be a result of an earlier warming of surface air temperatures in 2001 and possibly an earlier initiation of spring/summer phytoplankton productivity. Furthermore, the fall/winter season was one of the driest on record for the last 50 years which partly explains why chemical concentrations did not match between April 2000 and April 2001. These results will be combined with the particulate study findings (Chapter II) to form an integrated model of the modern pond biogeochemistry to interpret the environmental history of the area from the sediments beneath Ordy Pond.

1.5. ACKNOWLEDGEMENTS

This study was funded in part by a grant from the National Oceanic and Atmospheric Administration, project #R/EL-18, which is sponsored by the University of Hawai'i Sea Grant College Program, SOEST, under Institutional Grant No. NA86RG0041 from NOAA Office of Sea Grant, Department of Commerce. Total chlorophyll measurements were graciously provided by Dan Hoover at the University of Hawai'i. The nutrient enrichment experiment work and data interpretation was provided by Joji Uchikawa and graciously funded by the Department of Oceanography's Global

Environmental Science undergraduate program, Dr. Fred. T. Mackenzie, Program Coordinator. The views expressed herein are those of the authors and do not necessarily reflect the views of NOAA or any subagencies. This is University of Hawai'i SOEST contribution #XXXX and Sea Grant Publication #UNIHI-SEAGRANT-xx-00-xx. Additional funding for this research was provided by Sigma Xi as a Grants-in-Aid award for graduate research, by the Geologic Society of America as a graduate research award, and by William T. Coulbourn and Harold T. Stearns Fellowship Awards from the Department of Geology and Geophysics at the University of Hawai'i, Mānoa.

1.6. REFERENCES

Atlas R. M. and Bartha R. (1993) *Microbial Ecology*. The Benjamin/Cummings Publishing Company, Inc.

Athens, J.S., Tuggle, H.D., Ward, J.V., and Welch, D.J., 2002, Avifaunal extinctions, vegetation change, and Polynesian impacts in prehistoric Hawai'i: Archeologica Oceania, v. 37, p. 57-78.

Bleiker, W., and Schanz, F., 1997, Light climate as the key factor controlling the spring dynamics of phytoplankton in Lake Zuerich: Aquatic Sciences, v. 59, p. 135-157.

Chester, R. 1990. Marine Geochemistry, Boston, Unwin Hyman, 698 p.

Chivas, A.R., De Deckker, P., Cali, J.A., Chapman, A., Kiss, E., and Shelley, J.M.G., 1993, Coupled stable-isotope and trace-element measurements of lacustrine carbonates as paleoclimate indicators, *in* Savin, S., ed., Climate Change in Continental Isotopic Records, Volume 78: Geophysical Monograph: Washington, D.C., American Geophysical Union, p. 113-121.

Davies, C.W., 1962, Ion Association: London, Butterworths, 190 p.

De Carlo, E.H., 1992, Geochemistry of interstitial water and associated sediments from the Exmouth Plateau., *in* von Rad, U., Haq, B.U., et al., eds., Proceedings of the Ocean Drilling Program, Scientific Results, Volume 122, p. 295-308.

De Carlo, E.H., and Kramer, P.A., 2000, Minor and trace elements in interstitial waters of the Great Bahamas Bank: Results from ODP Leg 166., *in* Sarg, J.F., ed., Proceedings of the Ocean Drilling Program, Scientific Results, Volume 166, p. 99-111.

Gaedke, U., Ollinger, D., Kirner, P., and Baeuerle, E., 1998, The influence of weather conditions on the seasonal plankton development in a large and deep lake (L. Constance): III. The impact of water column stability on spring algal development; NATO Advanced Science Institutes Series 2: Environment, Management Of Lakes And Reservoirs During Global Climate Change, Volume 42: Dordrecht, Netherlands, Kluwer Academic Publishers, p. 323.

Glenn, C.R., and Kelts, K., 1991, Sedimentary Rhythms in Lake Deposits, *in* Seilacher, A., ed., Cycles and Events in Stratigraphy: Berlin Heidelberg, Springer-Verlag, p. 188-221.

Grasshoff, K., Ehrhardt, K., and Kremling, K., 1983, Methods of Seawater Analysis, Second Revised and Extended Edition: Germany, Verlag Chemie, 419 p.

Guzman, L., and Campodonico, I., 1978, Mareas rojas en Chile (Red tides in Chile): Interciencia, v. 3, p. 144-151.

Hama, T., Hama, J., and Handa, N., 1993, ^{13}C tracer methodology in microbial ecology with special reference to primary production processes in aquatic environments., *in* Gwynfryn Jones, J., ed., Advances in Microbial Ecology, v. 13: New York, Plenum Press, p. 39-83.

Hama, T., Handa, N., and Hama, J., 1987, Determination of amino acid production rate of a marine phytoplankton population with ^{13}C and gas chromatography-mass spectrometry: Limnology and Oceanography, v. 32, p. 1144-1153.

Hecky, R.E., and Kilham, P., 1988, Nutrient limitation of phytoplankton in freshwater and marine environments: A review of recent evidence on the effect of enrichment: Limnology and Oceanography, v. 33.

Kaiser, W., and Schulz, S., 1976, On the causes of the differences in time and location of the spring phytoplankton bloom in the Baltic: ASFA printed journals, v. 14, p. 77-81.

Klein, M., and Koren, N., 1998, The influence of the thermocline on sedimentation in the deeper part of Lake Kinneret, Israel: Limnologica. Jena, v. 28, p. 293-299, 1998.

Kroopnick, P, 1974, The dissolved O_2-CO_2-^{13}C system in the eastern equatorial Pacific. Deep-Sea Research, v. 21., p. 211-227.

Ku, T.-L., Kimmel, M.A., Easton, W.H., and O'Neil, T.J., 1974, Eustatic sea level 120,000 years ago on O'ahu, Hawai'i: Science, v. 183, p. 95a.

Maranon, E., Holligan, P.M., Varela, M., Mourino, B., and Bale, A.J., 2000, Basin-scale variability of phytoplankton biomass, production and growth in the Atlantic Ocean: Deep-Sea Research, v. 47, p. 825-857.

Millero, F.J., and Poisson, A., 1981, International one-atmosphere equation of state of seawater: Deep-Sea Research, v. 28A, p. 625-629.

Muhs, D.R., and Szabo, B.J., 1991, New uranium-series ages of the Waimanalo Limestone, O'ahu, Hawai'i, and paleoclimatic implications for the last interglacial period: Geological Society of America Abstracts with Programs, v. 23, p. A239.

Nozaki, Y., 2001, Elemental distribution overview, *in* Steele, J.H., Turekian, K.K., Thorpe, S.A., eds., Encyclopedia of Ocean Sciences, London, Academic Press.

Ogden, 1999, Remedial Investigation Report for BRAC - Related Activities, Regional Ground-Water System, Naval Air Station Barbers Point, O'ahu, Hawai'i, 3 Vol.: Honolulu, Hawai'i, Ogden Environmental and Energy Services Company, Inc.

Pierson, D.C., Pettersson, K., and Istvanovics, V., 1992, Temporal changes in biomass specific photosynthesis during the summer: Regulation by environmental factors and the importance of phytoplankton succession: The Dynamics and Use of Lacustrine Ecosystems, Hydrobiologia, v. 243-244.

Schlesinger, W.H., 1995, Biogeochemistry: an analysis of global change: San Diego, Academic Press, p. 588.

Sherman, C.E., Glenn, C.R., Jones, A.T. , Burnett, W.C. , Schwarcz, H.P., 1993, New evidence for two highstands of the sea during the last interglacial, oxygen isotope substage 5e: Geology, v. 21, p. 1079-1082.

Stearns, H.S., 1974, Submerged shorelines and shelves in the Hawaiian Islands and a revision of some of the eustatic submerged shorelines: Geological Society of America Bulletin, v. 85, p. 795-804.

Sverdrup, H.U., 1953, Journal Conseil Permanent pour l'Exploration de la Mer, v. 18, p. 287.

Szabo, B.J., Ludwig K.R., Muhs, D.R., Simmons, K.R., 1994, Thorium-230 Ages of Corals and Duration of the Last Interglacial Sea-Level High Stand on Oahu, Hawai'i: Science v. 266, p. 93-96.

Tribble, J.S., Garrison, G.H., Stens, J.S., Skillbeck, C.G., and Frankel, E., 1999, Evidence for early-mid Holocene sea level on O'ahu, Hawai'i from coastal pond sediments, *in* Fletcher, C.H. and Matthews, J.V., eds., The Non-Steady State of the Inner Shelf and Shoreline: Coastal Change in the Time Scale of Decades to Millennia in the Late Quaternary: Abstracts with Programs, Inaugural Meeting of IGCP Project #437, University of Hawai'i, Honolulu, HI, Nov. 9-12, 249p.

Uchikawa, J., 2002, Investigation of limiting nutrients in Ordy Pond, O'ahu: Correlations between nutrient cycles and growth responses of natural phytoplankton populations in a coastal eutrophic pond [Undergraduate thesis], University of Hawai'i at Mānoa.

Varela, M., 1996, Phytoplankton ecology in the Bay of Biscay: Scientia Marina (Barcelona), v. 60, p. 45-53.

Wanninkhof, R., 1992, Relationship between wind speed and gas exchange over the ocean: Journal of Geophysical Research, v. 97, p. 7373-7381.

Weiss, R.F., 1970, The solubility of nitrogen, oxygen and argon in water and seawater: Deep-Sea Research, v. 17, p. 721-735.

WOCE, 1994, WOCE Operations Manual, Volume 3: The Observational Programme: Woods Hole, MA, USA, World Ocean Circulation Experiment.

Wolery, T.J., 1992, EQ3NR, A computer program for geochemical aqueous speciation-solubility calculations: Oak Ridge, TN, Lawrence Livermore National Laboratory.

CHAPTER II.

Sedimentary responses to seasonal aquatic biogeochemistry in a stratified pond and implications for interpreting O'ahu's environmental history

ABSTRACT

Lacustrine sediments are effective paleoenvironmental proxies if the processes of sediment formation are clearly understood. This paper presents a time-series analysis between June 2000 and March 2001 of modern particulate production in Ordy Pond on O'ahu, Hawai'i. Modern particulate production closely reflected changes in the nature of the water column. Particulates consisted primarily of phytoplanktonic organic matter and an inorganically precipitated mix of microcrystalline kutnahorite and LMC. Kutnahorite is a Mn-bearing dolomite mineral. Increased primary productivity and CO_2 drawdown in the summer triggered a doubling of the carbonate particulate flux. Carbonate mineral $\delta^{13}C$ peaked at -1.8‰ (V-PDB) in July and fell to -3.3‰ (V-PDB) in March reflecting elevated primary productivity in the summer and increased remineralization of organic matter in the winter. Particulate carbonate $\delta^{18}O$ traced the pond's seasonal water balance; $\delta^{18}O_{carb}$ peaked at +2.9‰ (V-PDB) in the summer when pond water evaporation was strongest (as determined by changes in salinity), and $\delta^{18}O_{carb}$ fell to +0.9‰ (V-PDB) in the winter when water was added to the pond via rainfall and groundwater seepage. Organic particulate $\delta^{15}N$ peaked at +12.7‰ (AIR) in July and fell to +10.8‰ (AIR) in winter, apparently a function of biogenic NH_4^+ uptake and $NH_{3(aq)}$ volatization. The $\delta^{13}C_{POM}$ trend was controlled by the fractionation of ^{13}C during primary productivity (ε_p). Fractionation peaked at +17.4‰, (V-PDB) in the spring/summer and dropped to +12.9‰ (V-PDB) in the fall/winter. This shift may have been due to an increased abundance of anaerobic photo- and chemosynthetic bacteria, although changes in cell size, growth rate (μ), and photosynthetic HCO_3^- uptake can also affect ε_p. These results indicate that the sediment laminae are seasonal deposits, and that dark-light laminae couplets are varves.

2.1. INTRODUCTION

Lacustrine sedimentary records are effective tools for reconstructing historic changes in terrestrial ecosystems and local climate (Schelske and Hodell, 1991; Hollander et al., 1992; Hodell and Schelske, 1998; Mullins, 1998). Lake sediments are often well preserved and can record changes in rainfall, temperature, biological productivity, and surrounding land use (e.g., deforestation, agriculture). Laminated sediments are especially valuable because they imply cycling on seasonal, annual, or decadal time scales (Glenn and Kelts, 1991). However, in order to accurately use lacustrine sediments for paleoenvironmental study, we have to understand how those sediments formed. In this paper I present a time-series analysis of modern particulate production in a pond which holds a sedimentary paleoenvironmental record of the Holocene epoch on the island of O'ahu, Hawai'i.

Ordy Pond fills a 20+ m deep karst sinkhole 800 m from shore in the Kalaeloa region of 'Ewa Plain, also known as Barbers Point (Fig. 2.1). 'Ewa is an emerged Pleistocene carbonate reef complex. The area around the pond formed during O'ahu's interglacial Waimanalo sea level stand (oxygen isotope Stage 5e) which lasted between 135-120 kya and was ~ 8 m higher than today (Ku et al., 1974; Stearns, 1974; Muhs and Szabo, 1991; Sherman et al., 1993: Szabo et al., 1994). The most recent post glacial sea level rise inundated the sinkhole with groundwater, and today the pond is 0.5 ha in area, 5m deep. The pond is sheltered by a ring of American mangrove (*Rhizophora mangle)* within a forest of kiawe trees (*Prosopis pallida*) and sourbush (*Pluchea symphytifolia*) and does not physically overturn (Chapter I).

Sediments beneath the pond were first cored in 1994 as part of an archeological study of 'Ewa Plain (Athens et al., 2002). That effort recovered 8 m of core and found the sediments to hold a paleoenvironmental record. The pond was cored again in 1997, and 17 m of sediments were recovered spanning the entire lacustrine history of the pond (Tribble et al., 1999). A radiocarbon sample from just below the first lacustrine sediments has an age of 9780 ± 110 years before present, and four additional dates along the core indicate that sedimentation rates were between 0.3 and 3.1 cm/year (Athens et al. 2002, Tribble et al., 1999). The aquatic sediments are highly laminated and alternate between dark organic-rich and light carbonate-rich layers, which suggests the laminae are varves.

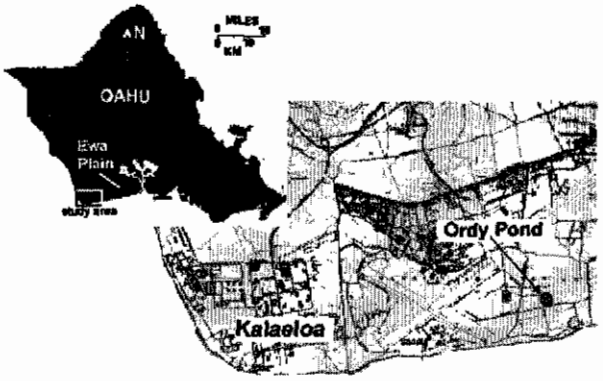

Figure 2.1. *Location map of Ordy Pond in the Kalaeloa area of 'Ewa Plain.*

A water chemistry time-series analysis made between April 2000 and April 2001 (Chapter I) found the pond to be brackish and eutrophic. During that study the pond was thermally stratified between early April and late September which was also a period of elevated organic mater production in the epilimnion; organic carbon fixation exceeded 470 mg C m^{-2} d^{-1}, a rate comparable to North Atlantic spring phytoplankton blooms (Chapter I). During the water column study, seasonal trends were noted in the $\delta^{13}C_{DIC}$, nutrient concentrations, and carbonate mineral saturation states which support the

interpretation of the sediment laminae as varves (Chapter I). The aim of this work was to compare modern particulate production to water chemistry in the pond and establish a model to interpret the environmental history recorded in the sediments beneath the pond.

2.2. METHODS

2.2.1. Sediment Traps

Sediment traps were placed in Ordy Pond and sampled six times between 7 June 2000 and 23 March 2001. The traps consisted of two Plexiglas tubes 7.6 cm diameter, 46 cm long, and closed at one end with a removable slip cover. These traps are similar in design to those used by the Hawaiian Ocean Time-series (HOTS, http://hahana.soest.hawaii.edu/hot/hot.html). The traps were suspended from a mooring to a depth of 4 m, 1 m above the bottom of the pond, and a full profile of the water column was made when the traps were both deployed and recovered. The pond never physical overturned during the study and the lower 3 m of the water column were always anoxic (Chapter I), so the traps probably did not collect any material resuspended from the bottom either by water currents or epifaunal bioturbation. Smear slides of each sample were made using UV-cured optical adhesive, and bulk content observations were made under a petrographic microscope. Samples were dried, weighed, and ground for chemical analyses. The material from each of the tubes was kept separate to evaluate sample homogeneity. The errors reported for analytical data are 1σ, and errors reported for calculated data are based on the 1σ analytical standard errors.

2.2.2. XRD

Sample mineralogy was determined on powdered samples with an automated Scintag Pad V X-ray diffractometer (XRD) scanning with Cu-Kα radiation ($\lambda = 1.5406$ Å) at rate of 2° 2Θ min^{-1}. Powdered fluorite was added to the samples before analysis, and the fluorite-111 hkl peak was used to standardize the sample XRD patterns. The mole percentage of Mg in calcite was calculated from the shift in the d-spacing of the calcite-104 peak (3.035 Å), according to an equation derived from data in Bischoff et al. (1983) (Bischoff, pers. comm.):

$$\text{Mol\%-Mg} = 100[(\text{calcite-104 d-space value}) - 3.035]/-0.291667 \qquad (1)$$

Replicated sample analyses had a standard deviation (σ) of 0.1% (n = 6). Particulate samples were mixtures of low magnesium calcite (LMC) and kutnahorite ($Ca(Mn_xMg_{1-x})(CaCO_3)_2$). In order to determine the relative fraction of each phase, kutnahorite to calcite peak areas ratios (PAR) were measured on twelve standard mixtures; results are presented in the Appendix. Replicated sample analyses had a standard deviation (σ) of 1.3% (n = 6).

2.2.3. Analytical Chemistry

Particulate inorganic and organic carbon weight percents were measured coulometrically. Inorganic carbon samples were acidified with 6% perchloric acid in a UIC Model 5130 Acidification Module, while total carbon samples were combusted at 1050° C in a UIC Model 5120 Total Carbon Aparatus. In both cases the CO_2 extracted from the samples was measured titrimetrically in a UIC Model 5001 CO_2 Coulometer. Replicated carbon analyses had a standard deviation (σ) of 0.2% (n = 6) for both inorganic and organic carbon. Carbonate stable isotope ratios, $\delta^{18}O_{carb}$ and $\delta^{13}C_{carb}$, were

measured using a modification of the sealed-vessel technique (McCrea, 1950; Epstein et al., 1953a; Epstein et al., 1953b; Emiliani, 1955). Samples were acidified under vacuum with 100% phosphoric acid at 50° C, and the evolved CO_2 was cryogenically trapped within sealed borosilicate ampoules. The CO_2 was analyzed on a Finnigan MAT 252 isotope-ratio-monitoring (IRM) mass spectrometer in the SOEST Stable Isotope Biogeochemistry Lab at the University of Hawai'i, Manoa. Corrections were made for temperature dependent oxygen isotopic exchange between the phosphoric acid and the sample carbonate (Swart et al., 1991). Particulate organic matter (POM) $\delta^{13}C$, $\delta^{15}N$, and C:N ratios were measured at the same facility with a Carlo Erba 2500NC Elemental Analyzer coupled to a Finnigan MAT Delta S mass spectrometer via a CONFLO II interface. Samples were first acidified with 6% sulfurous acid (H_2SO_3) in silver boats to remove carbonate material. Isotopic ratios are reported in standard delta notation; $\delta^{13}C$ and $\delta^{18}O$ are reported relative to Peedee Beleminite (V-PDB), and $\delta^{15}N$ is reported relative to atmospheric nitrogen (AIR). The weight percent organic nitrogen was calculated with the C:N ratio and the organic carbon weight percent. Replicated isotope sample analyses had a σ of 0.1‰ (n = 6) for $\delta^{13}C_{carb}$ $\delta^{18}O_{carb}$, and $\delta^{13}C_{org}$, 0.2‰ (n = 6) for $\delta^{15}N_{org}$, and 0.2% for weight percent N. Analytical precisions based on routine analyses of internal laboratory reference materials were ±0.10‰ for $\delta^{18}O_{carb}$, ±0.05‰ for $\delta^{13}C_{carb}$, ±0.15‰ for $\delta^{13}C_{POM}$, and ±0.30‰ for $\delta^{15}N_{POM}$. Internal reference materials for $\delta^{13}C$ and $\delta^{18}O$ analyses were calibrated against NBS-19 ($\delta^{18}O$ = -2.2‰, $\delta^{13}C$ = +1.95‰, V-PDB) and normalized to NBS-18 ($\delta^{18}O$ = -23.05‰, $\delta^{13}C$ = -5.04‰, V-PDB) standard reference materials in accordance with International Atomic Energy Agency (IAEA) guidelines.

2.3. RESULTS

2.3.1. Physical Particulate Description

The particulates collected within the traps were a loose mass of sapropelic material that included clumps of bright green and purple organic matter, presumably photoautotrophic green and purple sulfur and purple non-sulfur bacteria (Atlas and Bartha, 1993). Petrographic smear slide examination found that all the samples contained clear microcrystalline particles dispersed throughout brown-green amorphous organic material. The crystalline material ranged from 1 - 5 μm in size, was highly birefringent under crossed nicols, and was thus believed to be carbonate minerals. In some samples, occasional larger grains (10-20 μm) were also observed. The organic material had no discernable structure at a magnification of 500x, and no test-forming organisms of any kind were observed. Textural characteristics suggest that particulate material was almost entirely authigenic carbonate minerals or organic matter.

2.3.2. Mineralogy

Inorganic particulates consisted of a mix of LMC (<7.5 mol% Mg) and kutnahorite [rhombohedral, $Ca(Mn_xMg_{1-x})(CO_3)_2$] (Fig 2.2, Table 2.1), a hexagonal Mn-bearing dolomite mineral (Frondel and Bauer, 1955). The kutnahorite fraction of the carbonate particulates followed the average total dissolved Mn^{2+} concentration in the pond (Fig. 2.2a), and both were highest when the water column was in its most chemically reduced state (Chapter I); it appears that the availability of Mn^{2+} controlled how much kutnahorite formed. On the other hand, the Mg mole % in the calcite particles

appears to have been controlled by the dissolved molar Mg:Ca ratio; higher dissolved Mg^{2+} concentrations correlated with higher particulate calcite Mg mol% (Fig. 2.2b).

TABLE 2.1. Particulate XRD analytical results

	d-spacing (Å)		Peak Areas				
Sample	Calcite 104 peak	Kutn. 104 peak	Calcite 104 peak	Kutn. 104 peak	Calcite Mg-mole %	K/C PAR*	% of Carbonate as Kutn.**
7/27/2000	3.014	2.949	2012	970	7.3	0.5	47
9/7/2000	3.017	2.956	762	2292	6.1	3.0	77
10/25/2000	3.020	2.952	1638	10565	5.3	6.4	90
12/14/2000	3.021	2.960	3006	7637	4.7	2.5	74
1/31/2001	3.016	2.954	2995	11830	6.6	3.9	81
3/23/2001	3.022	2.958	940	3656	4.3	3.9	81

d-space peak values calculated with 2Θ values corrected with the fluorite-111 peak
* PAR – Peak Area Ratio **calculated with the standard curve described in the appendix

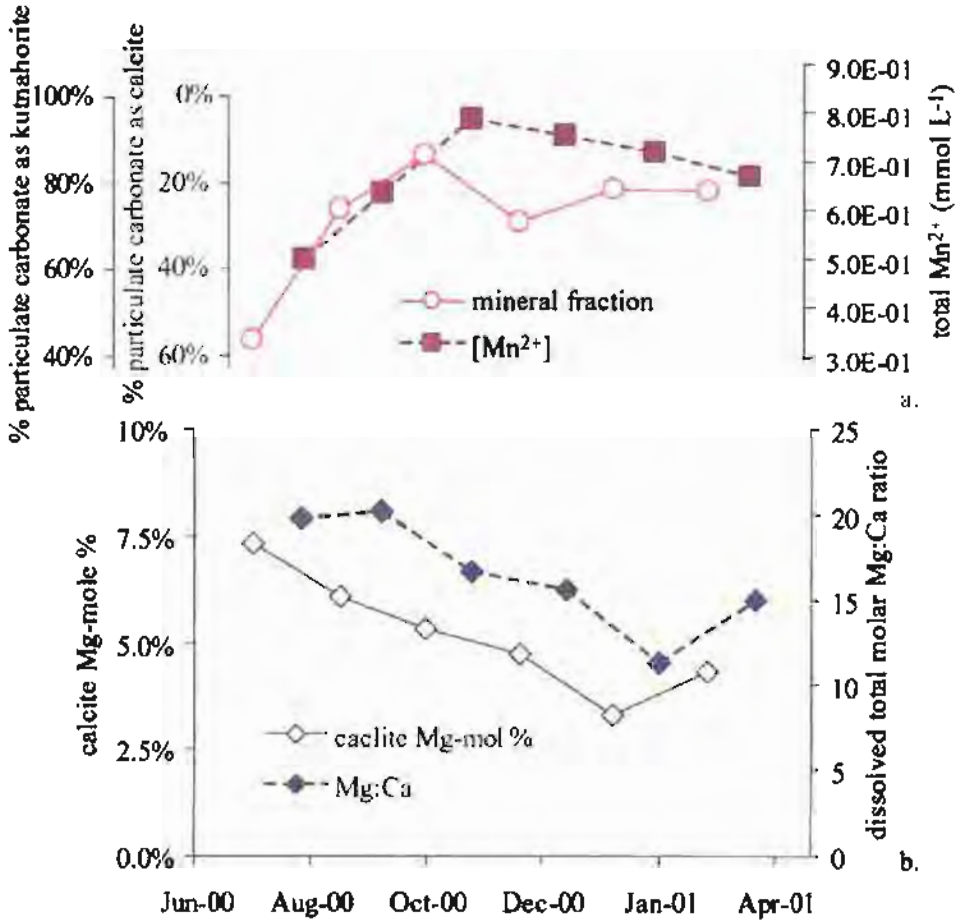

Figure 2.2. Particulate carbonate relative kutnahorite fractions and total $[Mn^{2+}]$ (2.2a), and calcite Mg-mole % and total $[Ca^{2+}]:[Mn^{2+}]$ ratio (2.2b) over time.

2.3.3. Particulate Fluxes and Geochemistry

The highest particulate fluxes occurred in the summer when the water column was stratified and POM production was at its peak (Tables 2.2 & 2.3, Fig. 2.3). The particulate carbonate Mn^{2+} and Mg^{2+} contents were not determined and the carbonate mineral flux calculations were made using a kutnahorite composition of $Ca(Mn_{0.7}Mg_{0.3})(CO_3)_2$ (205.83 g mol^{-1}) which is an average of reported kutnahorite values (Frondel and Bauer, 1955).

The POM aquatic fractions in Table 2.3 were calculated assuming the samples were conservative mixes of phytoplankton with a C:N ratio of 6.6 (Redfield, 1934, 1958), and terrestrial organic matter with a C:N ratio of 20+ (Meyers, 1994). The terrestrial organic fraction could have been as high as 16% in November/December. However, this is considered a maximum possible value since terrestrial C:N can exceed 50 (Meyers, 1994), and the C:N range observed in these samples can easily occur within phytoplankton (Menzel and Ryther, 1964; Downing and McCauley, 1992).

2.3.4. Particulate stable isotopic ratios: $\delta^{13}C_{POM}$, $\delta^{15}N_{POM}$, $\delta^{13}C_{carb}$, $\delta^{18}O_{carb}$

Particulate carbonates were more enriched in ^{13}C and ^{18}O in the summer and more depleted in the winter (Fig. 2.4). Carbonate $\delta^{18}O$ decreased from +2.9‰ (V-PDB) in August to +0.9‰ (V-PDB) in February/March, while in the same period $\delta^{13}C_{carb}$ decreased from -1.9‰ to -3.3‰ (V-PDB). Organic carbon became steadily more enriched in ^{13}C during the time-series, and $\delta^{13}C_{POM}$ increased from -29.9‰ to -26.9‰ (V-PDB). Particulate organic $\delta^{15}N$, on the other hand, decreased between June and November, from +12.7‰ to +10.8‰ (AIR), and then remained at an average value of +10.8‰ (AIR) until March.

TABLE 2.2. Particulate geochemistry and fluxes. Samples are identified in the text by the date they were collected.

sediment traps		Duration	total flux	particulate wt% inorganic carbon	% of carbonate particles as kutnahorite*	% of total particulates as calcite	% of total particulates as kutnahorite	total carbonate particulate flux
collected	installed	(d)	(mg m^{-2} d^{-1})					(mg m^{-2} d^{-1})
7/27/2000	6/7/2000	50	791 ± 20	1.7 ± 0.2	47	7.5	6.5	111 ± 3
9/7/2000	7/27/2000	42	887 ± 27	2.1 ± 0.1	77	4.1	13.8	160 ± 5
10/25/2000	9/7/2000	48	260 ± 38	2.3 ± 0.4	90	2.0	17.4	51 ± 7
12/14/2000	10/25/2000	50	397 ± 46	1.5 ± 0.2	74	3.3	9.5	51 ± 6
1/31/2001	12/14/2000	48	296 ± 2	1.6 ± 0.04	81	2.6	11.2	41 ± 1
3/23/2001	1/31/2001	51	292 ± 29	0.7 ± 0.02	81	1.2	5.1	19 ± 2

*from Table 2.1

TABLE 2.3. Particulate bulk organic carbon and nitrogen contents and fluxes

sample	particulate wt. % organic carbon	particulate wt. % organic nitrogen	molar organic C:N Ratio	% aquatic organic matter*	organic carbon flux (mmol m^{-2} d^{-1})	organic nitrogen flux (mmol m^{-2} d^{-1})
7/27/2000	28.4 ± 0.03	4.6 ± 0.3	7.2 ± 0.2	96 ± 1	18.7 ± 1.7	2.6 ± 0.2
9/7/2000	31.1 ± 0.02	4.9 ± 0.3	7.7 ± 0.1	92 ± 1	23.0 ± 1.7	3.1 ± 0.2
10/25/2000	30.5 ± 0.01	4.5 ± 0.1	7.8 ± 0.2	91 ± 2	6.6 ± 1.0	0.8 ± 0.1
12/14/2000	31.7 ± 0.002	4.2 ± 0.0	8.7 ± 0.0	84 ± 0	10.5 ± 1.2	1.2 ± 0.1
1/31/2001	27.6 ± 0.01	4.1 ± 0.3	7.9 ± 0.2	90 ± 2	6.8 ± 0.3	0.9 ± 0.1
3/23/2001	40.0 ± 0.02	6.4 ± 0.3	7.3 ± 0.1	95 ± 1	9.8 ± 1.1	1.3 ± 0.1

*marine organic matter fraction was calculated by considering the measured C:N ratio a mix between a marine C:N of 6.6 (Redfield, 1934, 1958) and a terrestrial C:N of 20 (Meyers, 1994); this is considered a minimum marine organic content

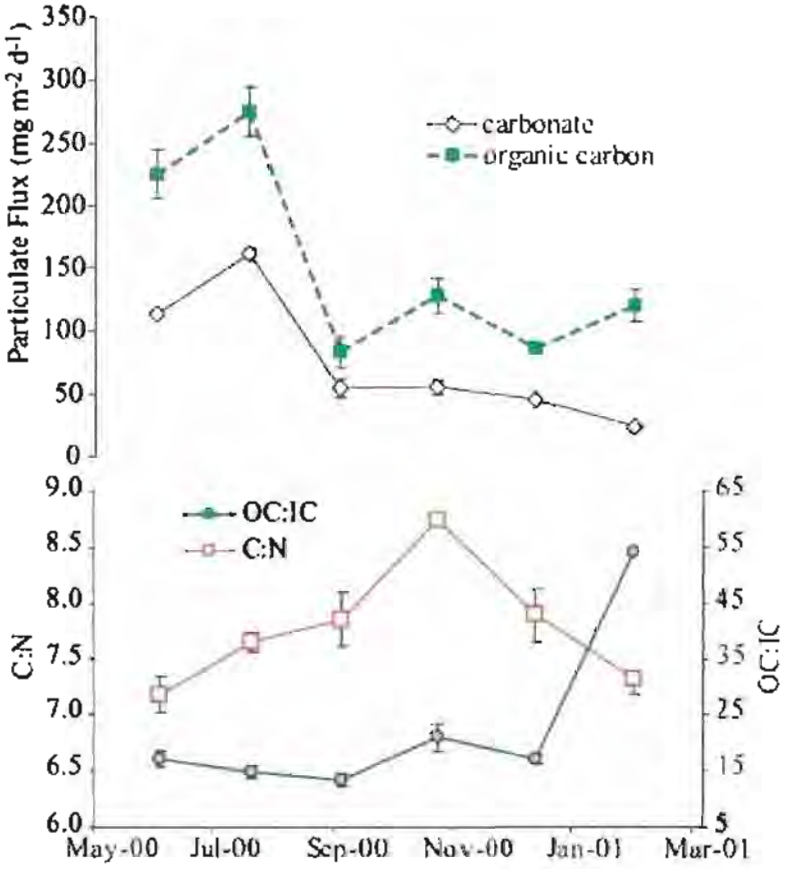

Figure 2.3. Upper panel: carbonate and organic carbon particulate fluxes. Lower panel: particulate organic molar C:N ratio, and organic carbon to inorganic carbon ratio (OC:IC).

TABLE 2.4. Particulate time-series stable isotope measurements

Sample	$\delta^{13}C_{carb}$ (V-PDB)	$\delta^{18}O_{carb}$ (V-PDB)	$\delta^{13}C_{POM}$ (V-PDB)	$\delta^{15}N_{POM}$ (AIR)
7/27/2000	-2.1 ± 0.2	+2.0 ± 0.1	-29.9 ± 0.0	+12.7 ± 0.1
9/7/2000	-1.9 ± 0.1	+2.9 ± 0.1	-29.0 ± 0.0	+12.5 ± 0.1
10/25/2000	-1.8 ± 0.1	+2.6 ± 0.0	-28.3 ± 0.0	+11.5 ± 0.1
12/14/2000	-1.8 ± 0.1	+2.1 ± 0.2	-28.2 ± 0.0	+10.9 ± 0.5
1/31/2001	-2.1 ± 0.2	+1.8 ± 0.0	-27.7 ± 0.3	+10.8 ± 0.4
3/23/2001	-3.3 ± 0.3	+0.9 ± 0.1	-26.9 ± 0.1	+10.8 ± 0.2

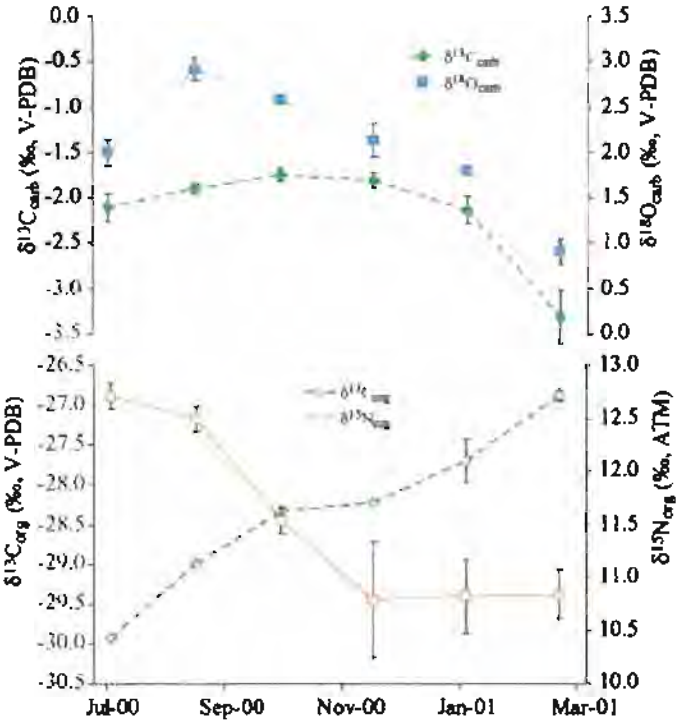

Figure 2.4. Upper panel: Particulate $\delta^{13}C_{carb}$ and $\delta^{18}O_{carb}$ over time.
Lower panel: Particulate $\delta^{13}C_{POM}$ and $\delta^{15}N_{POM}$ over time.

2.4. DISCUSSION

2.4.1. Controls on Carbonate Mineral Precipitation

Biological activity in the pond controlled the carbonate particulate flux by affecting the carbonate mineral saturation state according to Eq. (5):

$$\cancel{CO_2} + \cancel{H_2O} = CH_2O + O_2 \qquad (2)$$

$$2HCO_3^- = \cancel{CO_2} + \cancel{H_2O} + \cancel{CO_3^{2-}} \qquad (3)$$

$$Ca^{2+} + \cancel{CO_3^{2-}} = CaCO_3 \qquad (4)$$

$$\overline{Ca^{2+} + 2HCO_3^- = CH_2O + O_2 + CaCO_3} \qquad (5)$$

Biogenic $CO_{2(aq)}$ uptake (2) reduces acidity and shifts dissolved carbon equilibria towards CO_3^{2-} (3), thus raising the dissolved carbonate mineral saturation states (Ω) and

promoting precipitation (4) (Kelts and Hsu, 1978; Morse and Mackenzie, 1990; Hodell et al., 1998). Thus, the elevated organic and carbonate particulate production rates in the spring/summer (Fig. 2.3) are evidence of both increased primary productivity and increased carbonate mineral precipitation per Eq. (5). Kutnahorite and LMC precipitation lowered the carbonate mineral Ω's during the spring/summer (Fig. 2.5a & 2.5b) and brought the pond's saturation state closer to equilibrium (where $\Omega = 1$). The pond always remained oversaturated with respect to both LMC and kutnahorite, though, which indicated that carbonate mineral precipitation was being kinetically inhibited.

Phosphate may play an important kinetic role in retarding carbonate mineral precipitation. Both calcite and aragonite precipitation have been shown to be inhibited by even micromolar concentrations of PO_4^{3-} (Kelts and Hsu, 1978; Morse and Mackenzie, 1990), and the same may also be true for kutnahorite. Carbonate particulate fluxes peaked when surface water PO_4^{3-} levels dropped from 2.75 to 0.34 μM between April and June (Fig. 2.5c). The drop in carbonate particulate flux, however, preceded the late winter regeneration of dissolved PO_4^{3-}, which may indicate additional mechanisms of inhibition. Organic matter is also known to have a kinetic influence on carbonate mineralogy. The presence of certain dissolved organic compounds can slow carbonate precipitation rates (Morse and Mackenzie, 1990; Tucker and Wright, 1990), which may explain the water column's persistent oversaturation with respect to LMC and kutnahorite.

2.4.2. Mineralogy

Kutnahorite is usually found as a hydrothermal deposit (Tsusue, 1967; Mucci, 1991) and is rare in earth surface environments where it is associated with suboxic/anoxic conditions (Cannon and Force, 1983; Huckenridge and Meischner, 1996). Biologic

activity in Ordy Pond maintained the redox state of most of the water column somewhere between conditions of microbial nitrate and sulfate reduction (Chapter I), which kept Mn^{2+} activity high enough to supersaturate the water with respect to kutnahorite (Fig. 2.5a). Kutnahorite appears to have been the most thermodynamically stable carbonate mineral phase in the pond given the published data available (Fig.2.6). An exception was the September profile when reduced epilimnion [Mn^{2+}] placed the stability near the magnesite/rhodocrosite boundary; in October the water chemistry plotted back within the kutnahorite field. However, the presence of kutnahorite in the sediment traps is troubling because no kutnahorite was found in the sediments (Chapter III).

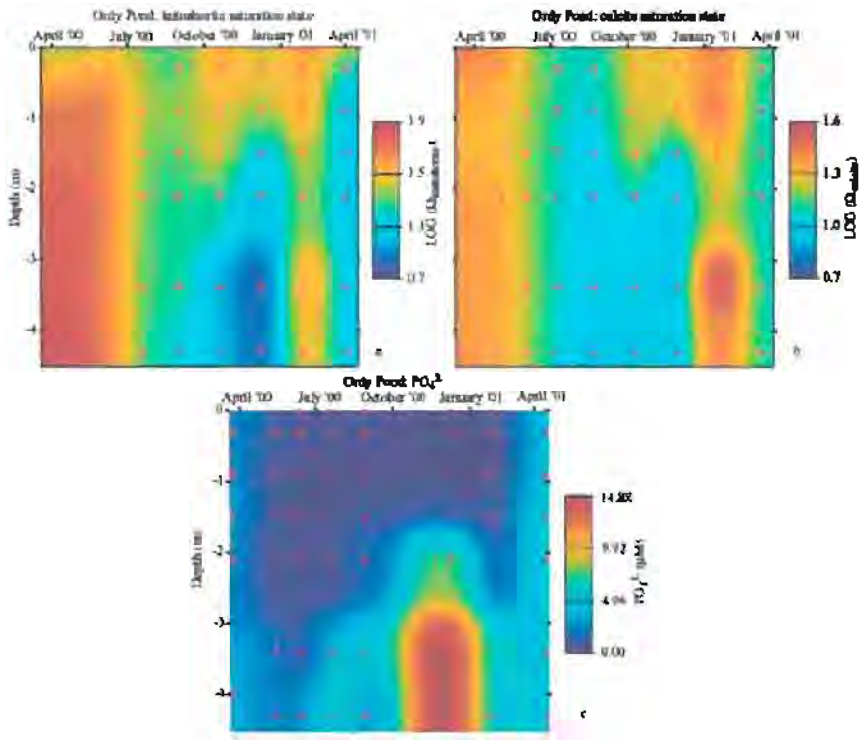

Figure 2.5. Dissolved saturation state (Ω=ionic activity product/K_{sp}) of Ordy Pond with respect to kutnahorite [$Ca(Mn,Mg)(CO_3)_2$, pK = 20.0 (Mucci, 1991)] and calcite [$CaCO_3$, pK = 8.46 (Millero et al., 1984)], and the year-long profile of PO_4^{3-}. Each sample is represented in depth and time by ○.

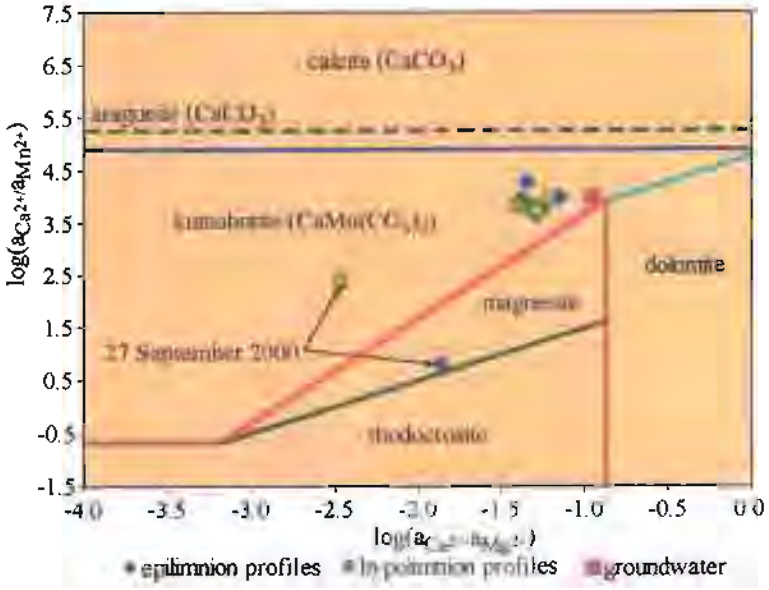

Figure 2.6. Equilibrium activity diagram representing the system CaO-MnO-MgO-CO_2 at 25° C and 1 atm pressure. CO_2 is considered to be ubiquitous and controlled outside the system. The equations used to construct the carbonate mineral stability fields are listed in Table 2.5, where: $5.709\log(K) = \Delta G_r^{\circ}$ (kJ mol^{-1}) (Morse and Mackenzie, 1990). Standard Gibbs free energy data (ΔG_f) are listed in Table 2.6. The average free ion activities in the epilimnion (0 – 0.9 m), hypolimnion (0.9 – 4.3 m), and groundwater in Ordy Pond between March 2000 and 2001 are also plotted. Free ion activities were calculated from analytical data with EQ3NR (Wolery, 1992).

TABLE 2.5. Equations used for Figure 2.6

calcite-kutnahorite $2CaCO_3 + Mn^{2+} = Ca(Mn)(CO_3)_2 + Ca^{2+}$ $\log(a_{Ca2+}/a_{Mn2+}) = \log K$	(6) K = 4.887	kutnahorite-dolomite $CaMn(CO_3)_2 + Mg^{2+} = CaMn(CO_3)_2 + Mn^{2+}$ $\log(a_{Ca2+}/a_{Mn2+}) = \log(a_{Ca2+}/a_{Mg2+}) - \log K$	(11) K = -4.782
calcite-dolomite $2CaCO_3 + Mg^{2+} = CaMg(CO_3)_2 + Ca^{2+}$ $\log(a_{Ca2+}/a_{Mn2+}) = \log K$	(7) K = 0.105	kutnahorite-magnesite $CaMn(CO_3)_2 + 2Mg^{2+} = 2MgCO_3 + Ca^{2+} + Mn^{2+}$ $\log(a_{Ca2+}/a_{Mn2+}) = 2\log(a_{Ca2+}/a_{Mg2+}) - \log K$	(12) K = -5.658
aragonite-kutnahorite $2CaCO_3 + Mn^{2+} = Ca(Mn)(CO_3)_2 + Ca^{2+}$ $\log(a_{Ca2+}/a_{Mn2+}) = \log K$	(8) K = 5.272	dolomite-magnesite $CaMg(CO_3)_2 + Mg^{2+} = 2MgCO_3 + Ca^{2+}$ $\log(a_{Ca2+}/a_{Mg2+}) = \log K$	(13) K = -0.876
rhodocrosite-kutnahorite $2MnCO_3 + Ca^{2+} = CaMn(CO_3)_2 + Mn^{2+}$ $\log(a_{Ca2+}/a_{Mn2+}) = -\log K$	(9) K = 0.683	dolomite-rhodocrosite $CaMg(CO_3)_2 + 2Mn^{2+} = 2MnCO_3 + Ca^{2+} + Mg^{2+}$ $\log(a_{Ca2+}/a_{Mn2+}) = 2\log(a_{Ca2+}/a_{Mg2+}) + \log K$	(14) K = -75.495
rhodocrosite-magnesite $MnCO_3 + Mg^{2+} = MgCO_3 + Mn^{2+}$ $\log(a_{Ca2+}/a_{Mn2+}) = \log(a_{Ca2+}/a_{Mg2+}) - \log K$	(10) K = -2.487		

It should be noted that the thermodynamic data available are for Mg-free kutnahorite (Mucci, 1991), but field studies have found that kutnahorite can contain as much as 1:1 Mg^{2+} to Mn^{2+} (Frondel and Bauer, 1955). Dissolved Mg^{2+} was abundant in the pond, and the total dissolved Mg^{2+}:Ca^{2+} ratio averaged 17:1 during the study. Therefore it can be expected that the Kutnahorite particles contained some Mg^{2+}, especially since the calcite particles averaged 5.2 mol% Mg^{2+} (Table 2.1). Depending on what the ΔG_f is for a Mg-bearing kutnahorite, the ΔG_r for a Mg-calcite – Mg-kutnahorite reaction may be greater than for Mg-free phases because Mg^{2+} has a lower ΔG_f than Mn^{2+} (Table 2.6). A greater ΔG_r would reduce the $K_{calcite\text{-}kutnahorite}$ value and shrink the kutnahorite stability field in Figure 2.6. If this was the case, the kutnahorite particulates that formed in Ordy Pond could be metastable with respect to both calcite and aragonite. If kutnahorite is a metastable phase, its absence in the sediments beneath the pond could be explained by recrystallization of kutnahorite in the sediments.

TABLE 2.6. Standard Gibbs free energies of formation of mineral and aqueous species shown in Figure 2.6

mineral or species	ΔG_f (KJ mol^{-1})	Source
calcite ($CaCO_3$)	-1129.90	1
aragonite ($CaCO_3$)	-1128.80	2
magnesite ($MgCO_3$)	-1029.00	3
rhodocrosite $MnCO_3$)	-816.00	4
kutnahorite ($CaMn(CO_3)_2$)	-1961.80	5
dolomite ($CaMg(CO_3)_2$)	-2161.70	4
Magnesian Calcite ($Ca_{0.85}Mg_{0.15}(CO_3)$)	-1114.5	6
Ca^{2+}	-553.50	4
Mn^{2+}	-227.60	4
Mg^{2+}	-454.80	4
CO_3^{2-}	-527.90	4

(1) Christ and Hostetler, 1970; (2) Morse et al., 1980; (3) Garrels et al., 1960; (4) Robie et al., 1979; (5) Mucci, 1991; (6) Bischoff et al., 1987

Two carbonate mineral phases that were not found in the particulate samples were aragonite and high magnesium calcite (HMC; Mg mol% = 12-19%; James and Choquette, 1983; Morse and Mackenzie, 1990), the two most common carbonate mineral phases in modern marine environments. Aragonite was found in the uppermost sediments beneath the pond in approximately the same percentage as kutnahorite in the particulate samples.

It is believed that the Mg:Ca ratio of marine waters is at least partially responsible for the inhibition of LMC precipitation, thus allowing metastable aragonite and HMC to form instead (James and Choquette, 1983). The aragonite and HMC mineral structures can accommodate Mg^{2+}, but the LMC crystal structure seems to be poisoned when Mg^{2+} is overly abundant (Morse and Mackenzie, 1990; Tucker and Wright, 1990). However, the Mg:Ca ratio in the modern ocean is 5.2 (Nozaki, 2001), while in Ordy Pond Mg:Ca ranged between 14 and 20 (Chapter I). Thus, the lack of particulate aragonite or HMC in the pond cannot be explained by a low Mg:Ca ratio. Aragonite precipitation over calcite has also been attributed to higher solution ionic strength (Anadon et al., 1998). The ionic strength measured in Ordy Pond never exceeded 0.5 (based on data from Chapter I), while sea water is typically around 0.7 (Morse and Mackenzie, 1990). Inhibition of LMC by Mg^{2+} may require a higher total ionic activity in the solution than was measured in Ordy Pond during this study. Furthermore, as mentioned earlier, both PO_4^{3-} and dissolved organic matter can reduce carbonate mineral precipitation rates. LMC formation is favored over aragonite and HMC at lower precipitation rates, even at elevated Mg:Ca ratios (Tucker and Wright, 1990), which may explain the lack or aragonite and HMC in the particulate samples.

2.4.3. Inorganic particulate carbonate carbon isotopic ratios ($\delta^{13}C_{carb}$)

Inorganic sedimentary $\delta^{13}C$ can be an effective geochemical proxy for studying relative changes over time in the level of phytoplankton primary productivity in an aquatic system. If Ordy Pond is truly a closed basin, then carbonate $\delta^{13}C$ and authigenic $\delta^{13}C_{carb}$ are controlled primarily by $\delta^{13}C$ of the dissolved CO_2 ($\delta^{13}C_{CO2(aq)}$), which in turn is controlled by biologic activity (Hollander and McKenzie, 1991; Rau et al., 1992; Fogel and Cifuentes, 1993). The isotopic equilibrium between the solution ($\delta^{13}C_{CO2(aq)}$) and the precipitate ($\delta^{13}C_{carb}$) was tested by calculating both the $\delta^{13}C_{CO2(aq)}$ of the water and the $\delta^{13}C_{CO2(aq)}$ that would have been in equilibrium with the measured $\delta^{13}C_{carb}$ (Figure 2.7, Table 2.7). $\delta^{13}C_{CO2(aq)}$ was calculated with DIC and $\delta^{13}C_{DIC}$ by isotopic mass balance and total concentration values of HCO_3^-, CO_3^{2-}, and $CO_{2(aq)}$. Dissolved carbon species concentrations were calculated with EQ3NR version 7.2c (Wolery, 1992). An extended Debye-Hückel model was employed with the activity coefficient equation of (Davies, 1962):

$$\log \gamma_i = -Az_i^2 (I/(1+(I) +0.2I) \qquad (16)$$

where γ_i is the ionic activity coefficient of the i-th aqueous solution species, A is the temperature dependent Debye-Hückel constant (0.5115 @ 25° C, 0.5161 @ 30° C), z_i is the ionic charge balance of the i-th species, and I is the ionic strength of the solution. A modification of the temperature-dependent equation for calcite-$CO_{2(aq)}$ carbon isotope fractionation (ε_{cl-CO2}) was used to calculate $\delta^{13}C_{CO2(aq)}$ that would have been in equilibrium with the measured $\delta^{13}C_{carb}$ (Romanek et al., 1992):

$$\varepsilon_{cl-CO2(aq)} = 10.98\ (\pm 0.13) - 0.12(\pm 0.01) \cdot T\ (^\circ C) \qquad (15)$$

The Romanek et al. (1992) experiments measured the fractionation of ^{13}C between calcite and CO_2 gas ($\varepsilon_{cl\text{-}CO_{2(g)}}$). To calculate the fractionation between calcite and dissolved CO_2 ($\varepsilon_{cl\text{-}CO_{2(aq)}}$), Eq. (15) adds +1‰ to the Romanek et al. (1992) equation to account for fractionation during CO_2 dissolution.

The quality of the $\delta^{13}C_{CO_{2(aq)}}$ data was evaluated by recalculating $\delta^{13}C_{CO_{2(aq)}}$ using CO2SYS (Lewis and Wallace, 1998) with the dissolved carbon speciation Ksp values of Roy et al. (1993). These results were compared with the EQ3NR data, and the two $\delta^{13}C_{CO_{2(aq)}}$ calculations were nearly identical. A linear correlation of the CO2SYS data against the EQ3NR data has a slope of 0.957 and an R^2 value of 0.9971 (n = 50).

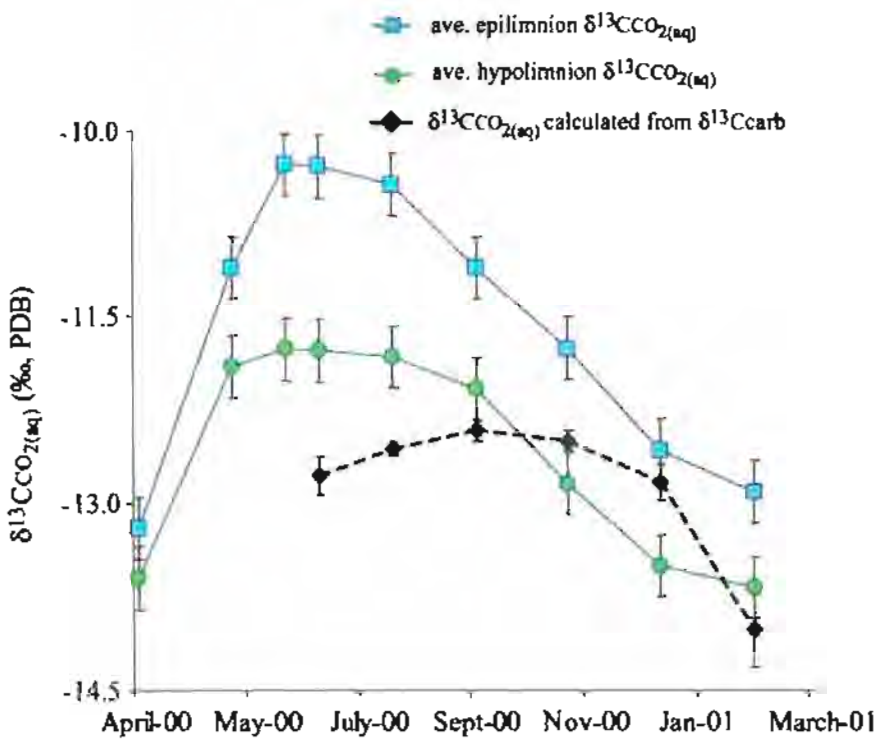

Figure 2.7. Profiles of $\delta^{13}C_{carb}$ and $\delta^{13}C_{CO_{2(aq)}}$ calculated for the epilimnion (0 – 0.9 m) and hypolimnion (0.9 – 4.3 m) with EQ3NR, Eq. (15), and water column DIC and $\delta^{13}C_{DIC}$ measurements

TABLE 2.7. $\delta^{13}C_{CO2(aq)}$ calculated from DIC and $\delta^{13}C_{DIC}$, and the equilibrium $\delta^{13}C_{CO2(aq)}$ calculated from $\delta^{13}C_{carb}$

Sample	$\delta^{13}C_{CO2(aq)}$ (V-PDB) calculated from DIC and $\delta^{13}C_{DIC}$							ave. epilimnion $\delta^{13}C_{CO2(aq)}$ (V-PDB)	ave. hypolimnion $\delta^{13}C_{CO2(aq)}$ (V-PDB)	$\delta^{13}C_{CO2(aq)}$ (V-PDB) calculated from $\delta^{13}C_{carb}$
	0 m	0.3 m	0.9 m	1.5 m	2.1 m	3.4 m	4.3 m	(0 – 0.9 m)	(0.9 - 4.3 m)	
4/4/2000	-13.0	-13.2	-13.4	-13.8	-13.9	NS	-13.3	-13.2	-13.6	
5/24/2000	-10.8	-11.0	-11.5	-11.8	-11.7	NS	-12.6	-11.1	-11.9	
6/21/2000	-10.1	-10.1	-10.6	-11.2	-11.7	-13.0	-12.3	-10.3	-11.8	
7/9/2000	-10.1	-10.1	-10.7	-11.3	-11.6	-13.0	-12.4	-10.3	-11.8	-12.8
8/17/2000	-10.8	-9.8	-10.7	-11.6	-11.4	-12.5	-12.9	-10.4	-11.8	-12.6
10/1/2000	-11.3	-10.5	-11.5	-11.6	-11.3	-12.5	-13.5	-11.1	-12.1	-12.4
11/19/2000	-11.8	-11.7	-11.9	-12.2	-12.4	-14.1	-13.8	-11.8	-12.8	-12.5
1/7/2001	-12.5	-12.1	-13.2	-13.3	-13.5	-13.9	-13.8	-12.6	-13.5	-12.8
2/25/2001	-12.6	-12.0	-14.1	-13.5	-13.5	-13.6	NS	-12.9	-13.7	-14.0

NS = no sample

Therefore, the carbonate particulates in Ordy Pond are in near carbon isotopic equilibrium with the surrounding water. The $\delta^{13}C_{carb}$ peak reflects the $\delta^{13}C_{CO2(aq)}$ peak in June-July (Fig. 2.7), when biogenic CO_2 uptake had enriched the DIC pool in ^{13}C. Between January and March, when POM production rates had fallen and increased microbial POM remineralization had depleted the DIC pool of ^{13}C, $\delta^{13}C_{carb}$ followed the return of $\delta^{13}C_{CO2(aq)}$ to pre-summer levels. Although the overlap between the hypolimnion $\delta^{13}C_{CO2(aq)}$ data and the particulate data seems to indicate that the carbonate particles formed in the deeper waters of the pond, changes water chemistry had indicated that mineral precipitation occurred in the epilimnion (Chapter I). However, Eq. (15) was computed for calcite alone, and there are no published data describing $\delta^{13}C$ fractionation during kutnahorite precipitation. By comparison, Romanek (1992) also found that $\delta^{13}C$ fractionation during aragonite precipitation was ~ +2‰ greater than for calcite. Thus, the 3‰ difference between the carbonate particulates and the surface waters in Figure 2.7 does not seem unreasonable.

The time lag between the peaks of the particulate ^{13}C and water ^{13}C trends can be explained by the difference in the time over which each chemical signal was integrated. The $\delta^{13}C_{DIC}$ analysis is a nearly instantaneous measurement of the ^{13}C:^{12}C ratio in the water; changes in biologic activity are translated to $\delta^{13}C_{DIC}$ on a scale of minutes to hours. The sediment traps, however, not only collected material that formed during the 7 weeks that they were deployed, but they also collected material that precipitated before deployment and had not yet settled. Thus, when the DIC analyses recorded a drop in $\delta^{13}C_{CO2(aq)}$ beginning in October, the sediment traps already contained material from early September that was isotopically more enriched in ^{13}C. It was not until the traps were emptied and redeployed in late October that a change in $\delta^{13}C_{carb}$ was observed.

2.4.4. Inorganic particulate carbonate oxygen isotopic ratios ($\delta^{18}O_{carb}$)

Carbonate mineral $\delta^{18}O$ is a function of both the reaction temperature and the water's $H_2{}^{18}O$:$H_2{}^{16}O$ balance, and it should serve as a proxy for changes in the physical nature of the pond over time (Talbot and Kelts, 1990). To evaluate the particulates' isotopic behavior, the water's $\delta^{18}O$ ($\delta^{18}O_{H2O}$) was calculated using the particulate $\delta^{18}O_{carb}$ and the temperature dependent equation for the calcite-water fractionation factor ($\alpha_{cl\text{-}water}$) of Kim and O'Neil (1997):

$$\alpha_{cl\text{-}water} = (R^{16}O_{cl}/R^{18}O_{cl})/(R^{16}O_{H2O}/R^{18}O_{H2O}) \quad (17)$$

$$\varepsilon_{cl\text{-}H2O} = 1000\ln\alpha_{cl\text{-}H2O} = 18.03(10^3 T(K)^{-1}) - 32.42 \quad (18)$$

Equation (18) was calculated for $\delta^{18}O_{H2O}$ relative to Vienna Standard Marine Ocean Water (VSMOW), and the $\delta^{18}O_{H2O}$ calculated here is also relative to VSMOW. Equation (18) removes the temperature effect and allows examination of $\delta^{18}O_{H2O}$ as a function of $H_2{}^{18}O$:$H_2{}^{16}O$. However, Eq. (18) is for pure calcite, and the isotopic fractionation associated with kutnahorite precipitation is not known. Since Ordy Pond doesn't experience ice formation (and presumably never did during the Holocene), it is assumed that the $H_2{}^{18}O$:$H_2{}^{16}O$ ratio of the pond is a function of precipitation input, evaporative output, and groundwater exchange. Salinity and $\delta^{18}O_{H2O}$ peaked together in the summer when temperatures were high and rainfall low (Fig. 2.8), indicating that the pond was experiencing net water loss due to evaporation. Once rainfall increased and temperatures fell, both salinity and $\delta^{18}O_{H2O}$ values dropped with the influx of fresher waters more depleted in $\delta^{18}O_{H2O}$. Carbonate $\delta^{18}O$ lagged behind salinity by one sampling period, as was observed in $\delta^{13}C_{carb}$, because the sample traps collected particulates over a period of weeks while salinity and temperature measurements were instantaneous.

The ^{18}O isotopic fractionation effect of temperature during carbonate particulate crystallization can be evaluated with Eq. (18) if $\delta^{18}O_{H2O}$ is kept constant. The 4.4° C drop in water temperature measured between July and March, would have resulted in an increase in calcite $\delta^{18}O$ of +0.9‰; the effect on kutnahorite-$\delta^{18}O$ is not known, but it would increase. The temperature effect on $\delta^{18}O_{carb}$ was opposite to, but overwhelmed by, the changes due to the $H_2{}^{18}O$:$H_2{}^{16}O$ balance. Thus, the sediment $\delta^{18}O_{carb}$ record should trace the water balance history of Ordy Pond, baring diagenetic alteration.

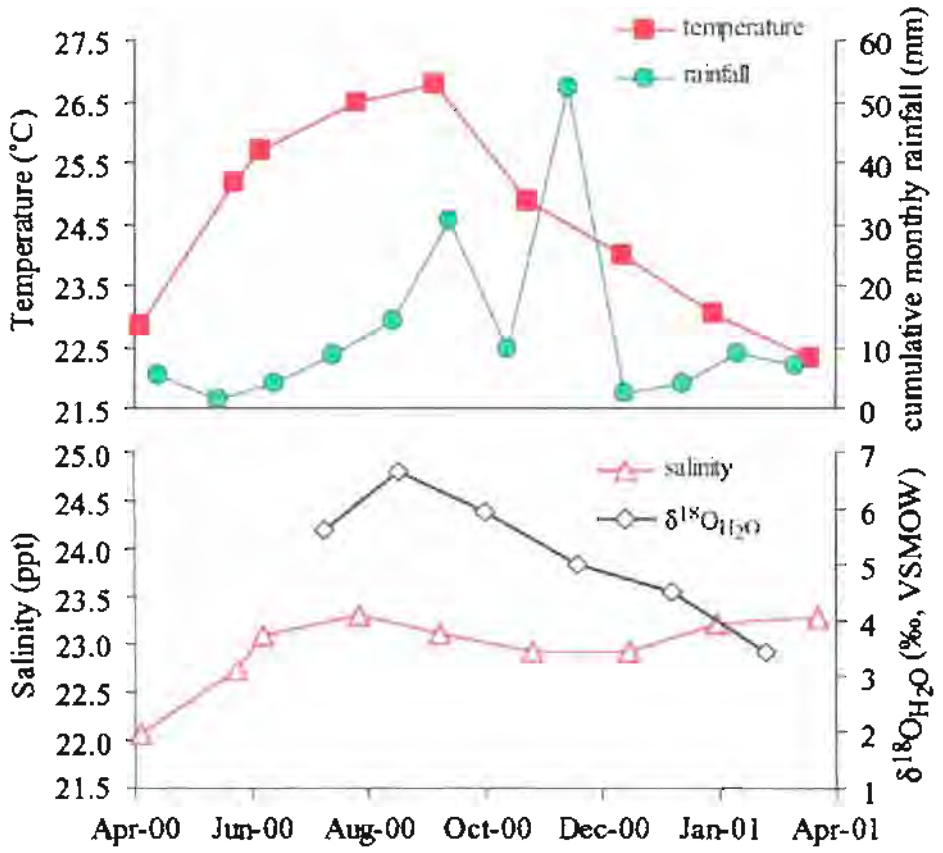

Figure 2.8. Upper panel: Average water temperature in Ordy Pond and rainfall at the BPNAS in Kalaeloa (NOAA National Climatic Data Center)
Lower panel: average pond salinity and $\delta^{18}O_{H2O}$ calculated from $\delta^{18}O_{carb}$

2.4.5. Organic particulate bulk nitrogen isotopic ratios ($\delta^{15}N_{POM}$)

The use of nitrogen isotopes to infer paleoenvironmental conditions is becoming common (Gu et al., 1996; Hodell and Schelske, 1998; Teranes and Bernasconi, 2000; Herczeg et al., 2001; Schubert et al., 2001), although the factors controlling $\delta^{15}N$ in dissolved inorganic nitrogen (DIN) and POM are not as well understood as $\delta^{13}C$ or $\delta^{18}O$. Caution must therefore be taken when interpreting the drop in $\delta^{15}N_{POM}$ observed over the time-series (Fig. 2.9). Phytoplankton preferentially uptake ^{14}N over ^{15}N, and if biogenic uptake exceeds supply, the residual DIN pool will become isotopically more enriched (Fogel and Cifuentes, 1993; Schubert et al., 2001). Consequently, during such periods phytoplankton can also become more enriched in ^{15}N (Goericke et al., 1994; Teranes and Bernasconi, 2000). However, since NH_4^+ was the main source of DIN in Ordy Pond waters (Chapter I), ammonium volatilization must also be considered. At the pond's pH (8.1 – 8.4), the concentration of $NH_{3(aq)}$ is about 1% that of dissolved NH_4^+ ($NH_{3(aq)}$ – NH_4^+ K_{sp} = 9.5). When $NH_{3(aq)}$ volatilizes, the fractionation effect is 25-35‰ (AIR; Delwiche and Steyn, 1970; Estep and Vigg, 1985; Macko et al., 1987; Cifuentes et al., 1989; Velinsky et al., 1989). More $NH_{3(aq)}$ would have been lost in the summer when water temperatures were 5° C higher. We cannot quantify how much NH_3 was actually lost, nor the expected isotopic effect, because wind speeds and air temperatures were not measured directly over the pond's surface. Elevated summer $\delta^{15}N_{POM}$ values are consistent with increased $NH_{3(aq)}$ volatilization. Fractionation of ^{15}N during NH_4^+ assimilation has been measured to range between -3 and -27‰ in laboratory cultures (Wada, 1980; Macko et al., 1987; Hoch et al., 1992), but field studies found fractionations to be more on the order of ~ -10‰ (Estep and Vigg, 1985; Cifuentes et al.,

1988). Ammonium-$\delta^{15}N$ in Ordy Pond could, therefore, have ranged between +14 and +40‰ (AIR) during the course of this study.

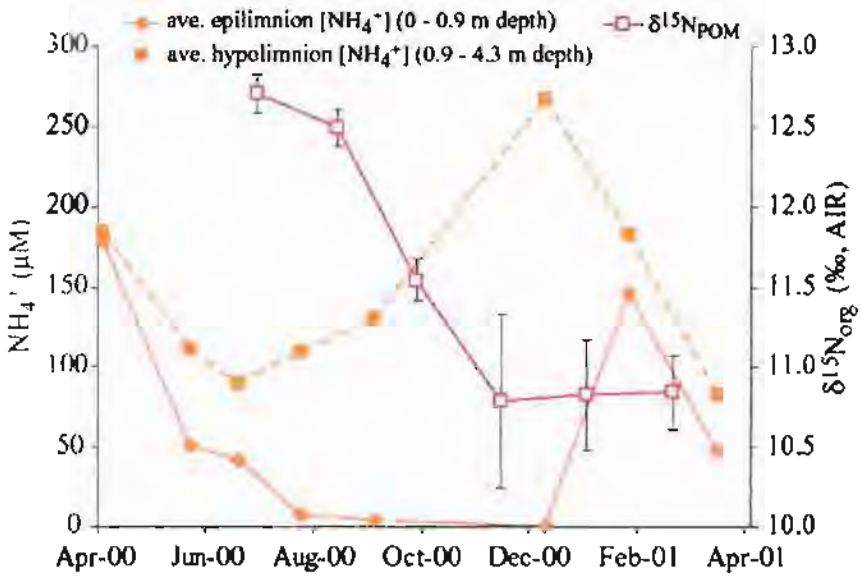

Figure 2.9. $\delta^{15}N_{POM}$ and average values of NH_4^+ in the surface water (0 – 0.9 m) and bottom water (0.9 – 4.3 m) over time.

The drop in $\delta^{15}N_{POM}$ between August and December may have been due in part to an increased supply of remineralized NH_4^+ from the bottom of the pond (Fig. 2.9). Microbial remineralization tends to favor ^{14}N-rich organic compounds such as amino acids (Macko et al., 1993). The absence of an increase in early winter epilimnion [NH_4^+] (Fig. 2.9) presumably indicates that phytoplankton were consuming NH_4^+ as quickly as it is was made available. The TIN:TIP ratio in December was below the 16:1 Redfield Ratio (Chapter I), and nitrogen could have been a limiting nutrient. When the pond became more mixed in January, surface water [NH_4^+] rose and the TIN:TIP ratio exceeded 16:1 (Chapter I). By that time, $\delta^{15}N_{POM}$ had leveled off, presumably indicating that isotopic equilibrium had been reached between NH_4^+ supply and biogenic uptake.

A third factor that could have affected $\delta^{15}N_{POM}$ in Ordy Pond is a shift in

community structure. Zooplankton would increase the bulk $\delta^{15}N_{POM}$ (DeNiro and Epstein, 1978), although no zooplankton were observed in the samples. There also could have been a shift to cyanobacterial $N_{2(aq)}$ fixation between July and January when TIN:TIP was below 16:1. There is little fractionation associated with the biologic assimilation of atmospheric N_2, which, by definition, has a $\delta^{15}N$ of 0‰ (Fogel and Cifuentes, 1993). The 1.9‰ drop in $\delta^{15}N_{POM}$ between July and January would require a cyanobacterial organic matter contribution of only 15%.

2.4.6. Organic particulate bulk carbon isotopic ratios ($\delta^{13}C_{POM}$)

The fractionation of ^{13}C between $CO_{2(aq)}$ and POM during photosynthesis (ε_p) is believed to be controlled primarily by the ratio of cellular carbon demand to carbon supply, cell size and shape, and community structure (Laws et al., 1995). The average full fractionation during carbon fixation in marine eukaryotic algae by the enzymes Ribulose 1,5-biphosphate carboxylase (RUBISCO) and PEP-carboxykinase (PEPCK) is ~25‰ (Arnellez and O'Leary, 1992; Popp et al., 1998; Elzenga et al., 2000). As Figure 2.10a shows, however, ε_p in Ordy Pond ranged between +12.8 and +17.1‰, which is 7-16‰ greater than would be expected for full photosynthetic fractionation. Thus, an understanding of what may control ε_p is needed to evaluate organic $\delta^{13}C$ as a paleoenvironmental signal.

As phytoplankton growth reduces the size of the ambient DIC pool, phytoplankton may become less isotopically discriminatory (Hollander and McKenzie, 1991; Rau et al., 1992). If $\delta^{13}C$ fractionation is affected by carbon availability, there should be a positive correlation between the concentration of $CO_{2(aq)}$ and ε_p. This was not the case in Ordy Pond as ε_p decreased as $CO_{2(aq)}$ became more concentrated (Fig. 2.10a & b). However, the effect of $[CO_{2(aq)}]$ on ε_p can be counteracted by changes in growth rate (μ); as μ increases, ε_p will fall if $[CO_{2(aq)}]$ remains constant (Laws et al., 1995; Cassar et

al., 2002). Thus, μ would have to have been greater in the winter than in the summer in Ordy Pond, which does not seem likely since winter was a time of increased mixing and reduced light availability for phytoplankton.

Phytoplankton can also become more enriched in ^{13}C when HCO_3^- is utilized instead of $CO_{2(aq)}$, because bicarbonate $\delta^{13}C$ is normally ~8‰ greater than $\delta^{13}C_{CO2(aq)}$ (Fogel and Cifuentes, 1993). Bicarbonate is an inefficient carbon source relative to $CO_{2(aq)}$, and HCO_3^- uptake normally occurs when phytoplankton growth becomes carbon limited (Burkhardt et al., 2001; Cassar et al., 2002). Hollander and Mackenzie (1991), for example, inferred HCO_3^- uptake when $CO_{2(aq)}$ concentrations fell below 10 μmol L^{-1}. In Ordy Pond, $[CO_{2(aq)}]$ fell below 10 μmol L^{-1} only once during late summer when $\delta^{13}C_{POM}$ was relatively depleted; between December and March $[CO_{2(aq)}]$ averaged 35 μmol L^{-1} (Chapter I). Moreover, the ratios of $CO_{2(aq)}$ to both dissolved inorganic nitrogen (DIN) and dissolved inorganic phosphorus (DIP) increased as ε_P fell (Fig. 2.10c). Thus, it does not seem likely that phytoplankton would need to assimilate HCO_3^- in the winter when $CO_{2(aq)}$ had become more abundant relative to other nutrients.

Cell geometry can also have a significant affect on ε_p. Larger phytoplankton with lower surface to volume ratios, e.g., *Porosira glacialis*, have an ε_p more dependent on $\mu/[CO_{2(aq)}]$ than those with larger surface area to volume ratios., e.g., *Phaeodactylum tricornutum* (Popp et al., 1998). However, species specific biologic surveys have not been made of the microbial community in Ordy Pond. Without knowledge of the cell geometry or species present, it is impossible to judge their potential effect on ε_p. The cyanobacterium *Synechococcus*, for example, has an ε_p that is insensitive to $\mu/[CO_{2(aq)}]$ and which is 7‰ greater than typical eukaryotic marine algae (Popp et al., 1998).

Finally, the 4‰ increase in ε_p in Ordy Pond between summer and winter could have resulted from an increase in the relative number prokaryotic organisms, specifically

anaerobic photosynthetic and chemosynthetic bacteria. Winter was a time of greater anoxia (Chapter I) which tends to favor anaerobic autotrophic bacteria (Atlas and Bartha, 1993). Instead of the Calvin cycle, common to aerobic photosynthesizing organisms, many aerobic photosynthetic bacteria use the reductive TCA pathway (or reverse Krebs cycle) to fix CO_2. The reductive TCA pathway discriminates less against ^{13}C than the Calvin cycle, and ε_p is around -10‰ (Sirevag, 1995; Tabita, 1995).

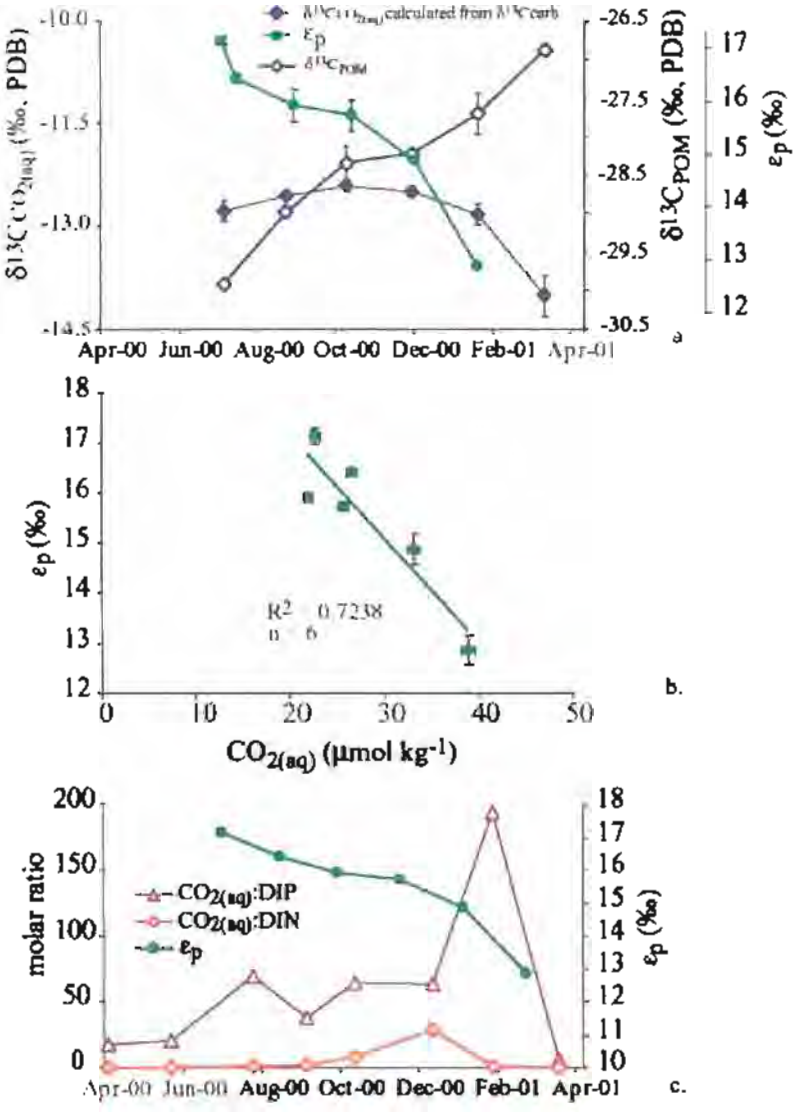

Figure 2.10. (a) $\delta^{13}C_{CO2(aq)}$, $\delta^{13}C_{POM}$, and ε_p over time.; (b) ε_p vs. surface water $[CO_{2(aq)}]$; (c) $\delta^{13}C_{POM}$ vs. $\delta^{13}C_{CO2(aq)}$ calculated from particulate $\delta^{13}C_{carb}$

2.5. CONCLUSIONS

Ordy Pond is a complex biogeochemical system that shows a significant seasonal variation due to the onset and decline of thermal stratification. Summer stratification appears to have triggered increased phytoplankton productivity, which impacted other geochemical signals such as a doubling of the inorganic carbonate particle flux. The suboxic to anoxic nature of the water column, maintained by microbial oxidation of POM, lead to the precipitation of both low Mg calcite and kutnahorite, a Mn-bearing dolomite isotype. Kutnahorite may be a metastable phase because it is not present in the sediments beneath the pond. Particulate $\delta^{18}O_{carb}$ was controlled by the pond's seasonal water balance which overwhelmed the effects of temperature. During the summer $\delta^{18}O_{carb}$ was high because the pond was affected by evaporation. During the winter $\delta^{18}O_{carb}$ decreased as waters depleted in ^{18}O relative to the pond were added by rainfall and groundwater seepage. Particulate $\delta^{13}C_{carb}$ was higher in the summer due to increased phytoplankton DIC uptake and lower in the winter due to elevated microbial organic matter remineralization. The $\delta^{15}N_{POM}$ was also highest in the summer and lowest in the winter, and it appears to have been controlled by the balance between microbially remineralized NH_4^+ versus $NH_{3(aq)}$ volatilization and/or preferential phytoplankton uptake of $^{14}NH_4^+$. Finally, particulate $\delta^{13}C_{POM}$ and ε_p may have been controlled by a number of factors including changes in growth rate (μ), HCO_3^- uptake over $CO_{2(aq)}$, and community structure. Without more information on the biologic communities present or measurements of phytoplankton growth rates over time, the specific controls on ε_p cannot be identified. However, the fact that ε_p fell as the water column became more reduced may support the hypothesis that ε_p shifted as a result of increased photo- and chemosynthetic anaerobic bacteria abundance. In conclusion, the particulate geochemistry in Ordy Pond reflected the seasonal changes in the aquatic biogeochemistry

of the water column. These results indicate that the laminae in the sediments beneath the pond are seasonal deposits, and that dark-light laminae couplets are varves. In Chapter III, the modern particulate data will be applied to the sediment record in conjunction with modern water data to interpret the Holocene environmental history of the area.

2.6. ACKNOWLEDGEMENTS

Many thanks go out to everyone who assisted with this project, especially Lauren Rogers who helped with the stable isotopic analyses of the sediment trap samples as part of the NSF Research Experience for Undergraduates program at the University of Hawai'i under the supervision of Craig Glenn and Jane Schoonmaker. This is University of Hawai'i SOEST contribution #XXXX. Funding for this research was provided by Sigma Xi as a Grants-in-Aid award for graduate research, by the Geologic Society of America as a graduate research award, and by the William T. Coulbourn Fellowship and Harold T. Stearns Fellowship awards from the Department of Geology and Geophysics at the University of Hawai'i, Mānoa.

2.7. APPENDIX

Standard curves were fitted to two pairs of kutnahorite-to-calcite peak area ratios (Fig. 2.11) in the standards listed in Table 2.8:

kutnahorite-012/calcite-102

$$\text{kutnahorite fraction} = 0.1629\ln(\text{PAR}) + 0.5157 \qquad (19)$$

kutnahorite peak-104 peak/calcite-104

$$\text{kutnahorite fraction} = 0.1652\ln(\text{PAR}) + 0.5875 \qquad (20)$$

Although the kutnahorite-012/calcite-102 PAR data had a better curve fit, both peaks were not always present in the particulate analysis and Eq. (20) was used to calculate the data listed in Table 2.2.

The kutnahorite used in these standards came from Sterling Mine in Ogdensburg, New Jersey, through the Excalibur Mineral Company. The Iceland spar calcite used was obtained from WARD'S Natural Science Establishment, Inc.

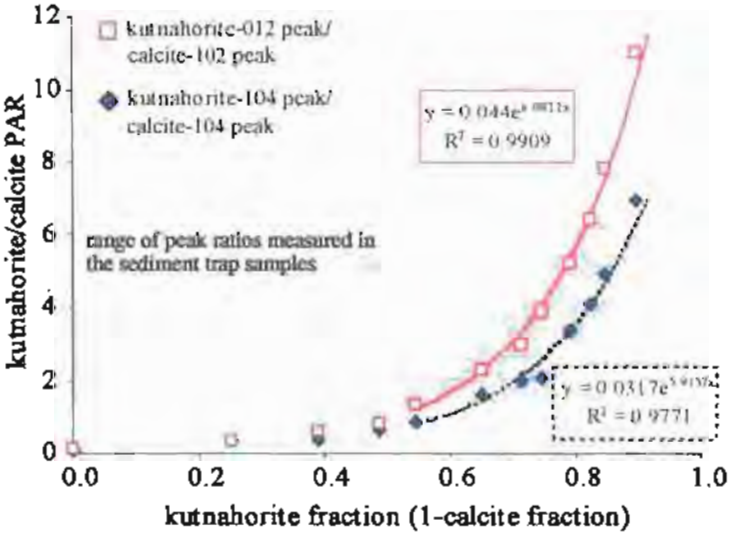

Figure 2.11. Kutnahorite/calcite PAR's vs. the kutnahorite fraction in the prepared standards listed in Table 2.8. The gray box represents the range of the PAR's measured in the particulate samples, and the standard curves are fitted only to those data within this range.

TABLE 2.8. Kutnahorite/calcite mixing curve mineral fractions, peak locations, peak areas, and kutnahorite:calcite peak area ratios (PAR)

Kutnahorite	Calcite	Kutnahorite – 012 peak			Calcite – 102 peak			K-012/C-102	Kutnahorite – 104 peak			Calcite - 104 peak			K-104/C-104
Fraction	Fraction	2Θ (°)	d(Å)	Area	2Θ (°)	d(Å)	Area	PAR	2Θ (°)	d(Å)	Area	2Θ (°)	d(Å)	Area	PAR
0.8955	0.1045	22.813	2.7336	3716	22.099	2.8473	337	11.0	29.505	2.0250	5714	29.505	2.0250	5714	6.95
0.8451	0.1549	22.811	2.7370	4437	22.102	3.8500	568	7.81	29.487	3.0291	847	29.487	3.0291	847	4.91
0.8217	0.1783	23.800	3.7391	4467	23.111	3.8481	696	6.42	29.436	3.0339	1010	29.436	3.0339	1010	4.11
0.7891	0.2109	23.810	3.7341	4640	23.107	3.8461	891	5.21	29.395	3.0361	10857	29.395	3.0361	10857	3.38
0.7440	0.2560	23.694	3.7521	4790	23.025	3.8596	1232	3.89	29.388	3.0368	18960	29.388	3.0368	18960	2.08
0.7132	0.2868	23.801	3.7355	3470	23.077	3.8510	1157	3.00	29.405	3.0351	18958	29.405	3.0351	18958	2.00
0.65	0.3500	23.706	3.7502	3232	23.063	3.8533	1405	2.30	29.389	3.0367	22342	29.389	3.0367	22342	1.59
0.5455	0.4545	23.705	3.7503	3364	23.067	3.8527	2548	1.32	29.375	3.0381	30149	29.375	3.0381	30149	0.861
0.4881	0.5119	23.695	3.7520	2051	23.047	3.8559	2544	0.806	29.390	3.0366	33994	29.390	3.0366	33994	0.628
0.3895	0.6105	23.713	3.7491	1941	23.035	3.8580	3235	0.600	29.364	3.0392	48101	29.364	3.0392	48101	0.375
0.2532	0.7468	23.696	3.7518	1091	23.028	3.8590	3000	0.364	29.389	3.0367	49603	29.389	3.0367	49603	0.359
0.0010	0.9990	23.682	3.7539	701	22.975	3.8678	4682	0.150	29.338	3.0418	64218	29.338	3.0418	64218	0.076

2.8. REFERENCES

Anadon, P., Utrilla, R., Vazquez, A. (1998). Paleohydrology of the upper Miocene Bicarb lake (eastern Spain) as inferred from stable isotopic data from inorganic carbonates: *Sedimentary Geology* **121**, 191-206.

Arnellez D. R. and O'Leary M. H. (1992) Binding of carbon dioxide to phosphoenolpyruvate carboxykinase deduced from carbon kinetic isotope effects. *Biochemistry* **31**, 4363-4368.

Athens, J.S., Tuggle, H.D., Ward, J.V., and Welch, D.J. (2002) Avifaunal extinctions, vegetation change, and Polynesian impacts in prehistoric Hawai'i: *Archeologica Oceania* **37**, 57-78.

Atlas R. M. and Bartha R. (1993) *Microbial Ecology*. The Benjamin/Cummings Publishing Company, Inc.

Bischoff J. L., Bishop F. C., and Mackenzie F. T. (1983) Biogenically produced magnesian calcite: inhomogeneities in chemical and physical properties; comparison with synthetic phases. *American Mineralogist* **68**, 1183-1188.

Bischoff J. L., Mackenzie F. T., and Bishop F. C. (1987) Stabilities of synthetic magnesian calcites in aqueous solution: Comparison with biogenic materials. *Geochimica et Cosmochimica Acta* **51**, p. 1413-1423.

Burkhardt S., Amoroso G., Riebesell U., and Sültemeyer D. (2001) CO_2 and HCO_3^- uptake by diatoms acclimated to different CO_2 concentrations. *Limnology and Oceanography* **46**(6), 1378-1391.

Cannon W. F. and Force E. R. (1983) Potential for high-grade shallow-marine manganese deposits in North America. In *Cameron Volume on Unconventional Mineral Deposits* (ed. I. Shanks, W.C), pp. 175-189. Society of Mineral Engineers.

Cassar N., Laws E. A., Popp B. N., and Bidigare R. R. (2002) Sources of inorganic carbon for photosynthesis in a strain of Phaeodactylum tricornutum. *Limnology and Oceanography* **47**(4), 1192-1197.

Christ C. L., and Hostetler P. B. (1970) Studies in the system MgO-SiO_2-CO_2-H_2O (II): The activity-product constant of magnesite. *American Journal of Science* **268**, p. 439-453.

Cifuentes, L. A., Fogel M.L., Pennock, J.R., Sharp, J.H. (1989) Biogeochemical factors that influence the stable nitrogen isotope ratio of dissolved ammonium in the Delaware estuary: *Geochimica et Cosmochimica Acta* **53**, 2713-2721.

Cifuentes L. A., Sharp J. H., and Fogel M. L. (1988) Stable carbon and nitrogen isotope biogeochemistry in the Delaware estuary. *Limnology and Oceanography* **33**(5), 1102-1115.

Davies C. W. (1962) *Ion Association*. Butterworths.

Delwiche, C.C., and Steyn, P.L. (1970) Nitrogen isotope fractionation in soils and microbial reactions. *Environmental Science and Technology* **4**, 929-935.

DeNiro M. J. and Epstein S. A. (1978) Influence of diet on the distribution of carbon isotopes in animals. *Geochimica Cosmochimica Acta* **42**, 495-506.

Downing J. A. and McCauley E. (1992) The nitrogen:phosphorus relationship in lakes. *Limnology and Oceanography* **37**(5), 936-945.

Elzenga J. T. M., Prins H. B. A., and Stefels J. (2000) The role of extracellular carbonic anhydrase activity in inorganic carbon utilization of Phaeocystis globosa

(Prymnesiophyceae): A comparison with other marine algae using the isotopic disequilibrium technique. *Limnology and Oceanography* **45**(2), 372-380.

Emiliani C. (1955) Pleistocene temperatures. *Journal of Geology* **63**, 538-578.

Epstein S., Buchsbaum R., and Lowenstam H. (1953a) Carbonate-water isotopic temperature scale. *Geological Society of America Bulletin* **62**, 417-425.

Epstein S., Buchsbaum R., Lowenstam H. A., and Urey H. C. (1953b) Revised carbonate water isotopic temperature scale. *Geological Society of America Bulletin* **64**, 1315-1326.

Estep M. L. F. and Vigg S. (1985) Stable carbon and nitrogen isotope tracers of trophic dynamics in natural populations and fisheries of the Lahontan Lake system, Nevada. *Canadian Journal of Fisheries and Aquatic Sciences* **42**(11), 1712-1719.

Fogel M. L. and Cifuentes L. A. (1993) Isotope fractionation during primary production. In *Organic Geochemistry* (ed. S. A. Macko), pp. 73-98. Plenum Press.

Frondel C. and Bauer L. H. (1955) Kutnahorite: a manganese dolomite, $CaMn(CO_3)_2$. *American Mineralogist* **40**, 748-760.

Garrels R. M., Thompson M. E., and Siever R. (1960) Stability of some carbonates at 25°C and one atmosphere total pressure. *American Journal of Science* **258**, p. 402-418.

Glenn C. R. and Kelts K. (1991) Sedimentary Rhythms in Lake Deposits. In *Cycles and Events in Stratigraphy* (ed. A. Seilacher), pp. 188-221. Springer-Verlag.

Goericke R., Montoya J. P., and Fry B. (1994) Physiology of isotopic fractionation in algae and cyanobacteria. In *Stable Isotopes in Ecology and Environmental Science* (ed. R. H. Michener), pp. 187-221. Blackwell Scientific Publications.

Gu B., Schelske C. L., and Brenner M. (1996) Relationship between sediment and plankton isotope ratios (d13C and d15N) and primary productivity in Florida lakes. *Canadian Journal of Fisheries and Aquatic Sciences* **53**, 875-883.

Herczeg A. L., Smith A. K., and Dighton J. C. (2001) A 120 year record of changes in nitrogen and carbon cycling in Lake Alexandrina, South Australia: C:N, d15N and d13C in sediments. *Applied Geochemistry* **16**, 73-84.

Hoch M. P., Fogel M. L., and Kirchman D. L. (1992) Isotope fractionation associated with ammonium uptake by a marine bacterium. *Limnology and Oceanography* **37**(7), 1447-1459.

Hodell D. A. and Schelske C. L. (1998) Production, sedimentation, and isotopic composition of organic matter in Lake Ontario. *Limnology and Oceanography* **43**(2), 200-214.

Hodell D. A., Schelske C. L., Fahnenstiel G. L., and Robbins L. L. (1998) Biologically induced calcite and its isotopic composition in Lake Ontario. *Limnology and Oceanography* **43**(2), 187-199.

Hollander D. J. and McKenzie J. A. (1991) CO_2 control on carbon-isotope fractionation during aqueous photosynthesis: A paleo-pCO_2 barometer. *Geology* **19**, 929-932.

Hollander D. J., McKenzie J. A., and ten Haven H. L. (1992) A 200 year sedimentary record of progressive eutrophication in Lake Greifen (Switzerland): Implications for the origin of organic-carbon-rich sediments. *Geology* **20**, 825-828.

Huckenridge H. and Meischner D. (1996) Origin and environment of manganese-rich sediments within black-shale basins. *Geochimica et Cosmochimica Acta* **60**(8), 1399-1413.

James, N.P., and Choquette, P.W. (1983) Diagenesis 5. Limestones: Introduction: *Geoscience Canada*, v. 10, p. 159-161.

Kelts K. and Hsu K. J. (1978) Freshwater carbonate sedimentation. In *Lakes: Chemistry, Geology, Physics* (ed. A. Lerman), pp. 295-323. Springer-Verlag.

Kim S.-T. and O'Neil J. R. (1997) Equilibrium and nonequilibrium oxygen isotope effects in synthetic carbonates. *Geochimica et Cosmochimica Acta* **61**(16), 3461-3475.

Ku T.-L., Kimmel M. A., Easton W. H., and O'Neil T. J. (1974) Eustatic sea level 120,000 years ago on Oahu, Hawaii. *Science* **183**, 95a.

Laws E. A., Popp B. N., Bidigare R. R., Kennicutt M. C., and Macko S. A. (1995) Dependence of phytoplankton carbon isotopic composition on growth rate and [CO2]aq: Theoretical considerations and experimental results. *Geochimica et Cosmochimica Acta* **59**(6), 1131-1138.

Lewis E. and Wallace D. W. R. (1998) *Program Developed for CO2 System Calculations.* Carbon Dioxide Information Analysis Center, Oak Ridge National Laboratory, U.S. Department of Energy.

Macko S. A., Engel M. H., and Parker P. L. (1993) Early diagenesis of organic matter in sediments. In *Organic Geochemistry* (ed. S. A. Macko), pp. 211-224. Plenum Press.

Macko S. A., Fogel E., Mare M., and Hoering T. C. (1987) Isotopic fractionation of nitrogen and carbon in the synthesis of amino acids by microorganisms. *Chemical Geology; Isotope Geoscience Section* **65**(1), 79-92.

McCrea J. M. (1950) On the isotopic chemistry of carbonates and a paleotemperature scale. *Journal of Chemical Physics* **18**(849-857).

Menzel D. W. and Ryther J. H. (1964) The composition of particulate organic matter in the western North Atlantic. *Limnology and Oceanography* **9**(2), 179-186.

Meyers P. A. (1994) Preservation of elemental and isotopic source identification of sedimentary organic matter. *Chemical Geology* **114**, 289-302.

Morse J. W. and Mackenzie F. T. (1990) *Geochemistry of Sedimentary Carbonates*. Elsevier Scientific Publication Company.

Morse J. W., Mucci A., and Millero F. J. (1980) The solubility of calcite and aragonite in seawater of 35‰ salinity and one atmospheric pressure. *Geochimica et Cosmochimica Acta* **44**, p. 85-94.

Mucci A. (1991) The solubility and free energy of formation of natural kutnahorite. *Canadian Mineralogist* **29**, 113-121.

Muhs D. R. and Szabo B. J. (1991) New uranium-series ages of the Waimanalo Limestone, Oahu, Hawaii, and paleoclimatic implications for the last interglacial period. *Geological Society of America Abstracts with Programs* **23**(5), A239.

Mullins H. T. (1998) Environmental change controls of lacustrine carbonate, Cayuga Lake, New York. *Geology* **26**(5), 387-390.

Nozaki, Y. (2001) Elemental distribution overview, *in* Steele, J.H., Turekian, K.K., Thorpe, S.A., eds., *Encyclopedia of Ocean Sciences*, London, Academic Press.

Popp B. N., Laws E. A., Bidigare R. R., Dore J. E., Hanson K. L., and Wakeham S. G. (1998) Effect of phytoplankton cell geometry on carbon isotope fractionation. *Geochimica et Cosmochimica Acta* **62**, 69-77.

Rau G. H., Takahashi T., Des Marias D. J., Repeta D. J., and Martin J. H. (1992) The relationship between $\delta^{13}C$ of organic matter and [CO_2 (aq)] in ocean surface water: Data from a JGOFS site in the Atlantic Ocean and a model. *Geochimica et Cosmochimica Acta* **56**, 1413-1419.

Redfield A. C. (1934) On the proportions of organic derivations in sea water and their relation to the composition of plankton. In *James Johnston Memorial Volume* (ed. R. J. Daniel), pp. 177-192. University Press of Liverpool.

Redfield A. C. (1958) The biological control of the chemical factors in the environment. *American Journal of Science* **46**(3), 1-18.

Robie R. A., Hemingway B. S., and Fisher J. R. (1979) *Thermodynamic Properties of Minerals and Related Substances at 298.15K and 1 Bar (10^2 Pascals) Pressure and at Higher Temperatures.* U. S. Geologic Survey Bulletin 1452, 456 pp.

Romanek C. S., Grossman E. L., and Morse J. W. (1992) Carbon isotopic fractionation in synthetic aragonite and calcite: effects of temperature and precipitation rate. *Geochimica et Cosmochimica Acta* **56**, 419-430.

Roy R. N., Roy L. N., Vogel K. M., Porter-Moore C., Pearson T., Good C. E., Millero F. J., and Campbell D. M. (1993) The dissociation constants of carbonic acid in seawater at salinities 5 to 45 and temperatures 0 to 45° C. Marine Chemistry. **44**, 269-267; --. 1994. Erratum. Marine Chemistry 45:337.; --. 1996. Erratum. Marine Chemistry 52:183.

Schelske C. L. and Hodell D. A. (1991) Recent changes in productivity and climate of Lake Ontario detected by isotopic analysis of sediments. *Limnology and Oceanography* **36**(5), 961-975.

Schubert C. J., Stein R., and Calvert S. E. (2001) Tracking nutrient and productivity variations over the last deglaciation in the Arctic Ocean. *Paleoceanography* **16**, 199-211.

Sherman, C.E., Glenn, C.R., Jones, A.T. , Burnett, W.C. , Schwarcz, H.P., 1993, New evidence for two highstands of the sea during the last interglacial, oxygen isotope substage 5e. *Geology* **21**, p. 1079-1082.

Sirevag, R., 1995, Carbon metabolism in green bacteria. *in* R.E. Blankenship, Madigan, M.T., and Bauer, C.E., eds., *Anoxygenic Photosynthetic Bacteria*. Kluwer, Amsterdam, 871-883.

Stearns H. S. (1974) Submerged shorelines and shelves in the Hawaiian Islands and a revision of some of the eustatic submerged shorelines. *Geological Society of America Bulletin* **85**, 795-804.

Szabo, B.J., Ludwig K.R., Muhs D.R., Simmons, K.R. (1994) Thorium-230 Ages of Corals and Duration of the Last Interglacial Sea-Level High Stand on Oahu, Hawai'i. Science **266**, 93-96.

Swart P. K., Burns S. J., and Leder J. J. (1991) Fractionation of the stable isotopes of oxygen and carbon in carbon dioxide during the reaction of calcite with phosphoric acid as a function of temperature and technique. *Chemical Geology (Isotope Geosciences Section)* **86**, 89-96.

Tabita, F.R., 1995, The biochemistry and metabolic regulation of carbon metabolism and CO_2 fixation in purple bacteria. *in* R.E. Blankenship, Madigan, M.T., and Bauer, C.E., eds., *Anoxygenic Photosynthetic Bacteria*. Kluwer, Amsterdam, 885-914

Talbot M. R. and Kelts K. (1990) Paleolimnological signatures from carbon and oxygen isotopic ratios in carbonates from organic carbon-rich lacustrine sediments. In *Lacustrine Basin Exploration. Case Studies and Modern Analogs* (ed. B. J. Katz), pp. 99-112. American Association of Petroleum Geologists Memoir 50.

Teranes J. L. and Bernasconi S. M. (2000) The record of nitrate utilization and productivity limitation provided by d15N values in lake organic matter—A study of sediment trap and core sediments from Baldeggersee, Switzerland. *Limnology and Oceanography* **45**, 801-813.

Tribble, J.S., Garrison, G.H., Stens, J.S., Skillbeck, C.G., and Frankel, E., 1999, Evidence for early-mid Holocene sea level on O'ahu, Hawai'i from coastal pond sediments, *in* Fletcher, C.H. and Matthews, J.V., eds., *The Non-Steady State of the Inner Shelf and Shoreline: Coastal Change in the Time Scale of Decades to Millennia in the Late Quaternary*: Abstracts with Programs, Inaugural Meeting of IGCP Project #437, University of Hawai'i, Honolulu, HI, Nov. 9-12, 249p.

Tsusue A. (1967) Manganese kutnahorite from Ryujima mine, Japan. *American Mineralogist* **52** 1751-1761.

Tucker M.E., Wright, V.P., 1990, *Carbonate Sedimentology*. Blackwell Scientific Publications, Boston, 482 p.

Velinsky, DJ; Pennock, JR; Sharp, JH; Cifuentes, LA; Fogel, ML, 1989, Determination of the isotopic composition of ammonium-nitrogen at the natural abundance level from estuarine waters. *Marine Chemistry* **26** (1) 351-361.

Wada E. (1980) Nitrogen isotope fractionation and its significance in biogeochemical processes occurring in marine environments. In *Isotope Marine Chemistry* (ed. K. Saruhashi), pp. 375-398. Uchida Rokakudo Pub. Co.

Wolery T. J. (1992) *EQ3NR, A computer program for geochemical aqueous speciation-solubility calculations*. Lawrence Livermore National Laboratory.

CHAPTER III.

A paleoenvironmental Holocene lacustrine sediment record from ʻEwa Plain, Oʻahu, Hawaiʻi

ABSTRACT

This work presents a 9800-year record of environmental change on O'ahu, Hawai'i, from laminated sediments in a eutrophic pond. Previous time-series analyses of modern water chemistry and particulate production provides a model for understanding the ancient sediments as a record of changes in the surrounding environment. Three general types of sediments occur: amorphous aquatic organic matter, inorganic carbonate minerals, and diatom tests. The alternating light and dark laminae color is a function of the relative fraction of each sediment type. Previous time-series analyses of the modern pond biogeochemistry showed these laminae are *spring/summer – fall/winter* varves.

Changes in Ordy Pond sediments record historic environmental conditions on O'ahu's 'Ewa Plain. The pond was initially inundated as groundwater was elevated by post-glacial sea level rise ~9700 years ago. Continued sea level rise created a deeper pond with different winter and summer depositional conditions. Sediments produced in the fall/winter seem to have retained their primary geochemical values, but sediments produced in the spring/summer appear to have been chemically altered before settling out of the water column. Evidence of significant changes in the water balance of the pond are found at 6.72 meters below the sediment surface (mbs), or ~ 1 kya. Coeval changes in carbonate mineralogy, carbonate stable isotopes, and the diatom species assemblage reveal an influx of meteoric water contemporaneous with aridification of the surrounding forest. These changes cannot be anthropogenic and are suggestive of a well documented 2m drop in sea level around O'ahu. Sediments become sapropelic at the first appearance of pollen associated with Western human contact at 5.21 mbs (1830 AD), which possibly resulted from the introduction of phosphorus fertilizers. The most recent sediments

indicate that the pond is returning to a state similar to its earliest period, perhaps the result of the reestablishment of a local forest and an end to large-scale agriculture on O'ahu.

3.1. INTRODUCTION

Important measures for modeled predictions of future climate change is to successfully hind-cast past climate change. Testing of future climate predictions relies on high-resolution records from the recent past (0 - 150,000 ka) such as ice cores, tree rings, and rapidly deposited sediments. Lacustrine sediments can be particularly good records because their small reservoir sizes respond quickly to both intrinsic and extrinsic change (Glenn and Kelts, 1991; Chivas et al., 1993). Laminated sediments are particularly good for paleoenvironmental study because their structure implies an undisturbed record of cyclic environmental change on millennial to interannual time scales (Kemp, 1996). Laminae deposited in annual sequences are called varves. Varved sediments are particularly useful for paleoenvironmental study because they can provide a high temporal resolution. Evidence of past environmental changes is more apparent in varved sediments than non-varved sediments because perturbations can be more easily identified in a cyclically alternating system.

This work presents a 9800-year record of environmental change recorded within a laminated lacustrine Holocene sediment record from Ordy Pond on O'ahu, Hawai'i. Time-series analyses in 2000/2001 define how changes in the aquatic biogeochemistry of the pond were incorporated into the character of the particulates produced in the modern system (Chapters I & II). The only sources of water to the pond are limited rainfall and groundwater seepage input, which made the pond sensitive to its surrounding environment. The sediments beneath the pond formed within the water column and are controlled by the biogeochemistry of the aquatic system. Furthermore, the studies of water chemistry (Chapter I) and modern particulate production (Chapter II) show that laminations in the sediment record are varves resulting from seasonal thermal stratification and changes in organic matter productivity. This paper thus explores the

cored sediment record of Ordy Pond, notes how that record changes with depth, and evaluates some of its significant features with respect to the timing and nature of past environmental changes on O'ahu.

The pond fills a 20+ m deep karst sinkhole 800 m inland from the shoreline in the Kalaeloa region of 'Ewa Plain, also known as Barbers Point (Fig. 3.1). 'Ewa Plain is an emerged carbonate reef complex, and the area around the pond formed during O'ahu's interglacial Waimanalo sea level stand (oxygen isotope Stage 5e) which lasted between 135-120 kya and was approximately 8 m higher than today (Ku et al., 1974; Stearns, 1974; Muhs and Szabo, 1991; Sherman et al., 1993; Szabo et al., 1994). The most recent post-glacial sea level rise inundated the sinkhole with groundwater and today the pond is circular, 0.5 ha in area, 5m deep, and surrounded by a ring of American mangrove (*Rhizophora mangle)* within a forest of kiawe (*Prosopis pallida*) and sourbush (*Pluchea symphytifolia*).

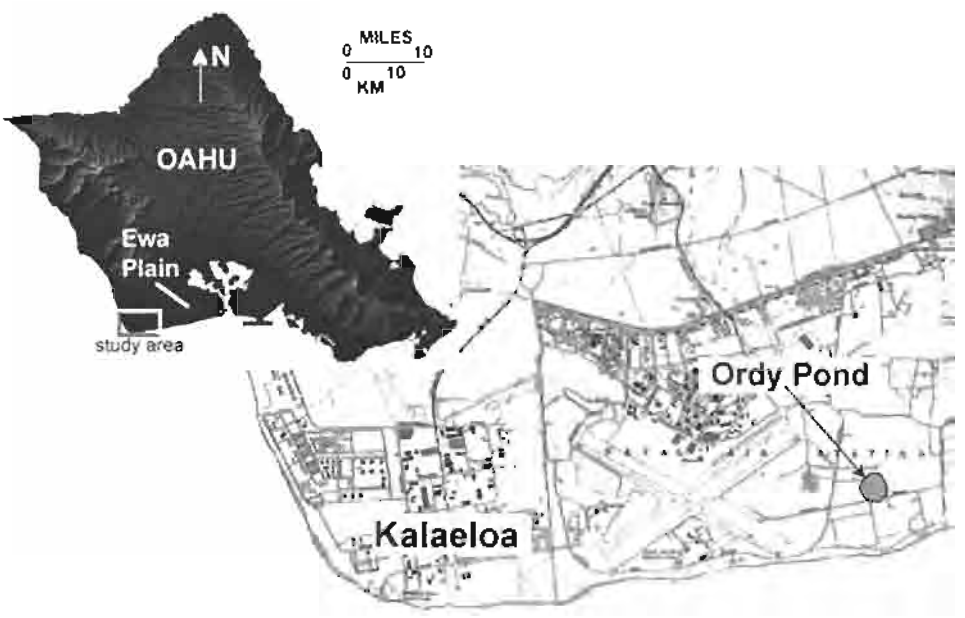

Figure 3.1. Location map of Ordy Pond in the Kalaeloa area of 'Ewa Plain.

3.2. METHODS

Athens et al. (2002) recovered 8 m of core from Ordy Pond in 1994 and showed the record to have sedimentation rates between 0.3 – 3 cm/yr. In 1997, a 7.5 cm ID vibracore system with aluminum core barrels was used to collect 8 m of sediments, below which a 3.5 cm ID aluminum-line piston core system was used to collect sediments to a total depth of 17.5 m below the sediment-water interface (mbs). These cores were split, photographed, and are stored in the SOEST Core Lab Facility at the University of Hawai'i. The work reported here is based on samples collected from the 1997 cores. The data collected from the 1994 cores (i.e., pollen assemblages, charcoal contents, ^{14}C dates, diatom species assemblages) were correlated to the 1997 cores based upon sediment descriptions and color images.

The sediment-water interface at the bottom of the pond is not a distinct boundary. The benthic boundary layer consists of a loose ~ 1.5 m thick sapropel, and it was not clear if the top of the sediment core could be considered the true top of the sediment record. A separate core tube of the sapropel was collected in 1999, identified as "SC-1" for Sapropel Core #1. A 7.62 cm OD PVC pipe was lowered from the pond's surface to a depth 1.5 m below the top of the sapropel. A SCUBA diver placed a rubber stopper into the bottom of the core tube while it was in place. Once closed, the core was returned to the lab without being overturned. In order to collect discrete samples, the entire core was frozen (-20° C) and cut into sections which were desiccated for 48 hours in a vacuum freeze-drier.

Sediment samples were mounted with optical adhesive on smear slides for petrographic microscopic inspection. Samples were also dried, ground, and their mineralogy determined using an automated Scintag Pad V X-ray diffractometer (XRD) scanning with Cu-Kα radiation (λ = 1.5406 Å) at rate of 2° 2Θ min^{-1}. Powdered fluorite was added to the samples before analysis,

and the fluorite-111 hkl peak was used to standardize the sample XRD patterns. The fluorite correction was also used to calculate the mole percentage of Mg in calcite sediment by noting the shift in the d-spacing of each sample's calcite-104 peak (3.035 Å) according to an equation derived from data in Bischoff et al. (1983; Bischoff, pers. comm.):

$$\text{Mg mol\%} = 100 \cdot [(\text{calcite-104 d-spacing})-3.035] \cdot -0.291667^{-1} \qquad (1)$$

The relative fractions of aragonite and calcite in the sediments were calculated using a standard curve generated for the Scintag instrument (Sabine and Mackenzie, 1995) based on the peak area ratio (PAR) of the aragonite-111 and the calcite-104 XRD peaks.

Inorganic carbon samples were acidified with 6% perchloric acid in a UIC Model 5130 Acidification Module, whereas carbon samples were combusted at 1050° C in a UIC Model 5120 Total Carbon Aparatus. In both cases the CO_2 extracted from the samples was measured titrimetrically in a UIC Model 5001 CO_2 Coulometer. Sedimentary organic carbon was taken as the difference between total and inorganic sedimentary carbon contents. Replicate sample analyses had a standard deviation (σ) of 0.2% for both inorganic carbon weight percent ($n = 230$) and organic carbon weight percent ($n = 186$). Inorganic and total sedimentary phosphorus were measured photometrically on a Brinkmann PC 800 Colorimeter according to the method of Aspila (1976), and replicated sample analyses had a σ of 0.005 weight % ($n = 3$). Sedimentary phosphorus was measured only in the upper 9 m of the sediments where anthropogenic land use impact was expected to be found.

Carbonate ^{18}O:^{16}O and ^{13}C:^{12}C ratios were measured using a modification of the sealed-vessel technique (McCrea, 1950; Epstein et al., 1953; Epstein et al., 1953b; Emiliani, 1955). Carbonate was removed from the samples by acidification with 100% phosphoric acid at 50° C under vacuum. Isotopic ratios of the CO_2 gas produced were analyzed on a Finnigan MAT 252

isotope-ratio-monitoring mass spectrometer in the SOEST Stable Isotope Biogeochemistry Lab at the University of Hawai'i, Mānoa. Corrections were made for temperature dependent oxygen isotopic exchange between phosphoric acid and sample carbonate (Swart et al., 1991). Sedimentary organic ^{13}C:^{12}C, ^{15}N:^{14}N, and molar C:N ratios were measured at the same facility with a Carlo Erba 2500NC Elemental Analyzer coupled to a Finnigan MAT Delta Plus mass spectrometer via a CONFLO II interface. Samples were first acidified with 6% sulfurous acid (H_2SO_3) to remove carbonate sediment. Isotopic ratios are reported in standard delta notation. Carbonate and oxygen isotope ratios are reported relative to Vienna PDB (V-PDB), and $\delta^{15}N$ is reported relative to atmospheric nitrogen (AIR). Replicated sample analyses had a σ of 0.6‰ (n = 9) for $\delta^{13}C_{carb}$, 0.4‰ (n = 8) for $\delta^{18}O_{carb}$, 0.7‰ (n = 6) for $\delta^{13}C_{org}$, and 0.7‰ for $\delta^{15}N_{org}$ (n = 5). Analytical precisions based on routine analyses of internal laboratory reference materials were ±0.10‰ for $\delta^{18}O$, ±0.05‰ for inorganic $\delta^{13}C$, ±0.15‰ for organic carbon, and ±0.34‰ for $\delta^{15}N$. Internal reference materials for $\delta^{13}C$ and $\delta^{18}O$ analyses at the SOEST Stable Isotope Biogeochemistry Lab have been calibrated against NBS-19 ($\delta^{18}O$ = -2.2‰, $\delta^{13}C$ = +1.95‰, V-PDB) and normalized to NBS-18 ($\delta^{18}O$ = -23.05, $\delta^{13}C$ = -5.04‰, V-PDB) standard reference materials in accordance with International Atomic Energy Agency (IAEA) guidelines.

3.3. RESULTS

3.3.1. Physical sedimentology

3.3.1.1. Lower Core Section, 17.5 – 13.3 mbs – The solid floor of the sinkhole was not encountered, but coring penetrated all the lacustrine sediments and reached a subaerially deposited paleosol. These earliest deposits (between 17.5 and 13.3 mbs; Fig. 3.2), were eroded from the surrounding carbonate platform and consist of a loose, poorly sorted, silty, light brown-

gray, calcitic mud with terrestrial gastropod shells and clasts of coral-algal reef carbonate. The upper contact of this unit is a darkening gradation into an overlying, 2 cm thick, olive-black organic-rich peat layer (Horizon B, Figs. 3.2a, 3.2b), and is considered a transition into lacustrine sediments. A sample of the shallowest subaerially deposited material (13.4 mbs) dated to 9,780 ± 110 yr BP marking this interval as an important point on the historical sea level curve for O'ahu (Tribble et al., 1999).

3.3.1.2. Laminated Core Section, 13.3 – 5.2 mbs – Above the basal aquatic layer, sediments are 2 – 50 μm in grain size and well laminated (Figs. 3.2b – 3.2c). Athens et al. (2002) collected radiocarbon dates on three samples of terrestrial plant material in this section (which they called Layers III–XVIII) and calculated a sedimentation rate of 0.3 cm yr^{-1} (Fig. 3.2f). There are nearly the same number of laminae within the sediments between the radiocarbon dates as there are years of calibrated time, supporting the interpretation that these are varved deposits (Fig. 3.2g). Laminations typically alternate between green-olive (dark) and buff-tan (light) layers 0.1-2.5 mm thick (Figs. 3.2a – 3.2d). Photomicrographs from this interval (Figs. 3.3c and 3.3d) reveal the sediment character to be very similar to modern particulate samples collected in 2000 (Fig. 3.3a). The primary difference between different colored laminae is the relative contribution of the sediment types: dark laminae are organic-rich, light laminae are carbonate-rich (low magnesium calcite and aragonite), and white laminae are diatom-rich. The sedimentary organic material is primarily filamentous mat-forming algae (Athens et al., 2002). Petrographic and SEM observations of the calcite and aragonite sediments showed them to consist of loose microcrystals between 2 and 30 μm in size (Fig. 3.4). The third and least common laminae type – labeled **D** in Figure 3.2c – are white and contain little organic or inorganic carbon. SEM examination revealed these laminae to consist entirely of monogenetic

diatom tests (Fig. 3.5), though not every diatomaceous lamina is of the same genus. The most frequent diatoms observed in these laminae were species of the genus *Synedra*, a needle-shaped non-symbiotic diatom found in fresh to slightly brackish waters (Round et al., 1990).

The upper part of this section is a transition zone with laminated sections interbedded with cm-scale banded sections, laminae decreasing upcore and mostly disappearing by 6.14 mbs (lower portion of Fig. 3.2e). These changes in layering accompanied by shifts in pollen assemblages. Below 6.72 mbs, ~1000 yr BP, the sedimentary pollen assemblage indicates that the area around Ordy Pond was dominated by a dry mesic forest (Athens et al., 2002). Above 6.71 mbs (Horizon E, Figs. 3.2a & 3.2d) the pollen indicate that the forest began to open up and allow the penetration of Cheno-Ams, a combined term for taxa in the *Chenopodiaceae* family and the genus *Amaranthus*, i.e., dryland shrubs. Gradually, the forest gave way entirely, and by 6.52 mbs (Horizon F, Figs. 3.2a & 3.2d, ~910 yr BP) the area became entirely dominated by dry shrubs and grasses (Athens et al., 2002).

3.3.1.3. Upper Core Section (sapropel), 5.2 – 0 mbs – The top of the core is a dark, low-density, organic-rich sapropel deposit with occasional subtle light-colored banding and was identified as Layer I by Athens et al. (2002). The sharp transition between the underlying fine carbonate sediments and this sapropelic section is labeled Horizon G in Figures 3.2a. and 3.2e; the subtle banding in the upper core section becomes more apparent in the horizontally exaggerated Figure 3.2a. The photomicrographs in Figure 3.3b show how these sediments resemble both the older sediments and modern particulates. At the base of this section, Athens et al. (2002) found the first appearance of what is termed "historic pollen" – an assemblage of pollen species that archeologists have correlated to Western contact with Hawai'i at 1830 AD. Thus, the average sedimentation rate across this section is 3.1 cm yr^{-1}.

Figure 3.2. Mosaic image of the sediment cores recovered from Ordy Pond in 1997 (Fig. 3.2a). The lower portion of the subaerial section of the core (17.5 – 13.8 mbs) is not shown. The magnified Figures 3.2b – 3.2e have a 1:1 vertical to horizontal scale. The oldest sediments, labeled **A** (Figs. 3.2a & 3.2b), are a paleosol eroded from the surrounding carbonate platform. Inundation following post-stadial sea level rise 9.7 kya left a peat at Horizon **B** (Figs. 3.2a & 3.2b). This organic-rich horizon (TOC = 22.5%) probably represents formation of a swampy marsh. As water level rose, seasonally variable sedimentation produced laminated deposits (**C**, Figs. 3.2a – 3.2c), which alternate between light colored carbonate-rich and dark organic-rich laminae. There are also occasional diatomaceous laminae (e.g., **D**, Fig. 3.2c, Fig. 3.5). Decline of the of the local forest began ~ 1 Kya (Horizon **E,** 6.72 mbs, Figs. 3.2a & 3.2d), as inferred from a palynological shift from dry forest to a grassland environment (Athens et al., 2002). The first Polynesian settlement on O'ahu is inferred at 0.9 Kya (Horizon **F,** 6.52 mbs, Figs. 3.2a & 3.2d) by charcoal deposits and exotic Polynesian flora (Athens et al., 2002). Horizon **G** (5.21 mbs, Figs. 3.2a & 3.2e) is the first appearance of Hawaiian "historic pollen" – a pollen assemblage correlated to Western contact with Hawai'i in 1830 AD (Athens et al., 2002). Sediments above this sharp boundary are sapropelic. The depth-to-age relationship is plotted in Figure 3.2f: the three youngest radiocarbon dates and the "historic" pollen date are from Athens et al. (2002); the oldest radiocarbon date is from Tribble et al. (1999). Figure 3.2g has plots of both the sediment radiocarbon ages and the cumulative number of laminae against sediment depth. The hypothesis that the laminae are varves is supported by the fact that number of laminae and the age of the sediment increase at the same rate with depth.

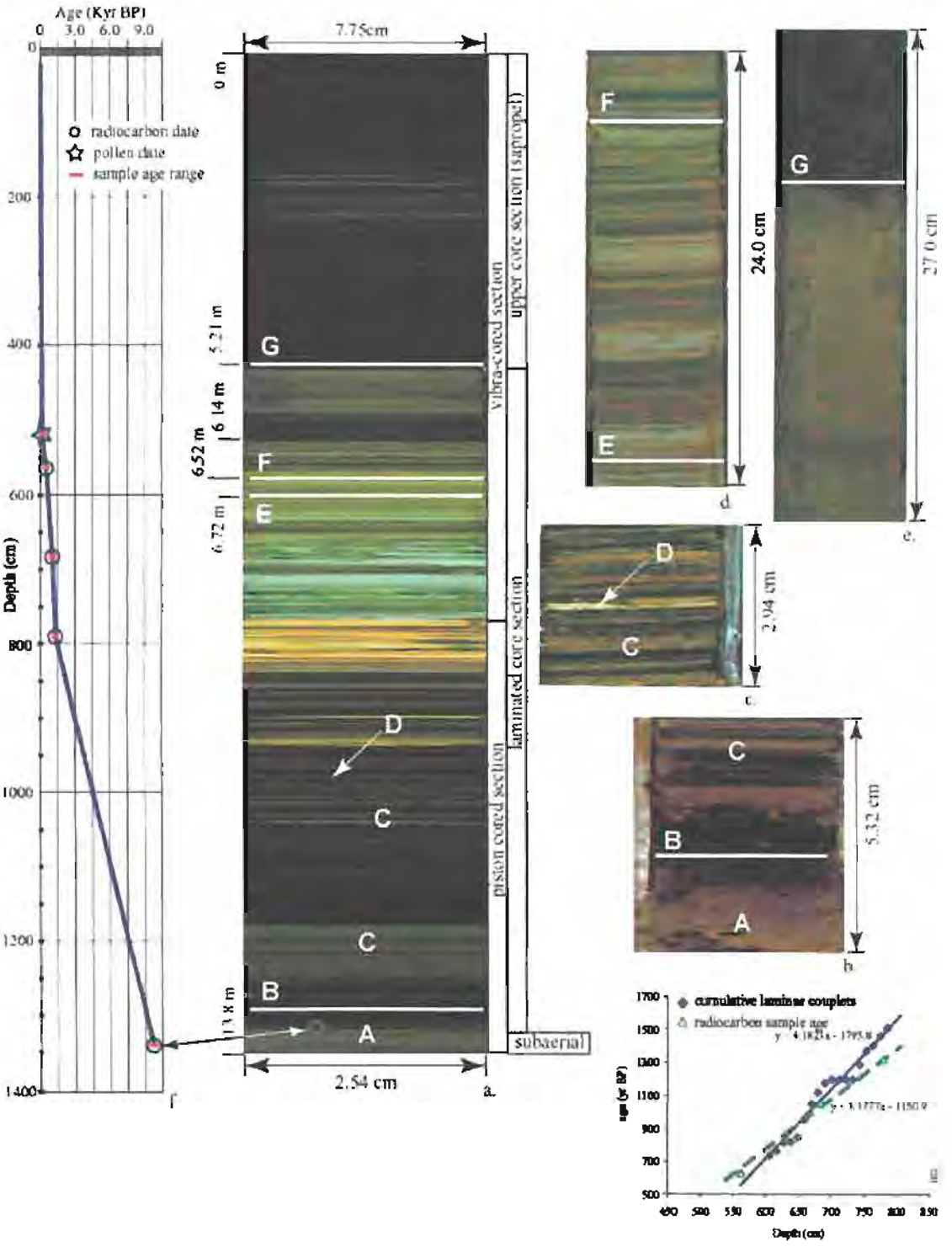
Age (Kyr BP)
0 3.0 6.0 9.0
radiocarbon date
pollen date
sample age range
Depth (cm)
0
200
400
600
800
1000
1200
1400
f
7.75cm
0 m
5.21 m
6.14 m
6.52 m
6.72 m
13.8 m
G
F
E
D
C
C
B
A
2.54 cm
a.
vibra-cored section
upper core section (sapropel)
laminated core section
piston cored section
subaerial
24.0 cm
d
27.0 cm
e.
2.94 cm
c.
5.32 cm
b.
cumulative laminae couplets
radiocarbon sample age
Depth (cm)

Figure 3.2.

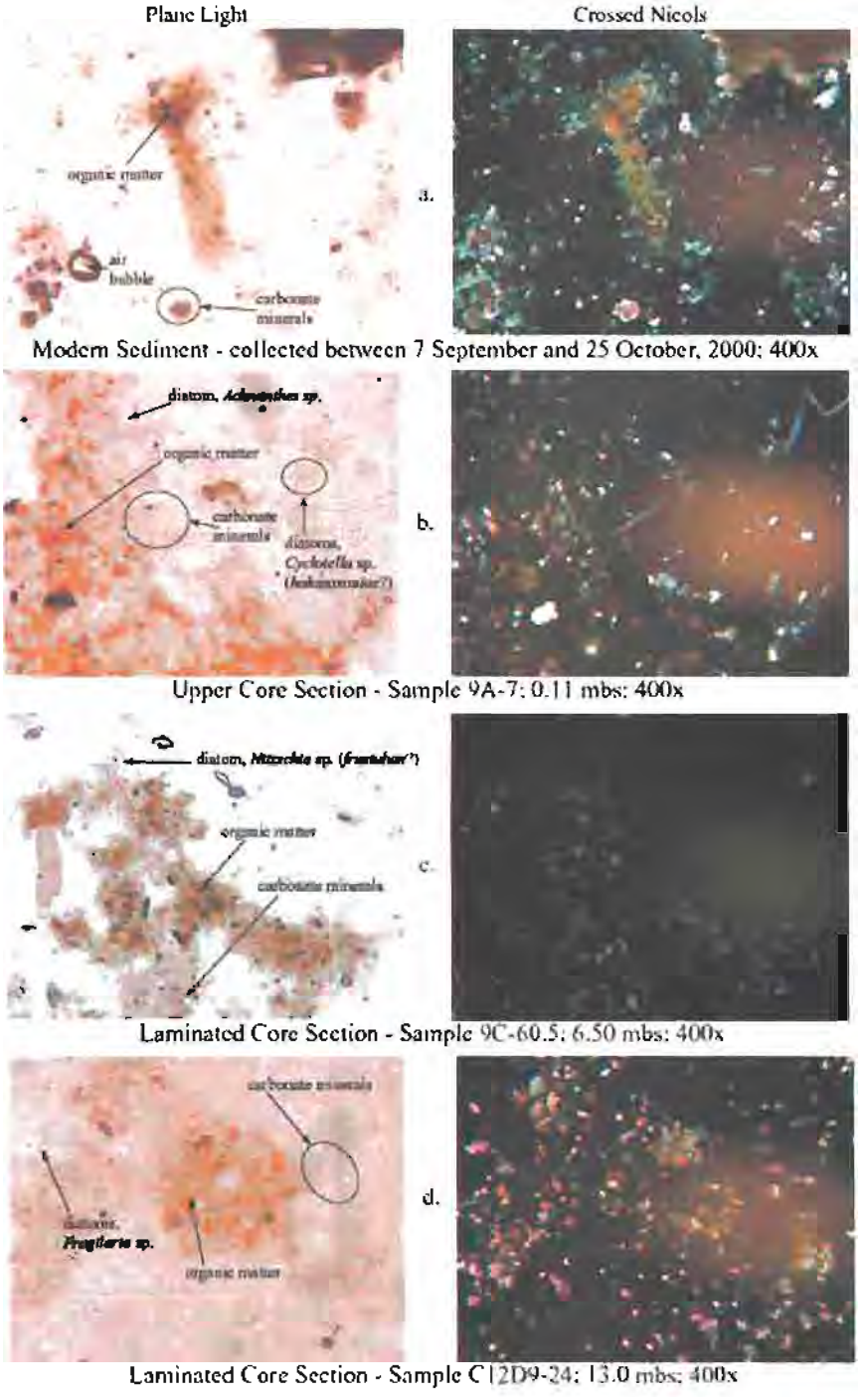

Figure 3.3. Photomicrographs in plane light and through crossed nicols: (3a) modern particulate; (3b) from the upper core section, 0.11 mbs; (3c&d) from the laminated core section, 6.50 mbs and 13.03 mbs. Sediment types are labeled.

Figure 3.4. SEM photomicrographs carbonate sediment within a typical light colored carbonate-rich lamina located at 10.58 mbs. The carbonate mineralogy of this particular lamina is 100% calcite.

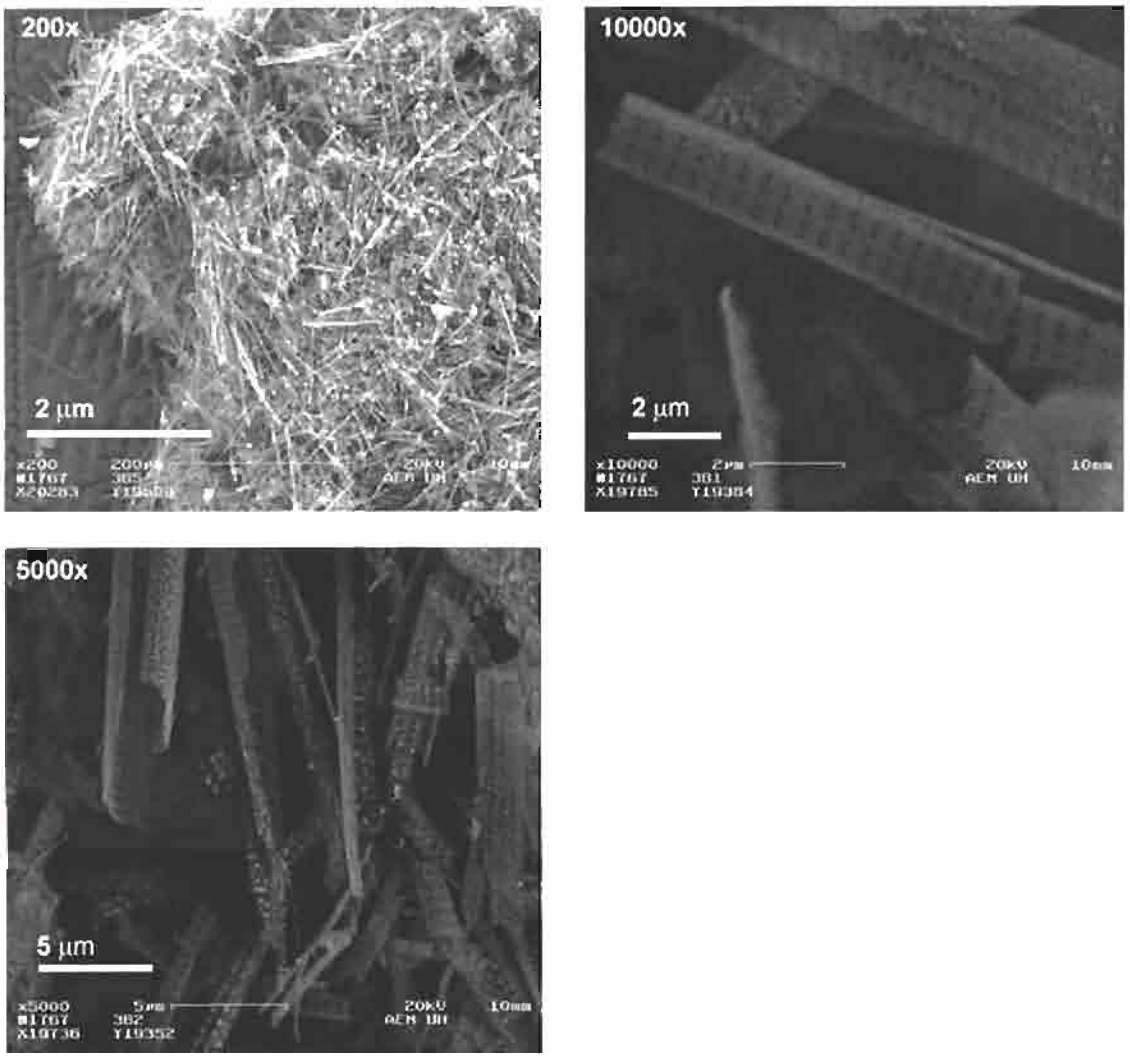

Figure 3.5. SEM photomicrographs of a white monospecific diatomaceous laminae from 8.90 mbs. This species is of the genus *Synedra*, which is found in fresh to slightly brackish waters (Round et al., 1990).

3.3.2. Elemental sediment chemistry

3.3.2.1. Laminated Core Section, 13.30 – 5.21 mbs – The light lamina have inorganic carbon contents between 6.1 – 11.4% by weight (wt%), while dark laminae inorganic carbon ranged between 0.5 – 7.0 wt% (Table 3.1, Fig. 3.6). The light laminae have organic carbon contents between 0.0 – 12.5 wt%., and organic carbon range between 3.3 – 22.9 wt% in the dark laminae. The white diatomaceous laminae have inorganic carbon contents of only 0.4 – 3.8 wt% and organic carbon contents of only 0.0 – 5.4 wt%.

3.3.2.2. Upper Core Section, 5.21 – 0.00 mbs – The sapropelic sediments in the upper core section are more homogenous than in the laminated section (Table 3.1). Inorganic carbon in light-colored sediments dropped to a range of 3.2 – 8.9 wt% and in the dark-colored sediments rose to a range of 1.3 – 6.2 wt%. Organic carbon in the light-colored sediments rose to range of 1.4 – 12.3 wt% but dropped to a range of 3.8 – 17.8 wt% in the dark-colored sediments. No diatom-rich layers were identified in the upper core section. Furthermore, Table 3.2 shows that there is nearly a three-fold increase in sedimentary phosphorus across the transition into the upper sapropelic sediments.

TABLE 3.1. – Average weight percent sedimentary inorganic and organic carbon specified by sediment type

	laminated core section			upper core section		
lamina/ layer type	wt% inorganic carbon	wt% organic carbon	OC:IC*	wt% inorganic carbon	wt% organic carbon	OC:IC*
light (carb-rich)	9.2 ± 1.3 n = 74	4.3 ± 2.9	0.5 ± 0.4	7.3 ± 1.0 n = 21	6.7 ± 1.9	0.9 ± 0.4
dark (org-rich	4.2 ± 1.8 n = 55	12.4 ± 5.5	2.9 ± 4.3	4.7 ± 1.3 n = 25	10.2 ± 4.3	2.2 ± 1.9
white (diatom)	1.4 ± 1.1 n = 15	2.6 ± 1.5	1.9 ± 1.8	n/a	n/a	n/a

errors are reported as 1 σ
n/a – no laminae present
*OC:IC = average of the wt% organic carbon:wt% inorganic carbon ratios

TABLE 3.2. – Average weight percent sedimentary phosphorus

lamina type	wt% inorganic phosphorus	wt% organic phosphorus	wt% total phosphorous
laminated core section	0.05 ± 0.05 n = 7	0.03 ± 0.02 n = 7	0.11 ± 0.06 n = 7
upper core section	0.17 ± 0.07 n = 5	0.09 ± 0.02 n = 5	0.25 ± 0.08 n = 5

3.3.3. *Carbonate Mineralogy*

The carbonate sediments of the core are entirely aragonite or low magnesium calcite (LMC; Fig. 3.7); the average calcite Mg content is 5.2 ± 2.1 mol%. The oldest aquatic sediments at the bottom of the laminated section contain 23% aragonite (heavy shading, Fig. 3.7), but sediments quickly become 100% calcite (light shading, Fig. 3.7) up the core. Sediments become aragonitic again between 9.93 and 9.48 mbs and also between 8.41 and 6.14 mbs, the same point at which lamination ends. Between 6.14 mbs and 5.21 mbs, the aragonite fraction drops to below 20%. Above 5.21 mbs, the sapropelic sediments of the Upper Core are mostly aragonitic (average = 80%) but range widely from 41% – 100% as aragonite. Sediment in the short core averaged 66% as aragonite similar to the uppermost sediments of main core.

3.3.4. Organic sedimentary stable isotope ratios

For the most part, $\delta^{13}C_{org}$ values centered around an average value of -22‰ (V-PDB) with some notable excursions (Fig. 3.7). Organic carbon $\delta^{13}C$ in the oldest aquatic sediments averages -21.4‰ (V-PDB) but is reduced up core to -29.3‰ (V-PDB) at 11.70 mbs coincident with a positive excursion in the $\delta^{13}C_{carb}$. Between 11.70 mbs and 6.72 mbs, organic sediments are more enriched in ^{13}C in the light laminae than in the dark and the separation reached a maximum of +6.6‰ at 8.7 mbs. At 6.72 mbs, the separation collapses and $\delta^{13}C_{org}$ values vary widely

between -31 and -14‰ (V-PDB). Finally, $\delta^{13}C_{org}$ decreases steadily from -16.3 to -28.4‰ (V-PDB) across the top 3 m of the sapropelic sediments with still no consistent difference between laminae types.

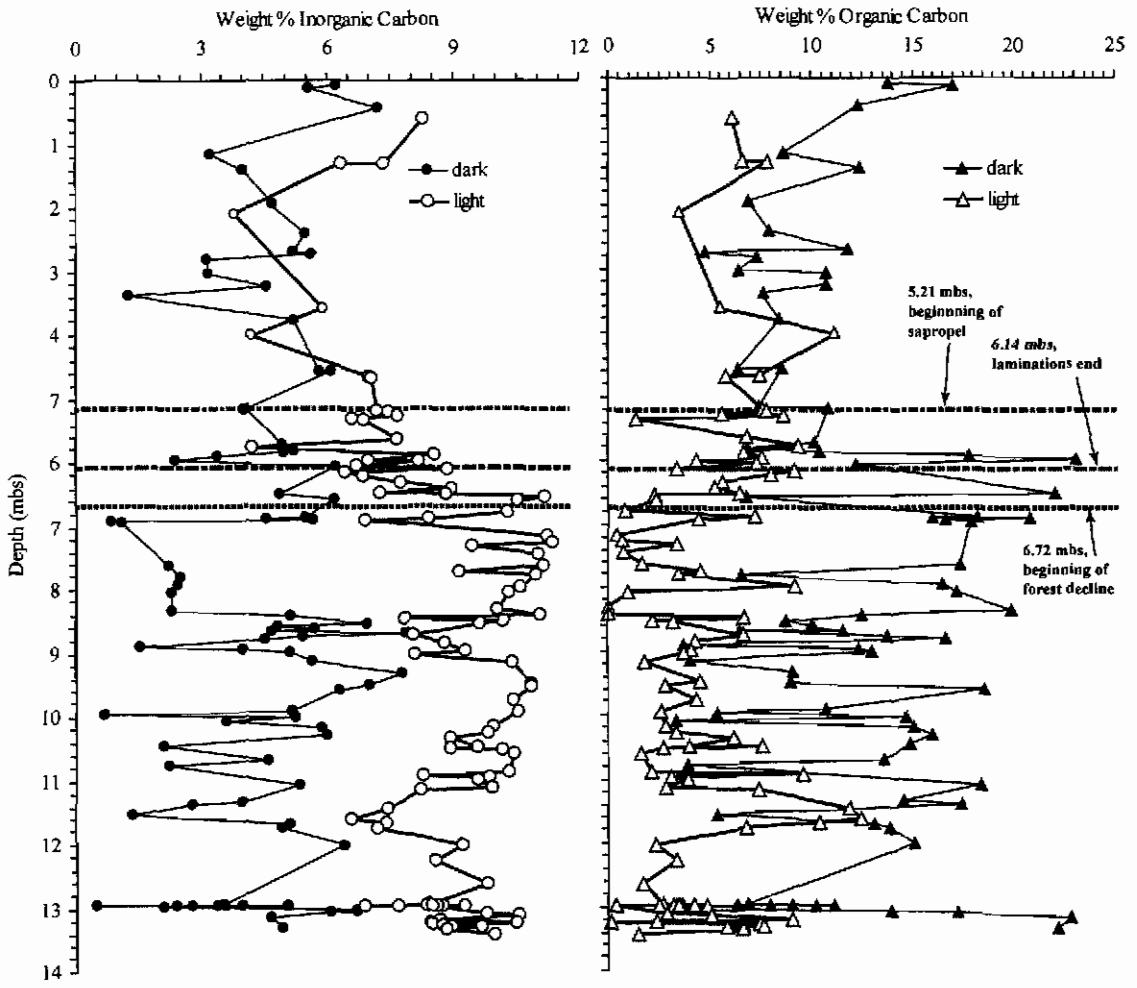

Figure 3.6. Left panel: weight percent of sediment as inorganic carbon; Right panel: weight percent of sediment as organic carbon. Data are differentiated between the dark and light sediments layers.

The organic sediment $\delta^{15}N$ does not show as much variability as $\delta^{13}C_{org}$. The oldest aquatic organic sediments are the most enriched with respect to ^{15}N, averaging +12.9‰ (AIR).

As with $\delta^{13}C_{org}$, there is a decrease in $\delta^{15}N_{org}$ up core to +4.2‰ (AIR) at 11.70 mbs, and then a steady increase in $\delta^{15}N_{org}$ up through the laminated core section. However, there is no discernable separation of $\delta^{15}N_{org}$ values between the laminae types. There is a brief +7‰ negative excursion in $\delta^{15}N_{org}$ just above 6.72 mbs, the same point at which forest trees began to give ground to dry Cheno-Ams shrubs. The C:N ratio averages 15.5 in the laminated core section and 11 in the upper core section with notable exceptions at the usual intervals; C:N varies between 8 and 19 in the oldest aquatic sediments, and there are excursions to 24 at 11.4 mbs and between 6.72 and 5.2 mbs which can probably be attributed to the presence of terrestrial organic matter.

3.3.5. Inorganic carbonate sedimentary stable isotope ratios

The youngest subaerial deposits below Horizon B (Fig. 3.2 and 3.7) have carbonate sediments more depleted in ^{18}O than the rest of the core (~ -2‰ vs. V-PDB). However, above Horizon B, $\delta^{18}O_{carb}$ values increase and separate between dark and light laminae; between 12.2 mbs and 6.72 mbs, $\delta^{18}O_{carb}$ rises from +2.4 to +3.3‰ (V-PDB) in the light laminae and from +1.4 to +2.6‰ (V-PDB) in the dark laminae. The more ^{18}O enriched carbonate sediments in the light laminae are considered evidence that these layers were deposited in the summers when the pond was evaporatively concentrated. The more ^{18}O depleted carbonates in the dark laminae are considered evidence that these deposits formed in the winters when the pond experience an influx of meteoric water. These interpretations are based on the findings of the particulate time-series analysis (Chapter II). Finally, above 6.72 mbs, where evidence of forest decline is first interpreted, $\delta^{18}O_{carb}$ drops 3‰ in both laminae types over a thickness of less than a meter. Within the sapropelic sediments, $\delta^{18}O_{carb}$ increases up core to +1.9‰ and +3.6‰ (V-PDB) in the youngest dark and light sediments, respectively.

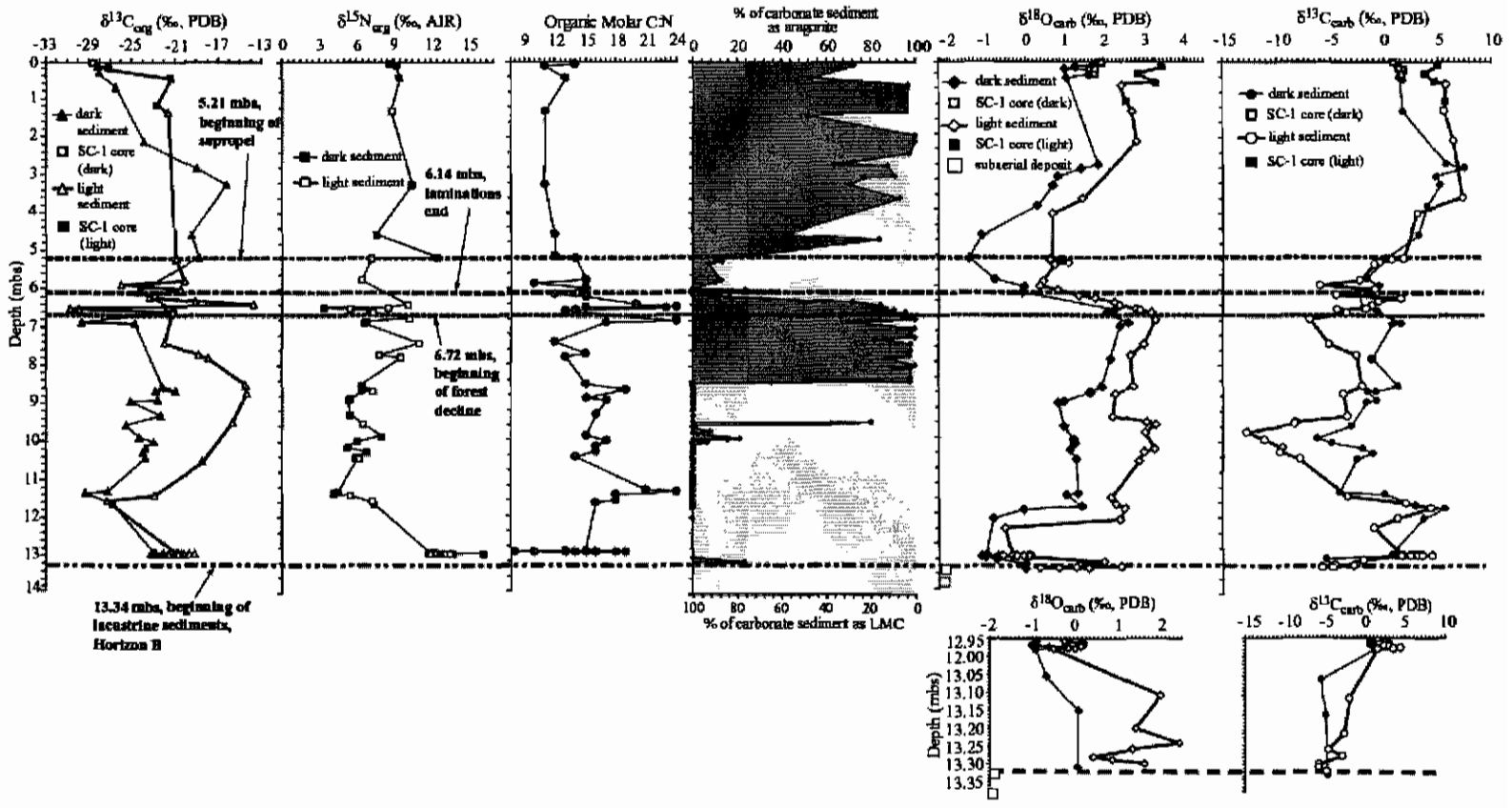

Figure 3.7. $\delta^{13}C_{org}$, $\delta^{15}N_{org}$, organic C:N molar ratio, carbonate mineralogy, $\delta^{18}O_{carb}$, and $\delta^{13}C_{carb}$ along the core. Data are differentiated between the dark and light sediments types. The section between 12.94 and 13.34 mbs is magnified for $\delta^{18}O_{carb}$ and $\delta^{13}C_{carb}$ to highlight the beginning of lacustrine sedimentation and the separation of carbonate isotope values between the dark and light laminae. Samples from the core of the modern sapropel matched the uppermost main core and are differentiated.

The trends of $\delta^{13}C_{carb}$ are not unlike those of $\delta^{18}O_{carb}$. The $\delta^{13}C_{carb}$ of the oldest lacustrine sediments is -4.7‰ (V-PDB) and increases up core to +5.6‰ at 11.7 mbs, coeval with the negative excursion noted in the $\delta^{13}C_{org}$ (Fig. 3.7). Between 12 mbs and the beginning of forest decline at 6.72 mbs, there is an average 4‰ separation of the $\delta^{13}C_{carb}$ values between the light and dark laminae. Also like $\delta^{18}O_{carb}$, there is an excursion in the light laminae $\delta^{13}C_{carb}$ centered near a depth of 10 mbs. At 6.72 mbs, the separation of $\delta^{13}C_{carb}$ values between laminae types breaks down from some major perturbation to the pond system. Above 6.14 mbs, $\delta^{13}C_{carb}$ steadily increases to a peak value of +7.5‰ (V-PDB) around 3 mbs. Above 2.7 mbs the $\delta^{13}C_{carb}$ values separate again between the organic-rich and carbonate-rich sediments layers, and the uppermost carbonate-rich sediments have an average $\delta^{13}C_{carb}$ of +4.9‰ (V-PDB), while the organic-rich sediment $\delta^{13}C_{org}$ drops to +0.9‰ (V-PDB).

3.4. DISCUSSION

Time-series analyses of the modern aquatic and particulate biogeochemistry in Ordy Pond was made between March 2000 and March 2001; the results of these studies are presented in Chapters I and II and summarized below.

3.4.1. Modern water chemistry

The water chemistry time-series profiled temperature, conductivity, salinity, oxygen, SO_4^{2-}, S^{2-}, NH_4^+, NO_3^-, NO_2^-, TDN, PO_4^{3-}, TDP, pH, total alkalinity, DIC, $\delta^{13}C_{DIC}$, Na^+, Ca^{2+}, Mg^{2+}, Sr^{2+}, Fe^{2+}, and Mn^{2+} (Chapter I). Ion activities and mineral saturation states were calculated with an extended Debye-Hückel model and the activity coefficient equation of Davies (1962) within EQ3NR version 7.2c, (Wolery, 1992). Between early May and late September the pond became thermally stratified, as seen in the separation of temperature values in the

epilimnion and hypolimnion (Fig. 3.8a). During this time, elevated $\delta^{13}C_{CO2(aq)}$ and dissolved O_2 (Fig. 3.8) indicated increased aerobic phytoplankton growth in the epilimnion (Fig. 3.8c & 3.8d). When the thermal gradient broke down in October (Fig. 3.8a), hypolimnion waters rich in NH_4^+, PO_4^{3-}, and dissolved inorganic carbon (DIC) depleted in ^{13}C relative to the surface waters mixed with the epilimnion. Subsequently, particulate organic matter production fell and the surface waters became suboxic to anoxic. It is believed that sunlight availability controlled the seasonality of photosynthetic productivity in the epilimnion (Chapter I). When the pond is not stratified, phytoplankton spend more time in the darker depths of the water column and more time in the respirative dark-phase of the photosynthetic cycle. However, when the pond is stratified, phytoplankton spend more time in the euphotic zone, more time in the oxygen-producing light-phase of the photosynthetic cycle (the photoperiod), and are more photosynthetically productive.

3.4.2. Modern particulate production

Modern particulates were collected in sediment traps deployed 1 m above the benthic boundary layer between 7 June 2000 and 23 March 2001 (Chapter II). The study showed the modern particulates to consist of phytoplanktonic organic matter, anaerobic bacteria, and an inorganically precipitated mix of microcrystalline kutnahorite LMC. Particulate production and geochemistry reflected the summer phytoplankton bloom which occurred once the water column became stratified: the particulate flux was >2x higher in the summer than the winter; $\delta^{13}C_{carb}$ reached -1.8‰ (V-PDB) in July/September and fell to -3.3‰ (V-PDB) in February/March as a result of changes in the balance between phytoplankton CO_2 uptake via photosynthesis and microbial CO_2 supply via organic matter remineralization. The particulate $\delta^{18}O_{carb}$ followed the pond's seasonal water balance which overwhelmed the effects of temperature. During the

summer, $\delta^{18}O_{carb}$ reached +2.9‰ (V-PDB) as the pond water became enriched in ^{18}O by evaporation (Fig. 3.9d). During the winter, $\delta^{18}O_{carb}$ fell to 0.9‰ (V-PDB) as waters depleted in ^{18}O relative to the pond were added via rainfall and groundwater seepage as noted by the drop in epilimnion salinity (Fig. 3.8b).

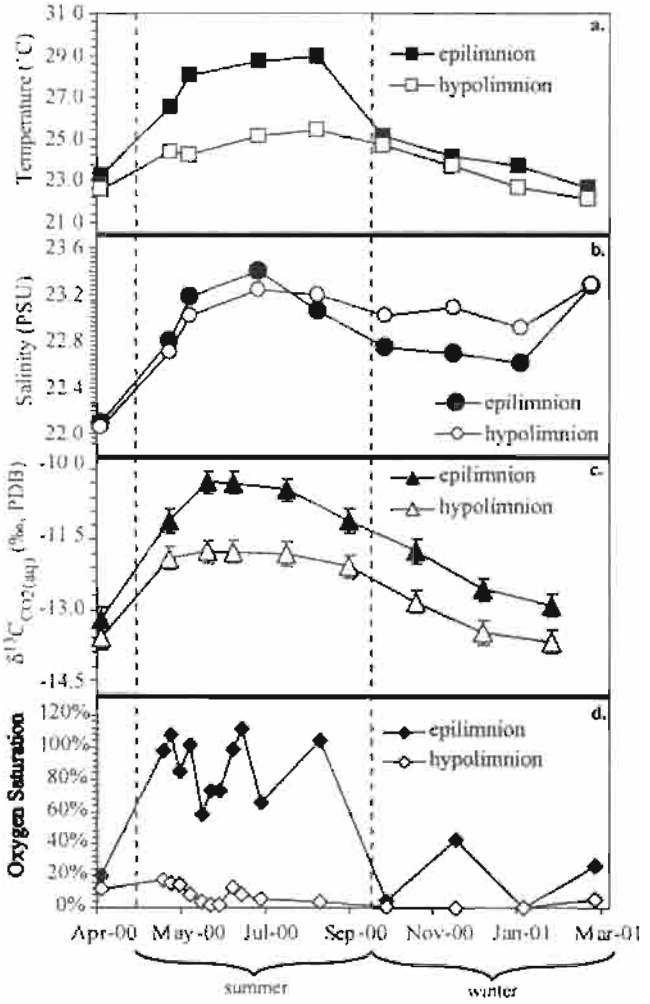

Figure 3.8. : Time-series averaged water properties in the epilimnion (0 – 0.9m) and hypolimnion (0.9 – 4.3 m) (Chapter I): Temperature (a); salinity (b); $\delta^{13}C_{CO2(aq)}$ (c) oxygen saturation (d).

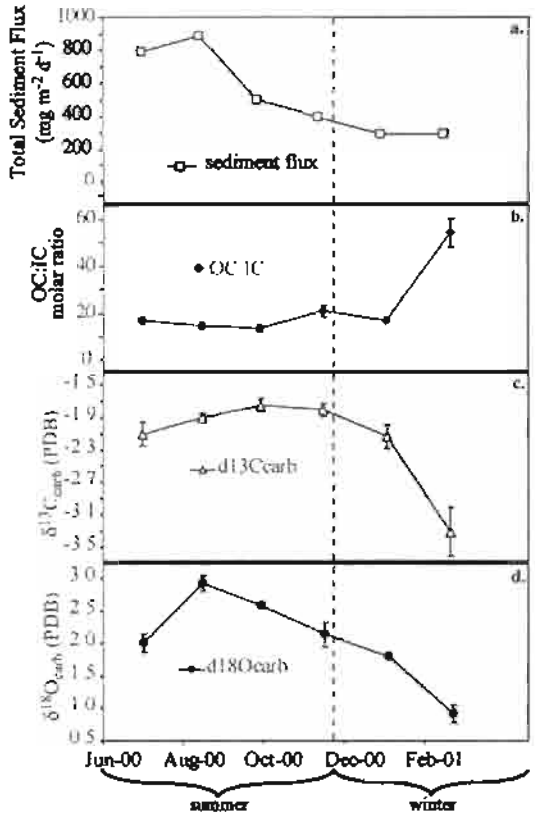

Figure 3.9. Particulate chemistry during the time-series analyses 1 m above the benthic boundary layer (Chapter II): bulk flux (3.9a); organic carbon to inorganic carbon (OC:IC) (3.9b); carbonate $\delta^{13}C$ ($\delta^{13}C_{carb}$) (3.9c); carbonate $\delta^{18}O$ ($\delta^{18}O_{carb}$) (3.9d).

3.4.3. Does the sediment record preserve primary signals from the pond?

An examination of the consistency between the modern particulates and the sediment record beneath the pond can tell us whether the time-series analyses are an accurate model for primary sediment formation. One concern is that the time-series analyses were made during an abnormally dry year. Rainfall during the time-series was 30% of the 50-year average – 151 mm of rain fell during the study versus the 508 mm average measured between 1949 and 1999. The reduced rainfall meant that loss of water from the pond by evaporation, and subsequent concentration of dissolved chemical constituents, must have been more significant than during a

more typical modern year. However, the cycle of events observed in the pond and the seasonal changes in the character of particulate production are consistent with the geochemical nature and cyclicity of the sediment record, as described below. Though the water column may have had a chemical composition more concentrated than average, the biogeochemical seasonality of the pond appears to have been a function more of changes in air temperature than of rainfall (Chapter I). Thus, the seasonal patterns are considered to be representative of a typical year. Nevertheless, comparisons between these time-series analyses and the sediment record should keep the anomalously low rainfall in mind.

3.4.3.1. organic sediment production – The presence of remineralized DIC, PO_4^{3-}, NH_4^+, as well as reduced S^{2-}, Mg^{2+}, and Fe^{2+} within the water column is evidence that particulate organic matter (POM) experiences significant remineralization before being incorporated into the sediment record (Chapter I). The particulate OC:IC ratios measured in the particulate time-series ranged between 13.4 in the summer and 54.1 in the winter (Chapter II), and the OC:IC in the upper core section is only 1.00 in the light layers and 2.56 in the dark layers (Table 3.1). The difference in these ratios represents a 93% loss of organic carbon from the light-colored sediments and a 95% loss from the dark-colored sediments. The remineralization also favored nitrogen-bearing organic compounds. The C:N ratio in the modern particulates ranged between 7.2 and 8.7 (Chapter II), but in the core C:N ranges between 11 and 14 in the surface sediments (Fig. 3.7). This change would represent loss of an additional 21 – 49% organic nitrogen relative to organic carbon if the sedimentary and particulate organic matter had the same initial C:N value. Preferential loss of N is typical and was observed in Lake Griefen, Switzerland, where surface water POM had an average C:N of 8.9 but the surface sediments beneath the lake had a C:N of 12.1 (Hollander, 1989). The Ordy Pond time-series also showed that in winter POM was

more depleted in ^{15}N than in summer which is evidence that microbial remineralization in the pond favors ^{14}N-rich compounds such as amino acids (Chapter II). However, the modern POM was more enriched in ^{15}N than the surface sediments in the core: winter $\delta^{15}N_{POM}$ = +10.8‰ (AIR), core top $\delta^{15}N_{org}$ = +8.7‰ (AIR; Fig. 3.7). The change in C:N not withstanding, the ^{15}N enrichment of organic sediment in the core relative to the modern sediments may indicate a recent shift in the biology of the pond. The $\delta^{13}C_{org}$, however, does not indicate a similar shift. The youngest core sediments have a $\delta^{13}C_{org}$ around -27.5‰ (V-PDB; Fig. 3.9), which is within the -29.9 to -26.9‰ (V-PDB) range measured in the modern $\delta^{13}C_{POM}$ (Chapter I).

3.4.3.2. inorganic sediment production – The pattern of modern carbonate mineral particulate production observed during the time-series analysis agreed well with a varved sediment record. Modern particulates were more depleted in ^{18}O when the organic carbon content was highest (Fig. 3.9), similar to the core (Fig. 3.7). The preservation of $\delta^{18}O_{carb}$ seasonality between the laminae is evidence that the $\delta^{18}O_{carb}$ of the sediments had not been altered by post-depositional diagenesis and that changes in the $\delta^{18}O_{carb}$ can be considered primary depositional signals. The light-colored sediments at the very top of the core had a $\delta^{18}O_{carb}$ between +2.9 and +3.6‰ (V-PDB), and the modern summer particulates had a $\delta^{18}O_{carb}$ of +2.9‰ (V-PDB). The dark-colored sediments at the top of the core had a $\delta^{18}O_{carb}$ between +1.0 and +1.9‰ (V-PDB), and the modern winter particulates had a $\delta^{18}O_{carb}$ of +0.9‰ (V-PDB). The 2‰ difference between sediment types is generally consistent throughout the core except between 6.74 and 6.14 mbs.

The period of greatest carbonate particulate flux during the time-series was also the period when carbonate particulates were most enriched in ^{13}C, also the same trend seen in the uppermost sediments in the core. However, the actual $\delta^{13}C_{carb}$ values measured during the time-

series were quite different from what is present in the core. The $\delta^{13}C_{carb}$ of the summer sediments was -1.8‰ (V-PDB), but the uppermost carbonate-rich sediments had a $\delta^{13}C_{carb}$ of +2.9 to +3.6‰ (V-PDB). The $\delta^{13}C_{carb}$ of the winter sediments was -3.3‰ (V-PDB), but the uppermost organic-rich sediments had a $\delta^{13}C_{carb}$ of +1.3 to +1.9‰ (V-PDB). Thus, there is evidence that the sediments in the core are not identical to what was measured during the time-series. The difference could be explained by a change in the balance between photosynthetic carbon uptake and microbial remineralized carbon supply to the water column.

3.4.3.3. mineralogy – The carbonate particles collected during the time-series contained 47 – 81% kutnahorite, while the rest were LMC (Chapter II). Kutnahorite ($Ca(Mn_xMg_{1-x})(CO_3)_2$) is a manganese-bearing dolomitic isotype (Frondel and Bauer, 1955) usually found as a hydrothermal deposit (Tsusue, 1967; Mucci, 1991). Kutnahorite is rare in earth surface environments and is associated with suboxic/anoxic environments (Cannon and Force, 1983; Huckenridge and Meischner, 1996). The reduced chemical state of the pond helped to maintain Mn^{2+} activities high enough that the waters remained oversaturated with respect to kutnahorite throughout the time-series (Chapter II). However, kutnahorite was not found in the sediment cores. Only aragonite and LMC were present in the uppermost sediments (Fig. 3.7) in the same relative proportions as kutnahorite and LMC in the time-series particulate samples.

There are two plausible explanations for the absence of kutnahorite in the sediments. Kutnahorite formation may be a recent phenomena in the pond due to increased reductive strength of the water column or an increased supply of manganese to the pond. However, given the high rate of sedimentation in the pond since 1830 AD (~3 cm yr^{-1}), kutnahorite formation would have to have begun probably no more than a decade ago to be undetectable in the sediments. In that case, the failure to detect kutnahorite would be explained by a failure to

recover the most recent sediments in the 1997 cores and the 1999 SC-1 core. On the other hand, kutnahorite particles precipitated in the water column may have been recrystallized as they were are incorporated into the sediment column. The modern kutnahorite particles may be a metastable phase with respect to LMC and aragonite. If LMC crystallization is inhibited in the sediment pore waters, kutnahorite particles could have recrystallized as less soluble (but still metastable) aragonite. The inhibition of LMC formation within the pore waters would also help explain why 9700-year-old metastable aragonite is still present in the sediments.

3.4.4. Paleoenvironmental interpretations

Changes in the relationship between $\delta^{13}C_{carb}$ and $\delta^{18}O_{carb}$ within the core (Fig. 3.10) are interpreted with respect to changes in the environment of the pond over time. The time-series analyses in Ordy Pond showed that on a seasonal time scale, $\delta^{18}O_{carb}$ is controlled by the water balance between evaporation and rainfall/groundwater seepage, while $\delta^{13}C_{carb}$ is controlled by the balance between phytoplankton CO_2 uptake and the supply of microbially produced DIC (Chapters I & II). Consequently, $\delta^{13}C_{carb}$ covaried positively with $\delta^{18}O_{carb}$ during the time-series ($R^2 = 0.776$, n = 6, Fig. 3.10) because biogenic CO_2 drawdown peaked when the epilimnion was most enriched in ^{18}O (Chapter I). Other modern lacustrine systems have shown that such positive covariance is indicative of sediments formed in closed basins (Talbot, 1990). The degree of $\delta^{13}C_{carb}$–$\delta^{18}O_{carb}$ covariance in a lacustrine system is controlled by the residence time of the water and of DIC, the size of the DIC inventory, the hydrologic balance, and the intensity of organic carbon production (Talbot, 1990; Li and Ku, 1997). Therefore, the relationship between $\delta^{13}C_{carb}$–$\delta^{18}O_{carb}$ in Ordy Pond sediments can be used as a paleoenvironmental signal.

3.4.4.1. 13.30 – 13.00 mbs, sinkhole inundation – LMC within uppermost sediments of the subaerial lower core section –below 13.30 mbs (Horizon B, Figs. 3.2a & 3.2b) – have a

$\delta^{18}O_{carb}$ of -2.0‰ (V-PDB). This $\delta^{18}O_{carb}$ is consistent with calcite precipitated from non-evaporated groundwater from the 'Ewa Plain. According to the temperature dependent calcite-water $\delta^{18}O$ fractionation ($\varepsilon_{cl\text{-}H2O}$ per Kim and O'Neil, 1997), a calcite with a $\delta^{18}O_{carb}$ value of -2.0‰ (V-PDB) would have precipitated in equilibrium with a 25° C solution with $\delta^{18}O_{H2O}$ = -4.4‰ (SMOW). By comparison, the $\delta^{18}O_{H2O}$ of groundwaters along the leeward (rain-shadow) coasts of the islands of both Hawai'i and Maui range between -4.5 and -5.5‰ (SMOW) (Scholl et al., 1996; Scholl et al., 2002). Like the leeward coasts of these islands, 'Ewa Plain sits in a rain shadow behind the Ko'olau Range, and 'Ewa groundwaters are expected to have comparable $\delta^{18}O_{H2O}$ values.

3.4.4.2. 13.00 – 11.70 mbs, a deeper pond – The increase of $\delta^{13}C_{carb}$ and decrease of $\delta^{18}O_{carb}$ in this interval relative to the underlying sediments (Fig. 3.10) can be explained by a deepening water column. Groundwater levels are believed to have been rising during this part of the pond's history (~ 9.1 to 7.2 kya) in response to continued post-glacial sea level rise around O'ahu (Grossman and Fletcher, 1998). As the volume of the pond increased, the $\delta^{18}O_{H2O}$ of the pond would have been less sensitive to evaporation and would have approach the $\delta^{18}O_{H2O}$ of the surrounding groundwater; $\delta^{18}O_{carb}$ values in this interval are closer to being in equilibrium with a $\delta^{18}O_{H2O}$ of -4.5 to -5.5‰ (SMOW) as found in the oldest subaerial sediments (Fig. 3.7). A deeper water column would also have a greater separation of surface and bottom waters and would have had reduced vertical mixing. Reduced mixing would have resulted in higher surface water $\delta^{13}C_{DIC}$ because ^{12}C sequestered in settling particulate matter would have been retained within the hypolimnion. Such an occurrence is consistent with the increased $\delta^{13}C_{carb}$ in this interval relative to the older sediments (Fig. 3.10).

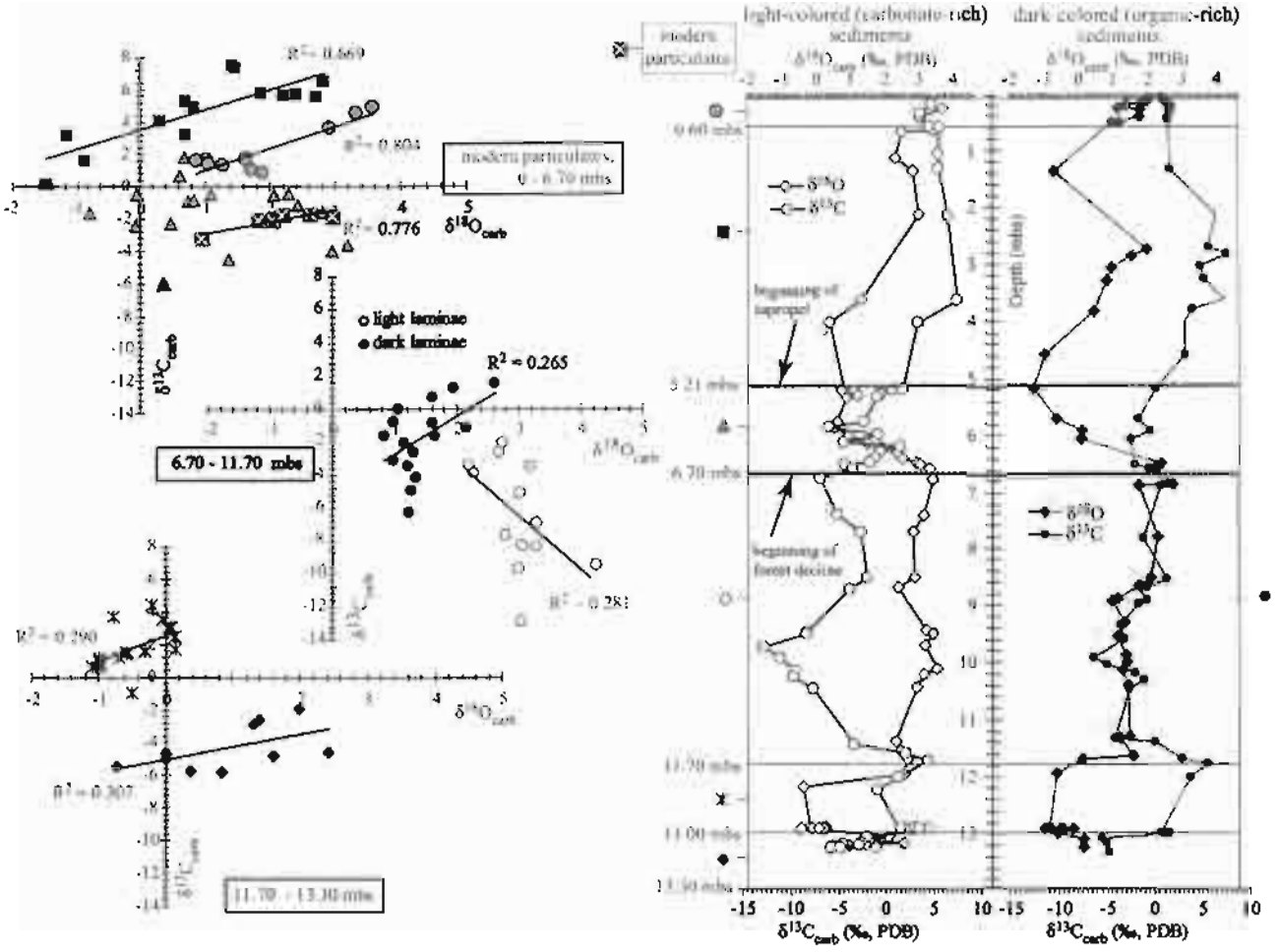

Figure 3.10. $\delta^{18}O_{carb}$ vs. $\delta^{13}C_{carb}$ within six sections along the core. Depths of samples graphed on the left are shown on the vertical axis of the plot on the right: ◆ - 13.30 – 13.00 mbs ; ✳ - 13.00 – 11.70 mbs; ○ - light laminae, 11.70 – 6.70 mbs: ● - dark laminae, 11.70 – 6.70 mbs; △ - 6.70 – 5.21 mbs; ■ - 5.21 – 0.60 mbs, ◉ - 0.60 – 0.00 mbs; ⊠ - modern particulates.

3.4.4.3. 11.70 – 6.70 mbs, particulate $\delta^{13}C$ alteration in the water column –

Carbonate sediments are more enriched in ^{18}O in this interval than in the underlying sediments (Fig. 3.10) as evaporation exceeded new water supply and the $H_2{}^{18}O$:$H_2{}^{16}O$ ratio increased during this period. The light and dark laminae $\delta^{13}C_{carb}$ and $\delta^{18}O_{carb}$ do not plot in the same region as they do in the other sections of the core. Instead, the light laminae carbonate sediments are more depleted in ^{13}C than the dark laminae carbonate sediments in a pattern that indicates diagenetic alteration in sulfate reducing waters. Talbot and Kelts (1990) showed that in sulfate-rich waters, where sulfate reduction is the dominant mechanism for anaerobic organic matter remineralization, diagenesis produces carbonate minerals depleted in ^{13}C relative to the primary material. Sulfate reduction produces HCO_3^- with the same $\delta^{13}C$ value as the organic matter being reduced. Carbonates diagenetically altered in such waters thus have $\delta^{13}C_{carb}$ values approaching that of the organic sediments. Since organic sediments are depleted in ^{13}C relative to the waters they formed in, carbonates undergoing diagenesis in sulfate reducing conditions have $\delta^{13}C_{carb}$ values which plot below the primary $\delta^{13}C_{carb}$–$\delta^{18}O_{carb}$ trend (Talbot and Kelts, 1990).

Furthermore, the reduced $\delta^{13}C_{carb}$ values in this interval are coeval with increased $\delta^{13}C_{org}$ values (Fig. 3.7). If these signals are primary $\delta^{13}C$ values, the $\delta^{13}C_{CO2(aq)}$ of the water would have been -23‰ according to the $\varepsilon_{carbonate\text{-}CO2(aq)}$ of Romanek et al. (1992), and the fractionation of ^{13}C due to organic uptake of $CO_{2(aq)}$, according to the ε_p of Freeman and Hayes (1992) would have been -2.7‰. During the time-series, ε_p in Ordy Pond ranged between +12.8 and +17.1‰ which is typical of marine environments; ε_p can range between +9.4 and +17.7‰ in the Indian Ocean (François, 1993) and between +12.9 and +21.9‰ (V-PDB) in the southern ocean (Popp et al., 1999). Therefore, it is more reasonable that the reduced $\delta^{13}C_{carb}$ and elevated $\delta^{13}C_{org}$ values in these light laminae relative to other sediments were due to alteration of the original signals

according to the explanation of Talbot and Kelts (1990). However, the dark laminae in this interval do not show the same trend. If the dark laminae $\delta^{13}C_{carb}$ is considered a primary value, then ε_p in these dark laminae ranged between +7.5 and +20.6‰ – values which suggest the dark laminae carbonate minerals have not been significantly altered. Therefore, the alteration of the light laminae carbon isotopic values must have occurred prior to sedimentation and is probably not diagenetic (i.e., occurring within the sediments beneath the pond).

The alteration of the particulate carbon isotope values must also have been seasonal because the laminae are varves. Therefore, the $\delta^{13}C$ indicates that during summers the primary carbonate sediments were recrystallized in the presence of intensified organic matter oxidation, presumably in the deeper waters of the pond as the particles settled out. Since anoxia slows organic matter remineralization (Arthur and Sageman, 1994), the lack of diagenesis in the dark laminae is evidence that the winter was a time of greater anoxia throughout the water column. A similar pattern was observed in the modern water column (Fig. 3.8). The modern pond is only 5 m deep, however, and modern summer sediments settle out quickly before they can be altered by organic matter oxidation.

The light laminae carbon signals appear most strongly affected at 9.51 mbs, where the difference between $\delta^{13}C_{carb}$ and $\delta^{13}C_{org}$ is at a minimum (Fig. 3.7). This depth is within an interval (10.48 - 9.46 mbs) where $\delta^{18}O_{carb}$ shows a positive ~1‰ shift to an average value of +3.1‰ (V-PDB; Fig. 3.7). Furthermore, there is also a narrow band of aragonitic sediment at this point; between 10.01 and 9.48 mbs carbonate sediments range between 8 and 80% as aragonite. As discussed for the deepest lacustrine sediments, coeval increases in aragonite and $\delta^{18}O_{carb}$ can be evidence of increased evaporative concentration of water in the pond, perhaps as a result of a reduced water supply. The 9.51 mbs depth dates to approximately 4.1 kya, and though the dating

resolution is poor, this depth is very near the time of O'ahu's mid-Holocene sea level high stand (Grossman and Fletcher, 1998). Initially, and elevated sea level would have flattened the groundwater gradient and reduced the seaward groundwater flowrate within the aquifer. However, dark laminae $\delta^{18}O_{carb}$ are not elevated around 9.51 mbs, which may indicate that in winter the pond $\delta^{18}O_{H2O}$ was controlled by rainfall input which remained unchanged. In conclusion, it appears that the alteration of the primary $\delta^{13}C$ values in these light laminae was related to intensified evaporation within the summer seasons during the mid-Holocene sea level highstand. However, at this point we do not have a clear explanation of how this relationship might have worked.

3.4.4.4. 6.72 – 5.21 mbs, fresh water inundation – Every geochemical signal changes dramatically above 6.72 mbs, the depth where the pollen reveals the first evidence that local forest was in decline. The organic C:N (Fig. 3.7) ratio exceeds 24 above this depth which is evidence of terrestrial organic matter input to the pond (Meyers and Ishiwatari, 1993), possibly from the die-off of the surrounding forest. More dramatically, above 6.72 mbs, $\delta^{18}O_{carb}$ drops steeply concomitant with a steady transition in the carbonate sediments from aragonite back to calcite (Fig. 3.7). By 6.14 mbs – the point at which the organic-rich laminae disappear – carbonate sediments are 100% LMC and $\delta^{18}O_{carb}$ falls to 0‰ (V-PDB). The switch to calcite and the drop in $\delta^{18}O_{carb}$ suggests a large influx of meteoric water. However, the pollen show that the area around the pond shifted to dry grassland fauna (Athens et al., 2002). Deforestation does not appear to be anthropogenic since the earliest evidence of humans, identified by charcoal deposits, was first seen 20 cm above the beginning of forest decline (Athens et al., 2002). Radiocarbon dates place the 6.72 mbs level near 1000 yr BP which is considered a time of falling sea level around O'ahu following the mid-Holocene high stand, or Kapapa stand (Grossman and

Fletcher, 1998). If rainfall remained relatively unchanged, a falling sea level would have steepened the coastal groundwater gradient and increased the fraction of meteoric groundwater around Ordy Pond as the meteoric/marine groundwater mixing zone was shifted towards the sea. The deeper water table would have aridified the soil and driven back a forest already challenged by the arid conditions of 'Ewa Plain. Additional evidence for sea level fall at this time was observed in terrestrial gastropod deposits elsewhere on 'Ewa Plain. Dye and Tuggle (1998) analyzed historical changes in land snail taxa on 'Ewa and noted a decline in diversity consistent with desiccation by a gradually falling water table around 1.0 kya. They found no evidence, however, of impact to the gastropod assemblages with the arrival of Polynesian settlers. Finally, evidence of decreased salinity is seen in the diatom fossil record with the Ordy Pond sediments. Below 6.14 mbs, Athens et al. (2002) found the most abundant diatom species is *Nitzschia frustulum* which prefers saline lacustrine habitats across western North America (Blinn, 1993). Above 6.14 mbs, Athens et al. (2002) found that *Nitzschia frustulum* disappears and the most abundant species is *Cymbella pusilla*, which favors less saline waters than *Nitzschia frustulum* (Blinn, 1993). At 5.90 mbs *Cymbella pusilla* is replaced by *Nitzschia palea* and *Nitzschia amphibian*, both of which prefer fresh water environments (Blinn, 1993).

Between 6.14 and 5.21 mbs, the sedimentary isotopic geochemistry does not provide a clear picture of the pond. At 5.90 mbs the $\delta^{18}O_{carb}$ of the light laminae reach a local minimum, and the carbonate fraction is 100% calcite (Fig. 3.7) indicating a minimum salinity. However, the light and dark layer $\delta^{18}O_{carb}$ values diverge across this interval as the light layer carbonate sediments become more enriched in ^{18}O up core than the dark layers. The inorganic and organic $\delta^{13}C$ values of both layer types do not differ significantly, but they do vary widely. The $\delta^{13}C_{carb}$ and $\delta^{18}O_{carb}$ data (Fig. 3.10) plot near modern values but do not covary. The changes observed

above 6.14 mbs may mark a switch to a more hydrologically open system, but the data in this interval are equivocal.

3.4.4.5. 5.21 – 0.60 mbs, the post-contact era – The transition to sapropelic deposits at 5.21 mbs is the most physically striking transition in the lacustrine sediments. The presence of "historic pollen" at this transition is evidence of the arrival of settlers from Europe and North America and is thought to date to about A.D. 1830 (Athens et al., 2002). Western contact brought widespread change to this part of the island, including cattle ranching, sugar cane plantations, and sisal production in the area immediately around Ordy Pond (Athens et al., 2002). This new agriculture also brought groundwater development and the introduction of phosphorus based fertilizers. Increased phosphorus supply to the pond at this time is seen in the three-fold increase in the sedimentary total phosphorus to inorganic carbon ratio across the sapropel horizon (Fig. 3.11) The phosphorus loading could have elevated productivity, altered the pond's aquatic flora, and created the ten-fold increase in the sedimentation rate (Athens et al., 2002).

The origins of sapropel deposits past and present have received a great amount of attention and have been attributed to one of two basic processes – increased organic matter preservation through anoxia and/or increase aquatic organic matter production (Arthur and Sageman, 1994). Nutrient enrichment experiments made during the time-series showed that phosphorus was the chemical nutrient most limiting to primary productivity in the pond (Chapter I). Therefore, the sapropel formation could have been due to increased POM production in response to phosphorus loading. However, the switch to sapropelic sediments was also accompanied by changes in the biology of the pond. Below 5.21 mbs the diatom assemblage is dominated by pennate species such as *Cymbella pusilla*, *Nitzschia frustulum*, *Nitzschia palea*, and *Nitzschia amphibian* (Athens et al., 2002). However, above 5.21 mbs diatoms are almost

exclusively centric, and the assemblage is dominated by *Chaetoceros muelleri*, *Cyclotella hakanssoniae*, and *Cyclotella meneghiniana* (Athens et al., 2002). Although the diatoms do not form the sapropel, they do indicate major biologic changes.

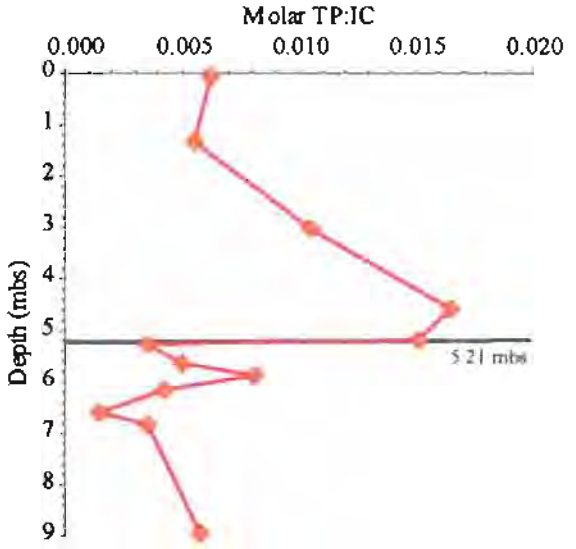

Figure 3.11. Sedimentary molar ratio of total P to inorganic carbon. Phosphorus is evaluated against inorganic carbon to remove dilutional effects changes in the signal caused by changes in the amount of carbonate sediment dilution (i.e., dilution).

The $\delta^{13}C_{carb}$ and $\delta^{18}O_{carb}$ from this interval (Fig. 3.10) have a strong linear correlation and indicate a closed system that behaved much as the pond does today. Elevated surface water temperatures and photosynthetic $^{12}CO_2$ drawdown in the summer seasons produced carbonates more enriched in both $^{13}C_{carb}$ and $^{18}O_{carb}$ than carbonate sediments formed in the winter. This interval has some of the most ^{13}C enriched carbonate sediment of the whole core, which supports the interpretation that the sapropel was partly due to elevated POM production; although the elevated $\delta^{13}C_{carb}$ values may be partly explained by the increased aragonite content (Fig. 3.7) since $\delta^{13}C$ fractionation during aragonite precipitation is ~ 2‰ greater than during calcite

precipitation (Romanek et al., 1992). Nonetheless, both $\delta^{13}C_{org}$ and $\delta^{15}N_{org}$ (Fig. 3.7) are also elevated in this interval and are further evidence of increased POM production.

3.4.4.6. 0.60 – 0.00 mbs, a return to normal? – At the top of the core the sediments show characteristics similar to what was observed in the oldest lacustrine sediments: carbonate-rich layers are more common; there is separation in the $\delta^{13}C_{carb}$ values between sediment layers; and carbonate sediments are more depleted in ^{13}C (Fig. 3.10). Organic sediment is also more depleted in ^{13}C and ^{15}N here than in the deeper sapropelic sediments (Fig. 3.7) indicating reduced phytoplankton productivity. These recent changes in the sedimentary geochemistry appear to be a response to changes in the surrounding area. The pollen record shows that by 3.00 mbs the pond had become reforested with exotic *koa haole*, *kiawe*, and mangrove (Athens et al., 2002). Furthermore, on April 15, 1942, a 3,500 acre area surrounding the pond was converted into the Barbers Point Naval Air Station (Kakesako, 1999). BPNAS brought an end to farming around the pond, and consequently the sedimentary phosphorus content drops significantly in these uppermost sediments (Fig. 3.11).

3.5. CONCLUSIONS

The sedimentary and aquatic biogeochemistry of the modern Ordy Pond is a suitable model for understanding the sediments beneath the pond as a record of changes in the surrounding environment. The inundation of the pond with groundwater elevated by a rising sea level initially produced a pond much like the one today, a shallow pond with no surface water features and impacted by evaporation. Varves and seasonal variability are present in these earliest lacustrine sediments which are very similar to what was seen in the modern pond. As sea level rose the pond became deeper and the sedimentary $\delta^{13}C$ show a departure from modern

conditions. The light laminae indicate carbonate mineral recrystallization in the presence of microbial organic matter oxidation, but the dark laminae sediments appear to retain more of their primary chemical values. The sediments indicate a significant change in the water balance of the pond at 6.72 mbs, or ~ 1 kya. Coeval changes in carbonate mineralogy, carbonate stable isotopic ratios, and the diatom species assemblage reveal an influx of meteoric water at the same time that the surrounding forest was being replaced by more arid-tolerant grasses and shrubs. These changes may have resulted from a 2m drop in sea level around O'ahu following the mid-Holocene highstand (Grossman and Fletcher, 1998) and is supported by contemporaneous changes in the local terrestrial gastropod assemblage (Dye and Tuggle, 1998).

It does not appear that these changes could have been caused by anthropogenic impacts, especially since the earliest evidence in the core of a human presence is 20 cm above where evidence of environmental changes are first observed. Finally, a major change is recorded in the sediments at the same point as the first evidence of Western contact in the area. Above 5.21 mbs, (1830 AD), the sediments become sapropelic possibly as a result of changes in the biology of the pond from the introduction of phosphorus fertilizers. The most recent sediments indicate that the pond is now returning to a state similar to its earliest period, perhaps the result of the reestablishment of a local forest of exotic species and the end of local agriculture with the commission of Barbers Point Naval Air Station in 1942; BPNAS was decommissioned in 1999.

3.6. ACKNOWLEDGEMENTS

This study was funded in part by a grant from the National Oceanic and Atmospheric Administration, project #XXXXX, which is sponsored by the University of Hawai'i Sea Grant College Program, SOEST, under Institutional Grant No. NA86RG0041 from NOAA Office of Sea Grant, Department of Commerce. The views expressed herein are those of the authors and do not necessarily reflect the views of NOAA or any subagencies. This is University of Hawai'i SOEST contribution #XXXX and Sea Grant Publication #UNIHI-SEAGRANT-XX-00-XX. Additional funding for this research was provided by Sigma Xi as a Grants-in-Aid award for graduate research, by the Geologic Society of America as a graduate research award, and by William T. Coulbourn and Harold T. Stearns Fellowship awards from the Department of Geology and Geophysics at the University of Hawai'i, Mānoa. Additional thanks go to Ellen Schulz who provided the sedimentary phosphorus analyses as part of the NSF Research Experience for Undergraduates program at the University of Hawai'i under the supervision of Fred T. Mackenzie.

3.7. REFERENCES

Arthur, M.A., and Sageman, B.B., 1994, Marine black shales: Depositional mechanisms and environments of ancient deposits: Annual Reviews of Earth and Planetary Sciences, v. 22, p. 499-551.

Aspila, K.I., Agemian, H., and Chau, A.S.Y., 1976, A semi-automatic method for determination of inorganic, organic, and total phosphate in sediments.: Analyst, v. 101, p. 187-197.

Athens, J.S., Tuggle, H.D., Ward, J.V., and Welch, D.J., 2002, Avifaunal extinctions, vegetation change, and Polynesian impacts in prehistoric Hawai'i: Archeologica Oceania, v. 37, p. 57-78.

Bischoff, J.L., Bishop, F.C., and Mackenzie, F.T., 1983, Biogenically produced magnesian calcite: inhomogeneities in chemical and physical properties; comparison with synthetic phases: American Mineralogist, v. 68, p. 1183-1188.

Bischoff J. L., Mackenzie F. T., and Bishop F. C. (1987) Stabilities of synthetic magnesian calcites in aqueous solution: Comparison with biogenic materials. *Geochimica et Cosmochimica Acta* **51**, p. 1413-1423.

Blinn, D.W., 1993, Diatom community structure along physicochemical gradients in saline lakes: Ecology, v. 74, p. 1246-1263.

Cannon, W.F., and Force, E.R., 1983, Potential for high-grade shallow-marine manganese deposits in North America, *in* Shanks, I., W.C, ed., Cameron Volume on Unconventional Mineral Deposits: New York, Society of Mineral Engineers, p. 175-189.

Chivas, A.R., De Deckker, P., Cali, J.A., Chapman, A., Kiss, E., and Shelley, J.M.G., 1993, Coupled stable-isotope and trace-element measurements of lacustrine carbonates as paleoclimatic indicators, *in* Savin, S., ed., Climate Change in Continental Isotopic

Records: Geophysical Monograph: Washington, D.C., American Geophysical Union, p. 113-121.

Davies, C.W., 1962, Ion Association: London, Butterworths, 190 p.

Dye, T., and Tuggle, H.D., 1998, Land snail extinctions at Kalaeloa: Pacific Science, v. 52, p. 111-140.

Emiliani, C., 1955, Pleistocene temperatures: Journal of Geology, v. 63, p. 538-578.

Epstein, S., Buchsbaum, R., and Lowenstam, H., 1953a, Carbonate-water isotopic temperature scale: Geological Society of America Bulletin, v. 62, p. 417-425.

Epstein, S., Buchsbaum, R., Lowenstam, H.A., and Urey, H.C., 1953b, Revised carbonate water isotopic temperature scale: Geological Society of America Bulletin, v. 64, p. 1315-1326.

François, R., 1993, Changes in the $\delta^{13}C$ of surface water particulate organic matter across the subtropical convergence in the SW Indian Ocean: Global Biogeochemical Cycles, v. 7, p. 627-644.

Freeman, K.H., and Hayes, J.M., 1992, Fractionation of carbon isotopes by phytoplankton and estimates of ancient CO_2 levels: Global Biogeochemical Cycles, v. 6, p. 185-198.

Frondel, C., and Bauer, L.H., 1955, Kutnahorite: a manganese dolomite, $CaMn(CO_3)_2$: American Mineralogist, v. 40, p. 748-760.

Glenn, C.R., and Kelts, K., 1991, Sedimentary Rhythms in Lake Deposits, *in* Seilacher, A., ed., Cycles and Events in Stratigraphy: Berlin Heidelberg, Springer-Verlag, p. 188-221.

Grossman, E.E., and Fletcher, C.H., III, 1998, Sea level higher than present 3500 years ago on the northern main Hawaiian Islands: Geology, v. 26, p. 363-366.

Hollander, D.J., 1989, Carbon and nitrogen isotopic cycling and organic geochemistry of eutrophic lake Greifen: Implications for preservation and accumulation of ancient organic

- carbon - rich sediments [unpublished Ph.D. thesis]: Switzerland: Eigenoissche Technische Hochschule, Zurich, 318 p. p.

Huckenridge, H., and Meischner, D., 1996, Origin and environment of manganese-rich sediments within black-shale basins: Geochimica et Cosmochimica Acta, v. 60, p. 1399-1413.

James, N.P., and Choquette, P.W., 1983, Diagenesis 5. Limestones: Introduction: Geoscience Canada, v. 10, p. 159-161.

Kakesako, G.K., 1999, Goodbye Barbers Point, Honolulu Star-Bulletin: Honolulu, p. A-1, -8.

Kemp, A.E.S., 1996, Laminated sediments as palaeo-indicators, *in* Kemp, A.E.S., ed., *Paleoclimatology and Paleoceanography from Laminated Sediments*: London, Geological Society Special Publication No. 116, p. vii-xii.

Kim, S.-T., and O'Neil, J.R., 1997, Equilibrium and nonequilibrium oxygen isotope effects in synthetic carbonates: Geochimica et Cosmochimica Acta, v. 61, p. 3461-3475.

Ku, T.-L., Kimmel, M.A., Easton, W.H., and O'Neil, T.J., 1974, Eustatic sea level 120,000 years ago on Oahu, Hawaii: Science, v. 183, p. 95a.

Laws, E.A., Popp, B.N., Bidigare, R.R., Kennicutt, M.C., and Macko, S.A., 1995, Dependence of phytoplankton carbon isotopic composition on growth rate and [CO2]aq: Theoretical considerations and experimental results: Geochimica et Cosmochimica Acta, v. 59, p. 1131-1138.

Li, H.-C., and Ku, T.-L., 1997, $\delta^{13}C$-$\delta^{18}O$ covariance as a paleohydrological indicator for closed-basin lakes: Palaeogeography, Palaeoclimatology, Palaeoecology, v. 133, p. 69-80.

McCrea, J.M., 1950, On the isotopic chemistry of carbonates and a paleotemperature scale: Journal of Chemical Physics, v. 18.

Meyers, P.A., and Ishiwatari, R., 1993, The early diagenesis of organic matter in lacustrine sediments, *in* Macko, S.A., ed., Organic Geochemistry: New York, Plenum, p. 185-209.

Mucci, A., 1991, The solubility and free energy of formation of natural kutnahorite: Canadian Mineralogist, v. 29, p. 113-121.

Muhs, D.R., and Szabo, B.J., 1991, New uranium-series ages of the Waimanalo Limestone, Oahu, Hawaii, and paleoclimatic implications for the last interglacial period: Geological Society of America Abstracts with Programs, v. 23, p. A239.

Müller, G., Irion, G., and Förstner, U., 1972, Formation and diagenesis of inorganic Ca-Mg carbonates in the lacustrine environment: Naturwissenschaften, v. 59, p. 158-164.

Popp, B.N., Trull, T., Kenig, F., Wakeman, S.G., Rust, T.R., Tilbrook, B., Griffiths, F.B., Wright, S.W., Marchant, H.J., Bidigare, R.R., and Laws, E.A., 1999, Controls on the carbon isotopic composition of Southern Ocean Phytoplankton: Global Biogeochemical Cycles, v. 13, p. 826-843.

Romanek, C.S., Grossman, E.L., and Morse, J.W., 1992, Carbon isotopic fractionation in synthetic aragonite and calcite: effects of temperature and precipitation rate: Geochimica et Cosmochimica Acta, v. 56, p. 419-430.

Round, F.E., Crawford, R.M., and Mann, D.G., 1990, The Diatoms: Biology & Morphology of the Genera: New York, Cambridge University Press, 747 p.

Sabine, C.L. and Mackenzie, F. T. 1995, Bank-derived carbonate sediment transport and dissolution in the Hawaiian Archipelago: Aquatic Geochemistry, v. 1, p. 189-230.

Scholl, M.A., Gingerich, S.B., and Tribble, G.W., 2002, The influence of microclimates and fog on stable isotope signatures used in interpretation of regional hydrology: East Maui, Hawaii: Journal of Hydrology, v. 264, p. 170–184.

Scholl, M.A., Ingebritsen, S.E., Janik, C.J., and Kauahikaua, J.P., 1996, Use of precipitation and ground water isotopes to interpret regional hydrology on a tropical volcanic island: Kilauea volcano area, Hawaii.: Water Resources Research, v. 32, p. 3525-3537.

Sherman, C.E., Glenn, C.R., Jones, A.T. , Burnett, W.C. , Schwarcz, H.P., 1993, New evidence for two highstands of the sea during the last interglacial, oxygen isotope substage 5e: Geology, v. 21, p. 1079-1082.

Stearns, H.S., 1974, Submerged shorelines and shelves in the Hawaiian Islands and a revision of some of the eustatic submerged shorelines: Geological Society of America Bulletin, v. 85, p. 795-804.

Swart, P.K., Burns, S.J., and Leder, J.J., 1991, Fractionation of the stable isotopes of oxygen and carbon in carbon dioxide during the reaction of calcite with phosphoric acid as a function of temperature and technique: Chemical Geology (Isotope Geosciences Section), v. 86, p. 89-96.

Szabo, B.J., Ludwig K.R., Muhs, D.R., Simmons, K.R., 1994, Thorium-230 Ages of Corals and Duration of the Last Interglacial Sea-Level High Stand on Oahu, Hawai'i: Science, v. 266, p. 93-96.

Talbot, M.R., 1990, A review of the palaeohydrological interpretation of carbon and oxygen isotopic ratios in primary lacustrine carbonates: Chemical Geology, v. 80, p. 261-279.

Talbot, M.R., and Kelts, K., 1990, Paleolimnological signatures from carbon and oxygen isotopic ratios in carbonates from organic carbon-rich lacustrine sediments, *in* Katz, B.J., ed., Lacustrine Basin Exploration. Case Studies and Modern Analogs: Tulsa, OK, American Association of Petroleum Geologists Memoir 50, p. 99-112.

Tribble, J.S., Garrison, G.H., Stens, J.S., Skillbeck, C.G., and Frankel, E., 1999, Evidence for early-mid Holocene sea level on O'ahu, Hawai'i from coastal pond sediments: The non-steady state of the inner shelf and shoreline: Coastal change in the times scale of decades to millennia in the late Quaternary.

Tsusue, A., 1967, Manganese kutnahorite from Ryujima mine, Japan: American Mineralogist, v. 52.

Tucker, M.E., and Wright, V.P., 1990, Carbonate Sedimentology: Oxford, Blackwell Scientific Publications, 482 p.

Wolery, T.J., 1992, EQ3NR, A computer program for geochemical aqueous speciation-solubility calculations: Oak Ridge, TN, Lawrence Livermore National Laboratory.

CHAPTER IV.

MEASUREMENT OF SUBMARINE GROUNDWATER DISCHARGE IN KAHANA BAY, O'AHU, HAWAI'I

ABSTRACT

Submarine groundwater discharge (**SGD**) is neither well understood nor commonly investigated in Hawai'i, but it is recognized as a potential pollutant source to coastal environments. Between 1998 and 2000, this study located and quantified both total SGD and the terrestrial SGD fraction (f_{TGW}) in Kahana Bay, O'ahu. CTD casts were used to profile the water structure and identify potential areas of SGD impact in the bay. Lee-type seepage meters were used to measure SGD rates and collect samples of SGD directly. Radon-222, Si, Cl^-, and total alkalinity (TA) were used as natural tracers to measure the terrestrial groundwater fraction within SGD. Nutrient concentrations were also measured to calculate total nutrient fluxes into the bay via SGD. Ninety percent of the SGD in Kahana Bay occurs in the inner bay within 1 km of the shoreline. The average total SGD flux measured was 90×10^6 L d^{-1}, 16% of which was terrestrial groundwater. By comparison, the average annual surface runoff from Kahana River is 90.7×10^6 L d^{-1}. Estimated fluxes of total dissolved phosphorus and nitrogen by SGD to the bay were 500% and 200% greater than fluxes via surface runoff, respectively. Thus, SGD in Kahana Bay has proved to be a significant source of both fresh water and total nutrient input comparable to that from the surface runoff of Kahana River.

4.1. INTRODUCTION

Submarine groundwater discharge (**SGD**) is the seepage of any fluids from coastal submarine sediments into the overlying coastal ocean. In this respect, coastal submarine sediments act as a subterranean estuary, an aquifer separate unto itself with a unique chemistry distinguishing it from either the meteoric or marine hydrologic systems (Moore, 1999). SGD is neither well understood nor commonly investigated in Hawai'i. However, SGD has recently become recognized as a potential pollutant source because it can include meteoric groundwater anywhere a terrestrial aquifer with positive head is in contact with the shoreline. In 1997, the Scientific Committee on Oceanic Research (SCOR) and the International Geosphere-Biosphere Program (IGBP) established Working Group 112 "to define... how SGD influences chemical and biological processes in the coastal ocean." Detailed research along the eastern seaboard of North America, the Caribbean, and the Gulf of Mexico has found SGD to be both present and often a startlingly significant aspect of coastal marine environments (Cable et al., 1996b; Moore, 1996; Corbett et al., 1999). Such findings are reason to give chemical oceanographers pause when evaluating the evolution of the global ocean (Moore, 1999).

One of the goals of this research reported here was to find if SGD could be recognized and quantified in a volcanic island setting. The fractured basalt/caprock structure along the coasts of O'ahu produces abundant meteoric groundwater supplies, and SGD is believed to play an important, though poorly understood, role (Takasaki et al., 1969; Lau, 1973; Kay et al., 1977). We furthermore sought to specifically identify the terrestrial groundwater fraction of SGD in light of its potential as a conduit of anthropogenic impact. There is concern that sewage-impacted SGD may provide an artificial nutrient supply, encouraging non-coral communities to flourish, and threatening reef-building corals with asphyxiating algae (Hallock and Schlager, 1986).

4.1.1. The Kahana Bay system - example of a coastal Hawaiian environment

The meteoric groundwater of O'ahu consists primarily of a Ghyben-Herzberg lens impounded within the island by a layer of caprock. Caprock is a regional term for the semi-impermeable calcareous reefal and volcanic alluvial deposits which overlie and confine the basaltic bedrock around the coastal edge of the island (Stearns and Vaksvik, 1935; Takasaki et al., 1969; Hunt, 1996). It is this caprock/floating lens system which has formed the large meteoric groundwater reservoir that supports O'ahu's urban development. Our hypothesis is that SGD from the system can be identified chemically within the overlying marine waters by naturally occurring tracers. The presence of elevated ^{222}Rn and Si relative to off-shore marine waters is considered evidence of SGD since both tracers are more concentrated in terrestrial groundwaters due to ^{238}U decay and silicate mineral dissolution (Cable et al., 1996a; Corbett et al., 1999). Conversely, dilution of dissolved Cl^- and total alkalinity (TA) relative to marine water is also considered evidence of SGD because these constituents are an order of magnitude less concentrated in Hawaiian meteoric groundwaters (Li, 1988).

Kahana Bay (Fig. 4.1) was selected as the study site because it is undeveloped and there is abundant rainfall in the adjacent valley; the valley receives over 500 cm of rain annually (Takasaki et al., 1969). Kahana Bay is the submarine extent of Kahana Valley, a deeply incised drainage in the Ko'olau Range extending 6.44 km back from the shoreline. The bay is characterized by a paleochannel bordered by two 10+ m vertical walls of Pleistocene coral-algal reef (Fig. 4.1). Within the channel, sediments are >10 m thick, and rudimentary seismic work observed two reflectors below the sediment surface, presumably an old reef surface or valley floor underlain by the basalt of the Ko'olau Range (Coulbourn et al., 1974). The topography and

bathymetry of the valley, bay, and offshore canyons reveal their pre-Pleistocene formation during 100+ m lower sea level stands (Coulbourn, 1971; Coulbourn et al., 1974).

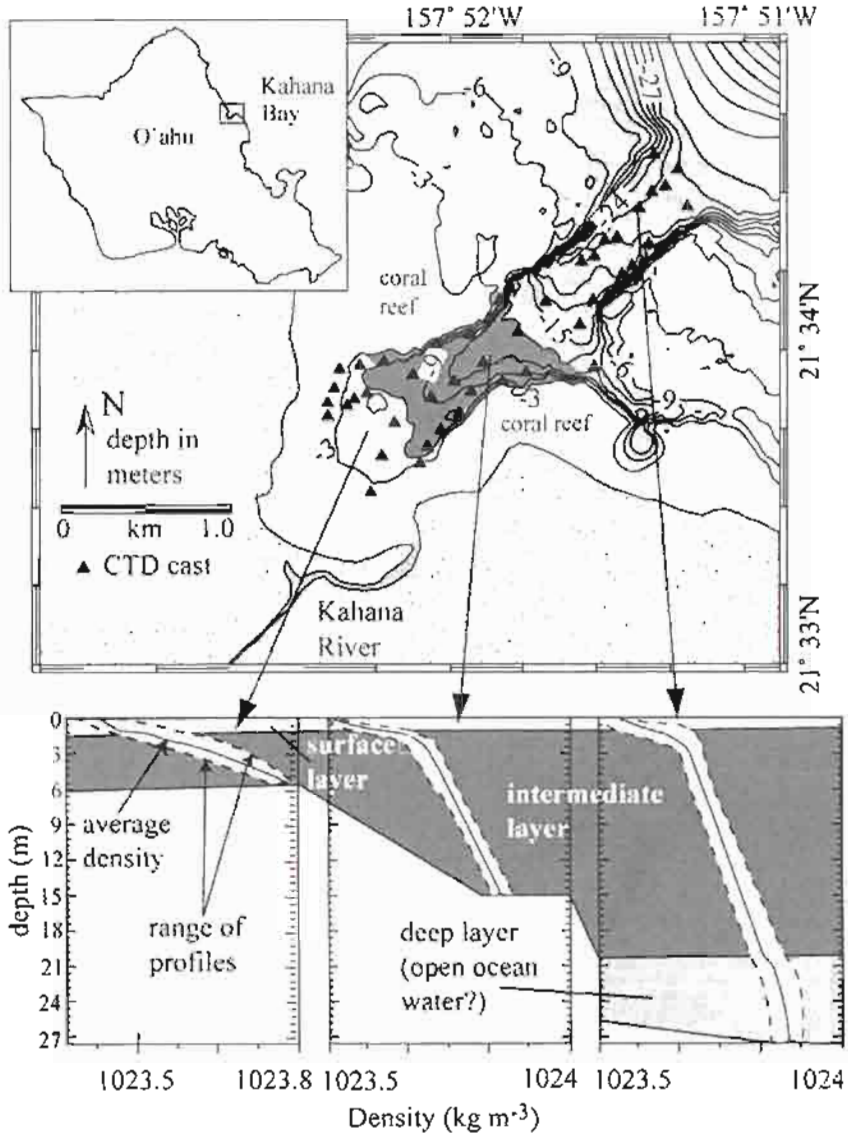

Figure 4.1. Map showing the location of Kahana Bay on the windward coast of O'ahu. Kahana Valley extends to the southwest. CTD sample locations are plotted on the map, and the density profiles from the inner, middle, and outer bays are shown below. The white swaths show the breadth of the density profiles within each area of the bay, while the solid line in each swath is the average of the profiles. The surface layer is formed by water from the Kahana River and becomes thinner and more saline farther from the river mouth. The intermediate layer has fairly constant salinity and may be due to seepage from the coastal aquifer.

Within the valley, there are three basic geologic units. The Ko'olau range, which forms and surrounds Kahana Valley, is the erosional remnant of the basaltic Ko'olau shield volcano. It is the Ko'olau basalts which serve as a Ghyben-Herzberg aquifer for the eastern half of the island (Stearns and Vaksvik, 1935), and in Kahana Valley it is identified by the Hawaiian Aquifer Code Nos. 306022212 and 306022122 (Mink and Lau, 1987). Dike-filled Ko'olau basalts, such as are found in Kahana Valley, have hydraulic transmissivities which range between 3×10^{-4} and 2×10^{-3} $m^2 s^{-1}$ (Takasaki et al., 1969). In the lower reaches of Kahana Valley, the Ko'olau basalts are overlain and confined by a sedimentary unit of weathered basaltic talus and alluvium. The unit is exposed from the head of the valley at 100 m elevation down to an elevation of 9 m, 1.5 km from the shore. This unit forms a separate aquifer identified by the Hawaiian Aquifer Code No. 30602116 (Mink and Lau, 1987), and well logs show this unit to be 49 m thick near the shoreline (Takasaki et al., 1969). The unit is believed to be at least Pleistocene in age based on its stratigraphy and elevation and is here referred to as the Pleistocene alluvium. Similar weathered alluvial units on O'ahu have transmissivities in the range of 10^{-6} $m^2 s^{-1}$ (Takasaki et al., 1969). At the mouth of Kahana Valley the Pleistocene alluvium is overlain by a younger and less lithified sedimentary deposit consisting of terrestrial alluvium and calcareous sands (Takasaki et al., 1969; Lau, 1973). The top of this unit reaches 9 m elevation, which was the approximate height of sea level on O'ahu during the mid-Holocene sea level high stand (Stearns, 1974; Grossman and Fletcher, 1998a). The unit forms the beach around Kahana Bay, is believed to be entirely Holocene in age, and is referred to here as the Holocene alluvium. According to the unpublished drilling log of USGS Well #405, located 100 m from the edge of the bay, the Holocene alluvium is approximately 15 m thick and reaches an elevation of -6 m near the shoreline (C. Lao, Honolulu Board of Water Supply). There is no hydraulic data on this unit, but it has greater

porosity and is less weathered than the Pleistocene alluvium and is believed to have a greater transmissivity. The last 3 km of the Kahana River are contained entirely within this unit.

In this paper the bay is described in three areas, illustrated in Figure 4.1: 1) the inner bay (water depths up to ~ 6 m, within ~ 1 km of the shore); 2) the middle bay (6 - 15 m depth, 1 - 2 km from shore); and 3) the outer bay (15+ m depth). The inner bay is the area that overlays the Holocene alluvium, which is not believed to extend beyond a water depth of 6 m. This depth is also believed to be the depth of closure for the Kahana Bay beach system. The depth of beach closure is the point farthest from shore beyond which sea floor sediments are not significantly influenced by surface energy, as defined by Komar (1998). Closure depth is estimated at Kahana based upon grain size measurements (Coulbourn, 1971), greatest annual ocean swell heights, and observations of the seafloor over the course of the study. The seaward extent of the middle bay was defined by the depths at which the intermediate water mass (as measured by preliminary CTD surveys) is no longer in contact with the seafloor, while the most seaward portion of Kahana is considered the outer bay.

4.2. METHODS

4.2.1. Sampling techniques

Field work was performed during the spring and summer months of 1998-2000, avoiding the high wave events for which the north-facing shores of O'ahu are famous. In January and February of 1998, a Sea Bird SEACAT conductivity, temperature, and depth (CTD) profiler was used to measure the physical water structure of Kahana Bay. These profiles were used to identify the areas with the highest potential for meteorically impacted SGD.

Typical Lee-type seepage meters were used both to measure SGD rates (Lee, 1977) and to collect waters seeping from the seafloor for chemical analyses, as described below. By

sampling waters directly from the chambers we were able to collect discrete SGD samples that were isolated from ambient water in the bay. Thus, wherever SGD chemical concentrations are discussed in this paper, we are referring to analyses made directly on waters collected in the meters. This is particularly important in isolating SGD characteristics from those of waters coming from the Kahana River. The Plexiglas hemispherical chambers used as seepage meters measure 43 cm in diameter, 0.15 m^2 in footprint area, 19 cm in height, and 19.4 L in volume. Each meter was fitted with a 1.9 cm exit port at its apex to which HDPE sampling bags were attached. At each sampling period the chambers were sunk into the seafloor 7-10 cm and left for at least 24 h to allow SGD equilibration and displacement of marine waters trapped in the chambers by SGD. Seepage was measured 1 to 4 times per tidal half-cycle (high-to-low tide, or vice versa) depending on the seepage rate. A control meter was also installed to assess potential artifacts during the sampling periods due to such phenomena as wave action. The control meters were identical to the regular seepage meters except that they were installed within a half-buried sediment-filled plastic kiddie pool. Any fluid exchange into or out of the control meters could not be due to SGD. In general, the control measurements found no significant artificial fluid flux, and the largest fluid flux measured in a control meter was less than 1% of the average SGD measured.

At the beginning of each sampling period, 1.00 L of ultrapure deionized water (18+ MΩ resistance) was added to each sampling bag to prevent anomalous influx (Shaw and Prepas, 1989; Cable et al., 1997). Prefilling also provides a volume of water that allows measurement of seepage into the seafloor sediments. Before collection, valves at the base of each bag were closed, the time recorded, and the bag removed and brought to shore. Once the samples were brought to shore the sampled waters were transferred to both the 4 L radon bottles (avoiding atmospheric exposure) and 125 ml HDPE bottles for return to the University of Hawai'i

laboratories. The radon bottles were evacuated 4L amber glass jars sealed with #6 stoppers and marine grade silicon sealant and fitted with tygon sampling tubes. These gas tight vessels, originally designed by the SGD group at Florida State University, can be directly attached to the radon extraction system with a reduced risk of sample loss.

In order to calculate the meteoric and marine mixing fractions in the fluids sampled from the seepage meters, water samples were collected from the bottom water surrounding the meters. These samples were used for the marine water end-member tracer concentrations (C_{MW}) for mixing calculations as listed in Table 4.1. Water samples were also collected from four piezometers installed in the Holocene alluvium at the mouth of the valley and from wells screened in the Pleistocene alluvium (HBWS well # 3453-07) and in the Ko'olau basalt bedrock (USGS well #W405). The piezometers consisted of 4.5 cm OD slotted PVC casings driven directly into the soil to a depth approximately 1.5 m below the groundwater table. The piezometer and well samples were used for the terrestrial groundwater end-member tracer concentrations (C_{SGD}) for mixing calculations as listed in Table 4.1.

TABLE 4.1: End-member concentrations and average calculated f_{TGW} for SGD in the inner and middle bays using different tracers.

4.1a. Inner Bay

TGW end-member – Holocene alluvium groundwater

MW end-member – inner bay ambient water

Tracer	Average C_{SGD}	Average C_{MW}	Average C_{TGW}	Average f_{TGW}
Cl^- (mmol L^{-1})	451.99 ± 2.16	546.43 ± 2.61	15.59 ± 4.19	0.2 ± 0.06
	n =10	n = 12	n = 4	
TA (meq L^{-1})	1.888 ± 0.009	2.174 ± 0.677	0.526 ± 0.164	0.2 ± 0.1
^{222}Rn (dpm L^{-1})	8.93 ± 0.71	1.48 ± 0.13	64.22 ± 14.16	0.1 ± 0.01
Si (mmol L^{-1})	9.90 ± 1.92	2.68 ± 1.02	175.41 ± 35.98	0.04 ± 0.01

4.1b. Middle Bay

TGW end-member – averages of the Pleistocene alluvium and Ko'olau basalt groundwaters
MW end-member – middle bay ambient water

Tracer	Average C_{SGD}	Average C_{MW}	Average C_{TGW}	Average f_{TGW}
Cl^- (mmol L^{-1})	546.10 ± 2.61 n = 17	547.63 ± 2.41 n = 35	4.94 ± 1.27 n = 8	0.003 ± 0.01
TA (meq L^{-1})	2.224 ± 0.011	2.247 ± 0.021	0.506 ± 0.040	0.009 ± 0.01
^{222}Rn (dpm L^{-1})	3.68 ± 1.52	2.10 ± 1.04	412.77 ± 295.58	0.003 ± 0.01
Si (mmol L^{-1})	9.30 ± 4.92	2.10 ± 1.40	621.44 ± 2.64	0.01 ± 0.01

C_{SGD} = SGD tracer concentration measured in fluids emanating from seepage meters
C_{MW} = mean tracer concentration in marine water surround the dome
C_{TGW} = mean tracer concentration in terrestrial groundwater source
f_{TGW} = the fraction of SGD as terrestrial groundwater

4.2.2. Analytical chemistry

Nutrient samples were filtered, frozen, and sent for analysis to either the SOEST Analytical Services (Ted Walsh, U. Hawai'i) or to the Marine Laboratory Facilities at the University of Washington (Kathy Krogslund). In either case, measurements were made using standard spectrophotometric flowthrough autoanalysis. Cl^- was measured titrimetrically with 0.1 mmol L^{-1} $AgNO_3$, a modification of the Mohr-Knudsen technique (e.g., Grasshoff et al., 1983). Total alkalinity (TA) was determined by Gran titration with a solution of 0.09553 mol HCl per kg of 600 mmol L^{-1} NaCl solution, and titrations were made with a Brinkmann Metrohm 655 Dosimat autotitrator. Radon-222 was measured using the technique described by Mathieu (Appendix I of Biscaye et al., 1976), modified such that the extracted radon was trapped in a stainless steel column placed in a bath of liquid nitrogen. Radon-222 decay was measured photometrically on an Applied Techniques Co. AC/DC-DRC-MK10-2 counting unit. Radon-222 concentrations were corrected for instrument and counter blanks, cell backgrounds, and radioactive decay between the sampling time and the end of scintillation counting.

4.2.3 Mixing calculations

Conservative chemical tracers were used to calculate mixing between marine and terrestrial waters using a simple mixing model:

$$C_{SGD} = (f_{TGW} \cdot C_{TGW}) + (f_{MW} \cdot C_{MW}) \qquad (1)$$

$$f_{MW} = 1 - f_{TGW} \qquad (2)$$

$$f_{TGW} = (C_{SGD} - C_{MW}) / (C_{TGW} - C_{MW}) \qquad (3)$$

where: C_{SGD} = SGD tracer concentration measured in fluids emanating from seepage meters

C_{TGW} = mean tracer concentration in terrestrial groundwater source

f_{TGW} = the fraction of SGD as terrestrial groundwater

C_{MW} = mean tracer concentration in marine water surrounding the dome

f_{MW} = the fraction of SGD as marine water

4.3. RESULTS

Figure 4.1 illustrates CTD cast locations and averaged density profiles from the inner, middle, and outer parts of the bay. The profiles reveal a three-layered water structure in the bay: 1) a light surface layer, up to 3 m thick, ranging in density between 1022.75 and 1023.67 kg m^{-3}; 2) an intermediate layer 10-20 m thick with an average density of 1023.75 kg m^{-3}; and 3) a bottom layer with a density averaging 1023.88 kg m^{-3}. Figure 4.2 shows the contoured profiles of dissolved ^{222}Rn, Si, and Cl^- in water samples collected from the ambient waters of Kahana Bay. Along the beach face ^{222}Rn and Si are enriched and Cl^- depleted, relative to offshore marine water. Within the middle bay are other areas of ^{222}Rn and Si enrichment and Cl^- depletion. These areas are smaller and not continuous with the inner bay waters.

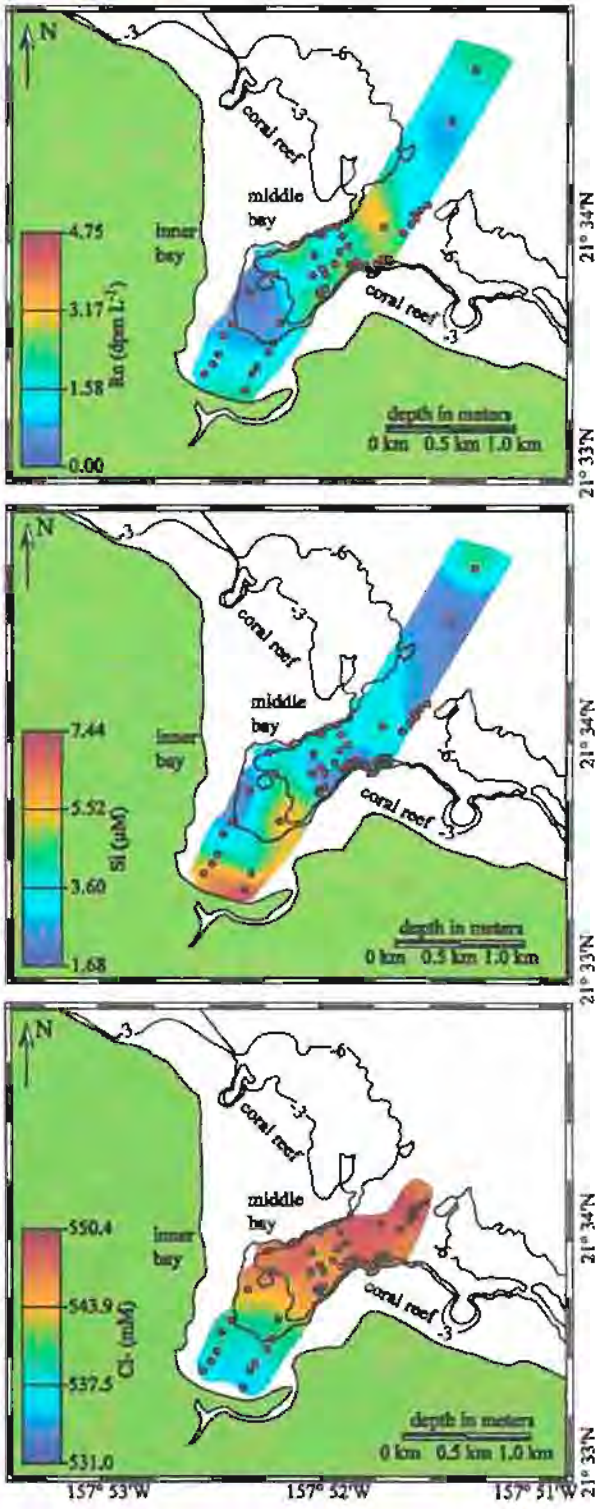

Figure 4.2. Contour plots of measured ^{222}Rn, Si, and Cl^- concentrations from ambient water samples. Sample location are indicated by the filled circles.

On a daily time scale, SGD rates are driven by sea level and tidal cyclicity. Figure 4.3 shows a plot of discharge rate from inner bay station D5 over the course of a tidal cycle on 15 April 2001. Also shown are sea level data taken from NOAA tide measurements at Honolulu Harbor and corrected for amplitude and arrival time at Kahana Bay. There is a clear inverse correlation between the two as maximum discharge rates were measured during the lowest tide level. This is not surprising, as the hydraulic gradient across the submarine aquifer will be steepest during low tide. There is also a time lag between the peak tides and the peak seepage rates.

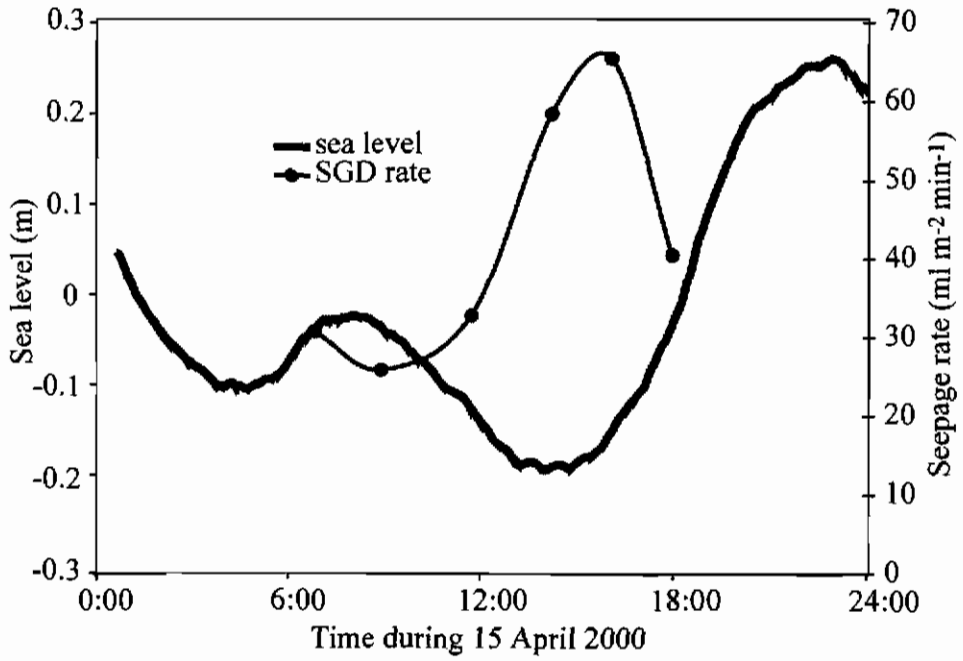

Figure 4.3. Seepage rates measured from seepage meter station D5 plotted over time on 15 April 2001. Also plotted is sea level during 15 April 2001. Sea level data come from NOAA and the amplitude and timing are corrected for Kahana Bay. Station D5 is located in the inner bay, at lat. 22.559750° N and long.157.870800° W, and at a water depth of 3.1 m.

^{222}Rn, Si, and TA are plotted separately against Cl^- in Figure 4.4 for the waters sampled from the seepage meters, while the expanded panel highlights the results from just the middle bay seepage meters. The elevated terrestrial groundwater seepage into the inner bay can be seen in the depleted Cl^- and TA and enriched ^{222}Rn and Si SGD concentrations relative to the middle bay. Furthermore, in both parts of the bay there is a strong linear correlation (R^2=0.987) between SGD Cl^- and TA, indicating that these constituents behave conservatively throughout the study area. Radon-222 and Si, however, behave differently between waters seeping into the inner bay versus the middle bay. Within the middle bay, ^{222}Rn and Si both trend inversely with Cl^- (R^2 = 0.7475 and 0.5391, respectively), while in the inner bay there is no discernable relation between either ^{222}Rn or Si and Cl^- ($R^2 < 0.1$).

Table 4.1 lists the end-member data used to calculate the fraction of terrestrial groundwater in the SGD. The table lists the arithmetically averaged tracer concentrations of Cl^-, TA, ^{222}Rn, and Si measured in the seepage meters (C_{SGD}), the ambient waters (C_{MW}), and the terrestrial groundwaters (C_{TGW}) for a) the inner bay and b) the middle bay. The fourth column of both tables is the average terrestrial groundwater fraction (f_{TGW}) measured in fluids emanating from the seepage meters using each tracer and Eq. (3); the f_{TGW} numbers listed are the average of values calculated for each seepage meter sample using the average C_{MW} and C_{TGW} end-member numbers. For the inner bay, the end-members used were the ambient water of the inner bay and the Holocene alluvium groundwater data. For the middle bay, the end-members chosen were the ambient water of the middle bay and the averaged Ko'olau basalt and Pleistocene alluvium groundwater data. Cl^- is considered the most conservative of all four and should most closely reflect the actual terrestrial fraction. Table 4.2 lists the expected and measured values of both tracer and nutrient concentrations in SGD using the f_{TGW} calculated

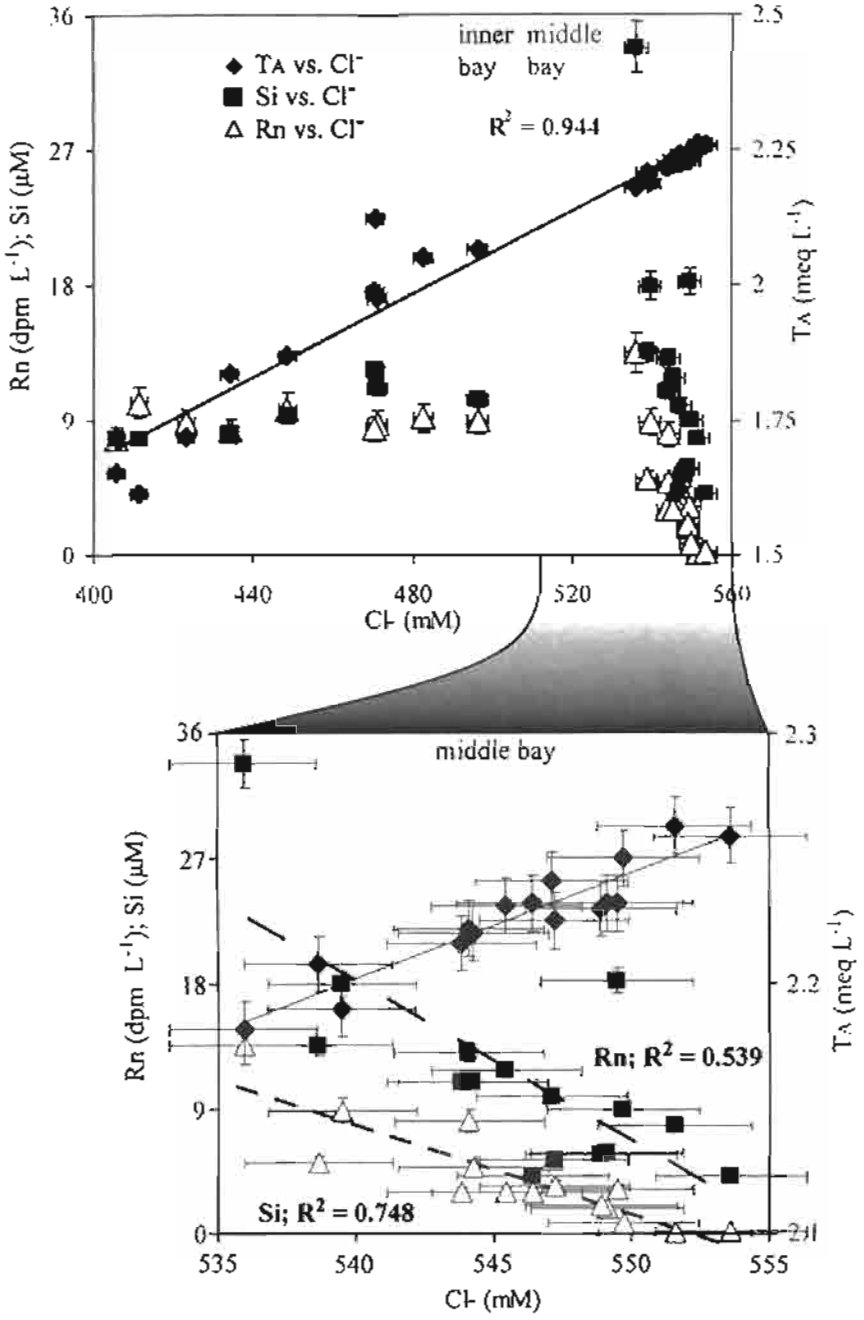

Figure 4.4. TA, ^{222}Rn, and Si plotted against CL^- for SGD water collected from seepage meters in Kahana Bay. The upper panel is data from all samples collected, while the lower panel is an expansion of the data only from those chambers placed in the middle bay. Notice that TA and Cl^- trend positively in all areas of the bay, while ^{222}Rn and Si trend inversely with Cl^- only in the middle bay.

using Cl^- in Eq. (3); the end-members are listed in Table 4.1. In the inner bay SGD, f_{TGW} calculated with TA and Cl^- are the most similar of all the tracers, while both ^{222}Rn and Si concentrations are lower than expected. In the middle bay, however, the ^{222}Rn f_{TGW} agrees with chloride and alkalinity values, while silicate concentrations remain lower than expected.

TABLE 4.2: Expected and measured SGD tracer concentrations calculated using the end-member values listed and Eq. (1)

INNER BAY	C_{TGW}	C_{MW}	f_{TGW}	Expected C_{SGD}	Measured C_{SGD}
Cl^- (mmol L^{-1})	15.6	546.43	0.2	451.45 ± 61.75	451.99 ± 2.16
TA (meq L^{-1})	0.526	2.174	0.2	1.89 ± 0.59	1.888 ± 0.009
^{222}Rn (dpm L^{-1})	64.22	1.48	0.2	12.29 ± 1.91	8.93 ± 0.75
Si (μM)	175.41	2.68	0.2	33.59 ± 14.62	9.90 ± 1.92
TDP (μM)	4.0	0.4	0.2	1.03 ± 0.71	0.75 ± 0.10
TDN (μM)	13.2	8.3	0.2	9.21 ± 6.15	17.45 ± 4.05
MIDDLE BAY					
Cl^- (mmol L^{-1})	4.94	547.63	0.003	545.95 ± 71.31	546.10 ± 2.61
TA (meq L^{-1})	0.506	2.247	0.003	2.24 ± 0.11	2.224 ± 0.011
^{222}Rn (dpm L^{-1})	412.77	2.10	0.003	3.43 ± 2.37	3.68 ± 1.21
Si (μM)	621.44	2.10	0.003	3.96 ± 1.33	9.30 ± 4.59
TDP (μM)	3.6	0.4	0.003	0.44 ± 0.13	1.06 ± 0.25
TDN (μM)	63.6	11.8	0.003	11.96 ± 7.52	24.24 ± 6.83

Table 4.3 lists the arithmetically averaged total and terrestrial fluid seepage rates, f_{TGW}, and net chemical fluxes measured from the seepage meters in different parts of Kahana Bay. Figure 4.5 shows logarithmically contoured plots of both the total seepage rates and f_{TGW}. 99% of both total and meteoric seepage is within the inner bay, and patchy SGD was found in the middle bay focused almost entirely in the central channel area. A total SGD rate of 90 x 10^6 liters per day (L d^{-1}) was measured within the study area as a whole, ~16% (14 x 10^6 L d^{-1}) of which is calculated to be meteoric groundwater. By comparison, the 37 year averaged daily flow from Kahana River (USGS gauging station #16296500; http://water.usgs.gov/hi/nwis/annual/) is 90.7

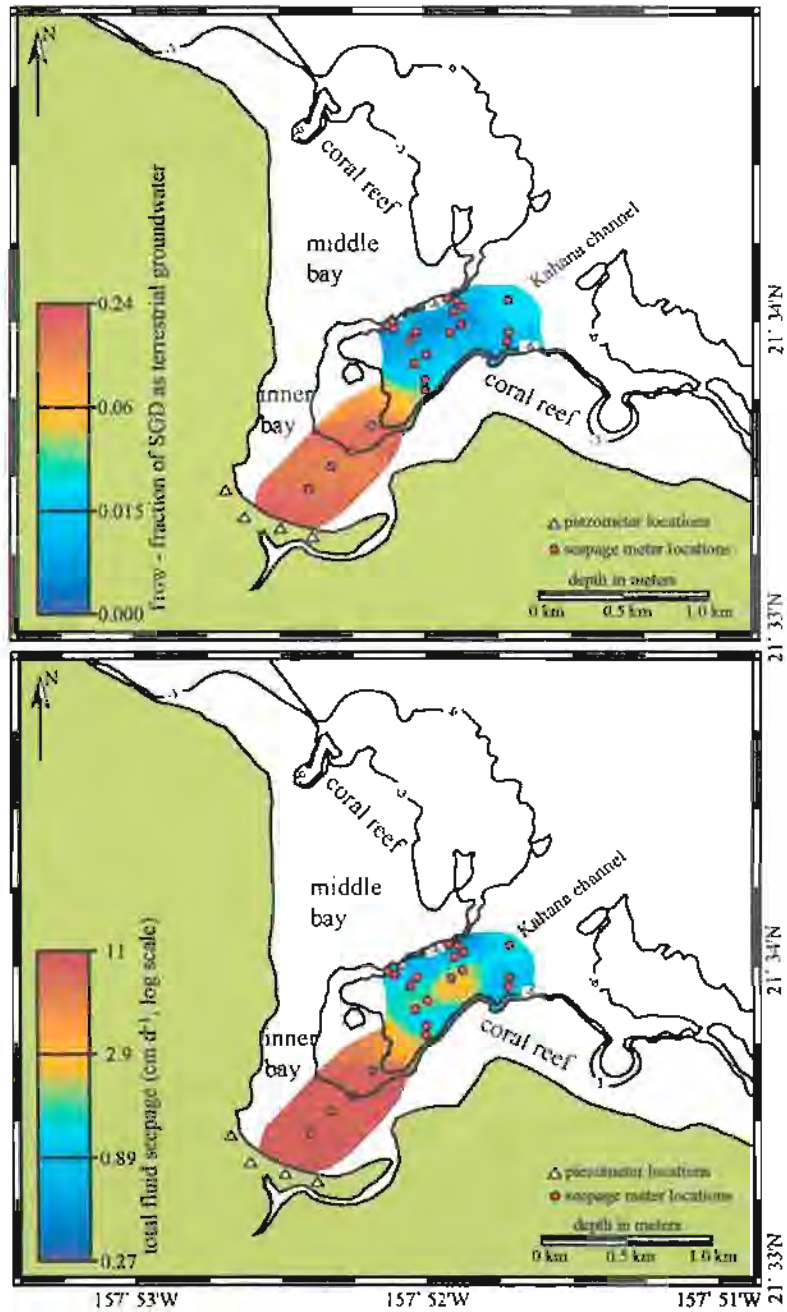

Figure 4.5. Contour plots of total SGD flux and the SGD as terrestrial groundwater fraction (f_{TGW}) across Kahana Bay as measured from Lee-type seepage meters. Meter locations are marked by the filled circles. Locations of the Piezometers installed to sample groundwaters from the Holocene alluvium are also shown. Data contours are plotted on a logarithmic scale.

x 10^6 L d^{-1}. Furthermore, in their terrestrial water budgets for Kahana Valley, Takasaki et al. (1969) calculated that 38 x 10^6 L d^{-1} should flow into the bay as meteoric groundwater, while Lau (1973) found that rate should be only 4 x 10^6 L d^{-1}.

TABLE 4.3: Averaged measurements of SGD characteristics within Kahana Bay. The data listed are the arithmetic averages of measurements from seepage meters located at different parts of the bay (Fig. 4.5).

	Inner Bay	Middle Bay
Surface area (10^5 m^2)	9.3	5.1
total SGD rate (cm d^{-1})	8.4 ± 2.1	2.3 ± 1.0
total SGD rate (10^6 L d^{-1})	78 ± 19	12 ± 1.5
f_{TGW}	0.2	0.003
terrestrial SGD (10^6 L d^{-1})	14 ± 0.3	0.038 ± 0.007
TA flux (meq m^{-2} d^{-1})*	5.9 ± 1.2	-13 ± 2
^{222}Rn flux (dpm m^{-2} d^{-1})*	570 ± 250	16 ± 5
Si flux (μM m^{-2} d^{-1})*	640 ± 180	99 ± 38
TDP flux (μM m^{-2} d^{-1})*	37 ± 11	9 ± 3
TDN flux (μM m^{-2} d^{-1})*	920 ± 300	160 ± 57

*flux calculations are net fluxes (total SGD flux from the submarine aquifer – marine flux into the aquifer)

Table 4.4 lists the annual net SGD nutrient loads to Kahana Bay. The fluxes were calculated by integrating the averaged chemical fluxes over the surface areas of the inner and middle bays – the total flux – and then subtracting the chemical fluxes into the sediments due to marine water recharge. Recharge chemical fluxes were calculated with Eq. (2) using the marine water end-member concentrations and the SGD marine fraction (f_{MW}) as listed in Table 4.2. Also listed in Table 4.4 are the comparative ratios of the SGD nutrient fluxes to those measured from Kahana River from 1997 through July 2000, data produced by Dan Hoover (unpublished dissertation, *U. Hawai'i*, 2002). The SGD brings 5 times as much total phosphorus to Kahana Bay and 2 times as much total nitrogen as Kahana River, but less than one-tenth as much silica.

TABLE 4.4: Annual SGD Nutrient Loads To Kahana Bay

Nutrient	Annual Load Via SGD	Ratio of SGD nutrient fluxes to Kahana River nutrient fluxes
TDP	5×10^4 mol yr^{-1}	5:1
TDN	1×10^6 mol yr^{-1}	2:1
Si	6×10^5 mol yr^{-1}	1:11

4.4. DISCUSSION AND CONCLUSIONS

Radon-222 proved to be a more effective tracer of terrestrial SGD in Kahana Bay than Si. Silica does show evidence of mixing when compared to Cl^- in the middle bay SGD, but Si concentrations were lower than expected (Table 4.2) and may indicate biogenic uptake. In the inner bay SGD silica actually has a positive correlation with Cl^- which would seem to indicate a marine source, although inner bay ambient water Si concentrations are far too low. Instead, consider that the inner bay SGD silica concentrations are a third of what we would expect based on conservative mixing (Table 4.2). It is possible that silica is being taken up from the shallow porewaters of the Holocene alluvium by terrestrial vegetation (Fox, 1967) and that the positive correlation may be just coincidental. The data do not present a more clear explanation.

SGD in Kahana Bay provides a significant source of dissolved nutrients (Table 4.4), and terrestrial SGD provides a important contribution to that nutrient supply. Figure 4.6 shows plots of SGD concentrations of a) total dissolved nitrogen (TDN) and b) total dissolved phosphorus (TDP) against f_{TGW} for the inner and middle bays. The positive correlation in both areas indicates that the higher the terrestrial groundwater fraction, the greater the SGD nutrient load to the bay. However, terrestrial groundwater is not the only source of nutrients in SGD. Table 4.2 also lists the expected TDP and TDN concentrations based on chloride f_{TGW}. Except for TDP in the inner bay, TDP and TDN are more concentrated in SGD than conservative mixing alone would predict.

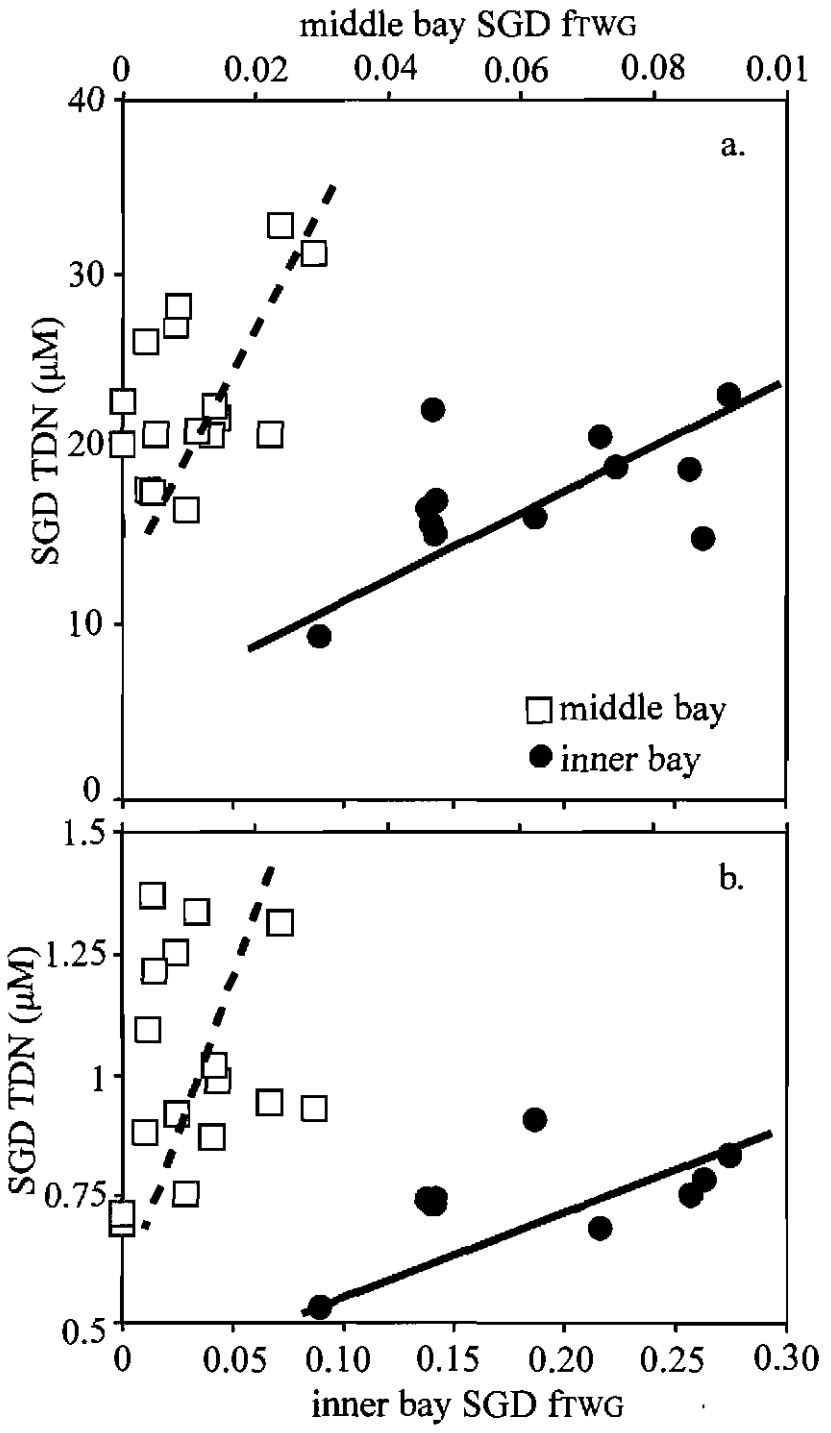

Figure 4.6. Seepage a) TDN and b) TDP concentrations vs. fTGW (the fraction of SGD as *terrestrial groundwater) in samples collected from the seepage meters. Note the* different abcissae on each graph for inner and middle bay samples.

This may be evidence that sediment diagenesis is adding dissolved nutrients to the pore waters of the submarine aquifer.

The chemical tracer data indicate that there are different sources of terrestrial SGD in different parts of the bay and support the terrestrial end-members chosen in Table 4.1. Figure 4.4 differentiates the TA, ^{222}Rn, and Si concentrations vs. Cl^- in SGD between the inner and middle bays. TA vs. Cl^- shows the SGD in the inner bay to be fresher than the middle bay and that both parts of the bay have a common tracer source, i.e., sea water. The ^{222}Rn and Si data, however, reveal the difference in terrestrial SGD sources. The exploded panel shows the inverse correlation between Cl^- and ^{222}Rn and Si in the middle bay SGD, reflecting a dilution of ^{222}Rn and Si by marine waters. In the inner bay, however, ^{222}Rn remains invariant relative to Cl^- and Si actually has a positive correlation.

Figure 4.7 is a plot of ^{222}Rn vs. Cl^- data from the terrestrial aquifers, the ambient waters of the inner and middle bays, and the waters sampled from the seepage meters. Linear regressions are plotted separately for the inner and middle bay SGD, and the exploded panel magnifies the inner and middle bay SGD data. The ^{222}Rn-intercept of for the middle bay SGD is 350 dpm L^{-1}, falling almost evenly between the averaged values measured in groundwaters from the Ko'olau basalt and Pleistocene alluvium (USGS well# W405 and Honolulu Board of Water Supply well# 3453-07, respectively). The data do not identify a specific source of terrestrial groundwater for the middle bay SGD. However, since the ^{222}Rn intercept exceeds radon concentrations in both the Pleistocene and Holocene alluvium groundwaters, we consider this to be evidence of at least partial groundwater input from the Ko'olau basalt. The intercept could be affected by a mixture of waters between aquifers, addition or predation of ^{222}Rn along the flowpath, or simply radioactive decay of ^{222}Rn. The data are not conclusive on this point as porewater radon concentrations could be easily affected in all three ways.

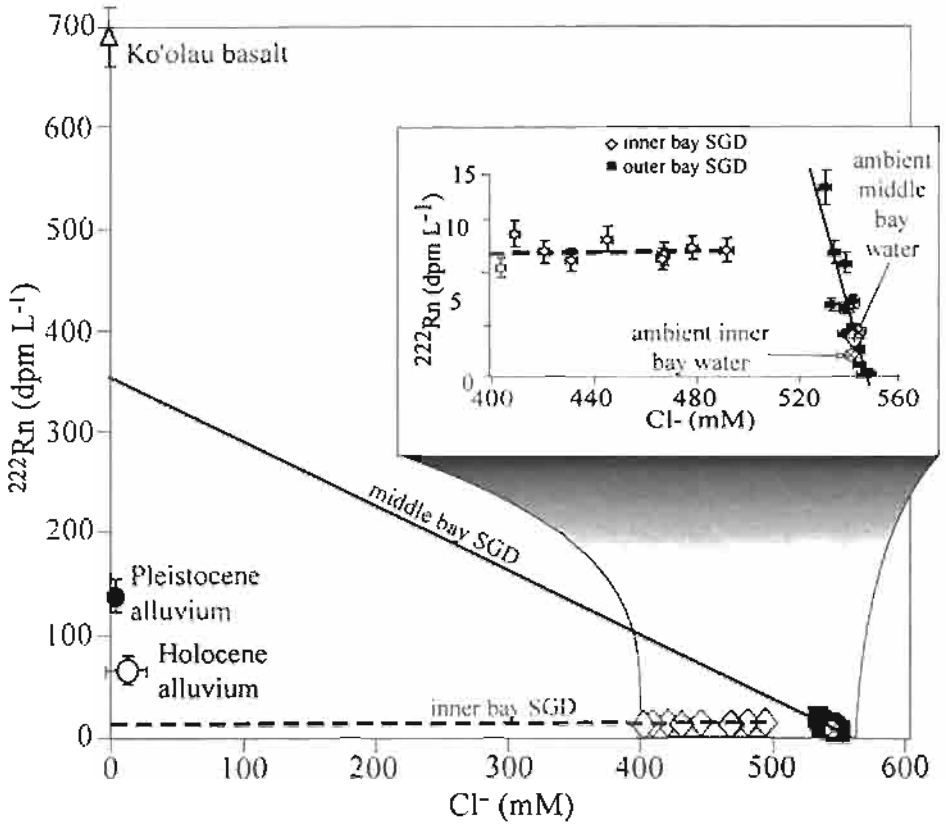

Figure 4.7. Plot of ^{222}Rn vs. Cl^- measurements from SGD, Holocene alluvium groundwater, Pleistocene alluvium groundwater (Honolulu BWS well "3453-07"), and Ko'olau basalt groundwater (USGS well "W405"). The inner panel is an expansion of the SGD data.

Looking at the inner bay SGD regression, and considering that this area is underlain by the Holocene alluvium, it appears that the primary source of terrestrial SGD in the inner bay is the Holocene alluvium groundwater. Inner bay SGD ^{222}Rn does not, however, show evidence of mixing when plotted against Cl^-. This absence of a trend may be a function of how marine and meteoric groundwaters mix in the Holocene alluvium. Figure 4.8 is a conceptualized cross section of the lower Kahana Valley and Bay. Because Cl^- and TA have a marine source, submarine groundwater concentrations will begin to increase at the landward edge of the mixing

zone, labeled position **1**. Radon-222, however, is produced by the sediments of the Holocene alluvium. Pore water ^{222}Rn concentrations won't begin to be diluted until the pore waters leave the submarine aquifer at position **2**. Thus, ^{222}Rn concentrations are essentially the same in the inner bay SGD regardless of the fraction of fresh water present. The same behavior is not seen for middle SGD because, unlike the inner bay, ^{222}Rn dilution and Cl^- enrichment occur at the same time. The fact that the inner bay SGD ^{222}Rn is so much lower than that measured in the piezometers (9 dpm L^{-1} vs. 64 dpm L^{-1}) may indicate that either porewater ^{222}Rn is lower in the submarine part of the Holocene alluvium than in the terrestrial part, or that there is a vertical ^{222}Rn gradient in the Holocene alluvium porewater.

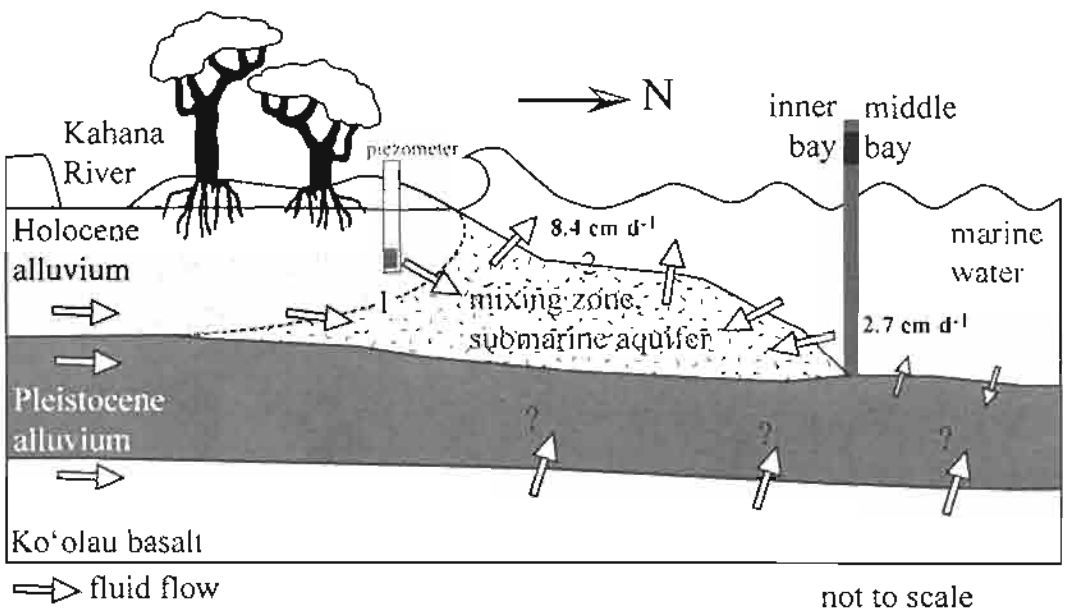

Figure 4.8. A conceptual cross section of the inferred pathways of subsurface fluid flow along a shore normal transect from the base of Kahana Valley into Kahana Bay. Total SGD rates are shown in bold; the inner bay had an average total seepage rate of 8.4 cm d^{-1}, while the middle bay had an average seepage rate of 2.7 cm d^{-1}. Position **1** is the landward edge of the meteoric/marine mixing zone. Position **2** is the seaward edge of the mixing zone where the submarine Holocene alluvium pore waters cross the sediment-water interface.

The results presented here can be considered first order approximations of the total SGD impact within Kahana Bay. Seasonal variability in the valley hydrology (precipitation, river flow, and groundwater head) does not exceed 25% of the mean values (Takasaki et al., 1969; Lau, 1973), thus constraining potential SGD variability. This work has demonstrated the applicability of natural chemical tracers and seepage meters to identify and quantify submarine groundwater discharge in Hawaiian waters. SGD is indeed present, and it provides an important chemical source to the waters of Kahana Bay. Furthermore, the intermediate water mass identified by the CTD surveys (Fig. 4.1) is in contact with the seafloor in the same areas where terrestrial groundwater seepage was identified. Thus, CTD meters may prove a simple but effective tool for identifying areas of terrestrial SGD impact on a wider scale than is possible by discrete sampling alone. This study found SGD provides total phosphorus and nitrogen loads equal or greater than those carried by surface runoff to the bay. Furthermore, the bay's SGD meteoric water flux is one-sixth as great as the river runoff. This study calculated that an average of 14×10^6 L of meteoric water per day enters Kahana Bay via SGD, a value which falls between the two previous hydrologic budget calculations that have been made for Kahana Valley.

4.5. ACKNOWLEDGEMENTS

We would like to thank those who have assisted in conducting this research, especially help in the field from John Kronen Jr. and Eric Grossman, and the generous supply of field equipment by the Coastal Geology Group of the Department of Geology and Geophysics at the University of Hawai'i. We would also like to thank the two anonymous reviewers' insightful commentary added depth and clarity to this paper. This study was funded in part by a grant to CRG and GMM from the National Oceanic and Atmospheric Administration, project #R/EL-18, which is sponsored by the University of Hawai'i Sea Grant College Program, SOEST, under

Institutional Grant No. NA86RG0041 from NOAA Office of Sea Grant, Department of Commerce. The views expressed herein are those of the authors and do not necessarily reflect the views of NOAA or any subagencies. Matching funds for this project were also graciously provided by the City and County of Honolulu Board of Water Supply. This is University of Hawai'i SOEST contribution #XXXX and Sea Grant Publication #UNIHI-SEAGRANT-XX-00-XX. This work was also supported in part by the William T. Coulbourn and Harold T. Stearns Fellowship Awards to GHG from the Department of Geology and Geophysics at the University of Hawai'i, Mānoa.

4.6. REFERENCES

Biscaye, P. E., W. S. Broecker, H. W. Feely, and R. D. Gerard. 1976. Transport and Transfer Rates in the Waters of the Continental Shelf. Lamont-Doherty Geological Observatory.

Cable, J. E., G. C. Bugna, W. C. Burnett, and J. P. Chanton. 1996a. Application of ^{222}Rn and CH4 for assessment of groundwater discharge to the coastal ocean. Limnology and Oceanography **41:** 1347-1353.

Cable, J. E., W. C. Burnett, and J. P. Chanton. 1996b. Magnitude and variations of groundwater seepage along a Florida marine shoreline. Biogeochemistry **38:** 189-205.

Cable, J. E., W. C. Burnett, J. P. Chanton, D. R. Corbett, and P. H. Cable. 1997. Field evaluation of seepage meters in the coastal marine environment. Estuarine, Coastal, and Shelf Science **45:** 367-375.

Corbett, R. D., C. J., W. Burnett, K. Dillon, and C. Rutowski. 1999. Patterns of groundwater discharge into Florida Bay. Limnology and Oceanography **44:** 1044-1055.

Coulbourn, W. T. 1971. Sedimentology of Kahana Bay, O'ahu, Hawai'i. Hawai'i Institute of Geophysics Report 71-14.

Coulbourn, W. T., J. F. Campbell, and R. Moberly. 1974. Hawaiian submarine terraces, canyons, and Quaternary history evaluated by seismic reflection profiling. Marine Geology **17:** 215-234.

Fox, R. L. 1967. Soil and plant silicon and silicate response by sugar cane. Soil Science Society of America Proceedings **35:** 897-901.

Grasshoff, K., K. Ehrhardt, and K. Kremling. 1983. Methods of Seawater Analysis, Second Revised and Extended Edition. Verlag Chemie.

Grossman, E. E., and C. H. Fletcher, III. 1998. Sea level higher than present 3500 years ago in the northern main Hawaiian Islands. Geology **26:** 363-366.

Hallock, P., and W. Schlager. 1986. Nutrient excess and the demise of coral reefs and carbonate platforms. Palaios **1:** 389-398.

Hunt, C. D. 1996. Geohydrology of the island of O'ahu, Hawai'i. U. S. Geological Survey Professional Paper **1412-B**.

Kay, A. E., L. S. Lau, E. D. Stroup, S. J. Dollar, D. P. Fellows, and R. H. F. Young. 1977. Hydrological and ecological inventories of the coastal waters of West Hawai'i. University of Hawai'i, Water Resources Research Center Technical Report 105: 94.

Komar, P. D. 1998. Beach Processes and Sedimentation. Prentice Hall Inc.

Lau, L. S. 1973. The quality of coastal waters: Second annual progress report. University of Hawai'i, Water Resources Research Center Technical Report 77.

Lee, D. R. 1977. A device for measuring seepage flux of lakes and estuaries. Limnology and Oceanography **22:** 140-147.

Li, Y. H. 1988. Denudation rates of the Hawaiian Islands by rivers and groundwaters. Pacific Science **42:** 253-266.

Mink, J. F., and L. S. Lau. 1987. Aquifer identification and classification of O'ahu: groundwater protection strategy for Hawai'i. Water Resources Research Center, University of Hawai'i at Mānoa, Technical Report No. 179.

Moore, W. S. 1996. Large groundwater inputs to coastal waters revealed by ^{226}Ra enrichments. Nature **380:** 612-614.

---. 1999. The Subterranean Estuary: A Reaction Zone of Groundwater and Sea Water. Marine Chemistry **65.**

Shaw, R., and E. E. Prepas. 1989. Anomalous, short-term influx of water into seepage meters. Limnology and Oceanography **34:** 1343-1351.

Stearns, H. S. 1974. Submerged shorelines and shelves in the Hawaiian Islands and a revision of some of the eustatic submerged shorelines. Geological Society of America Bulletin **85:** 795-804.

Stearns, H. T., and K. N. Vaksvik. 1935. Geology and Groundwater Resources of the Island of O'ahu, Hawai'i. Hawai'i Division of Hydrography Bulletin *1:* 479.

Takasaki, K. J., G. T. Hirashima, and E. R. Lubke. 1969. Water resources of Windward O'ahu, Hawai'i. U. S. Geological Survey Professional Paper **1894**.

CHAPTER V.

CONCLUSION SUMMARY

This dissertation studies the aquatic geochemistry of two different environments on O'ahu influenced by inputs from groundwater seepage and runoff. The biogeochemical system in Ordy Pond responds rapidly to changes in the surrounding environment. The environmental sensitivity of the pond is due largely to the fact that the pond is a closed system with limited rainfall and limited groundwater seepage input. On an annual scale, changes in the pond's biogeochemical system appeared to be extrinsically forced by changes in air temperature and not by changes in external chemical inputs or outputs. In contrast, Kahana Bay is influenced by significant groundwater seepage, a large surface water influx, and mixing with coastal ocean water. The larger reservoir size and significant fluid exchange should buffer seasonal changes in the biogeochemistry of this bay. Therefore, any historical record of changes in the surrounding environment held within the waters and sediments of Kahana Bay have coarser temporal resolution than Ordy Pond waters and sediments. Thus, while the Ordy Pond study is a better tool for studying Oahu's past environmental history, the Kahana Bay study demonstrates the applicability of natural chemical tracers to quantify modern groundwater discharge into Oahu's coastal waters and their affects on the aquatic geochemistry of the bay.

The study of Ordy Pond consisted of three parts: a time-series analysis of the modern water column, a time-series analysis of the modern particulate production, and study of sediment cores collected from the pond. The period during the time-series was abnormally dry when compared to historical rainfall records – 151 mm of rain fell during the study versus the 508 mm average measured between 1949 and 1999. The reduced rainfall meant that loss of water from the pond by evaporation, and subsequent concentration of dissolved chemical constituents, must

have been more significant than during a more typical modern year. However, the cycle of events observed in the pond and the seasonal changes in the character of particulate production are consistent with the geochemical nature and cyclicity of the sediment record. Though the water column may have had a chemical composition more concentrated than average, if the seasonal cycle observed during the time-series can be considered representative of seasonal variability in pond biogeochemistry, then particulate production appears to respond more to changes in air temperature rather than rainfall. Thus, the patterns observed are considered to be indicative of the type of seasonal signals that would be found during a more normal year of rainfall. Nevertheless, comparisons between these time-series analyses and the sediment record should keep the anomalously low rainfall in mind. For example, the hydrologic balance during a normal rainfall year may have a more significant role on the biogeochemistry of the pond, in which case seasonal differences may be even more extreme.

Seasonal changes in the water chemistry of the pond appeared to be controlled primarily by changes in the air temperature. The pond was thermally stratified between May and September, 2000, and epilimnion primary productivity increased dramatically, as inferred from profiles of dissolved O_2, dissolved inorganic carbon (DIC), $\delta^{13}C_{DIC}$, and rates of particulate production. Once the density gradient waned, the anoxic hypolimnion mixed with the epilimnion, organic matter productivity fell, and surface waters became suboxic to anoxic. Primary productivity is believed to have been controlled by the availability of sunlight. When phytoplankton were restricted to the surface waters during stratification, they had a longer daily photoperiod resulting in greater organic matter production. Without stratification, phytoplankton mixed below the euphotic zone, spent more time in the dark and respirative photosynthesis phase, and organic matter production decreased. In turn, primary productivity controlled the pond's carbonate mineral saturation state. The pond was always oversaturated with respect to

low magnesium calcite (LMC) and kutnahorite [$Ca(Mn_xMg_{1-x})(CaCO_3)_2$], and the dissolved saturation states of these minerals dropped significantly in the spring/summer epilimnion due to increased mineral precipitation.

Modern particulate production closely reflected changes in the nature of the water column. Particulates consisted primarily of phytoplanktonic organic matter and an inorganically precipitated mix of microcrystalline LMC and kutnahorite. Kutnahorite is a Mn-bearing isotype of dolomite. Increased rates of primary productivity and subsequent CO_2 drawdown in the summer epilimnion triggered a doubling of the carbonate particulate flux and a reduced organic carbon to inorganic carbon (OC:IC) ratio. Carbonate mineral $\delta^{13}C$ peaked at -1.8‰ (V-PDB) in July and fell to -3.3‰ (V-PDB) in March reflecting elevated primary productivity in the spring/summer and increased organic matter remineralization in the fall/winter. Particulate carbonate $\delta^{18}O$ followed the pond's seasonal water balance; $\delta^{18}O_{carb}$ peaked at +2.9‰ (V-PDB) in the summer when evaporation of water from the pond was strongest (as determined by changes in salinity) and $\delta^{18}O_{carb}$ fell to +0.9‰ (V-PDB) in the winter when water was added to the pond via rainfall and groundwater seepage. Particulate organic $\delta^{15}N$ peaked at +12.7‰ (AIR) in July and fell to +10.8‰ (AIR) in the winter apparently a function of biogenic NH_4^+ uptake and $NH_{3(aq)}$ volatization. The $\delta^{13}C_{POM}$ trend was controlled by the fractionation of ^{13}C during organic carbon production (ε_p). Fractionation peaked at +17.4‰, (V-PDB) in the spring/summer and dropped to +12.9‰ (V-PDB) in the fall/winter. This shift in ε_p may have been due to an increased abundance of anaerobic photo- and chemosynthetic bacteria, although changes in cell size, growth rate (μ), and photosynthetic HCO_3^- uptake can also affect ε_p. Regardless of the ultimate extrinsic forcing, these results indicate that the laminae in the sediments beneath the pond are seasonal deposits, and that dark-light laminae couplets are varves.

The aquatic sediments beneath Ordy Pond extend back approximately 9800 years, the point when post-glacial sea level rise first inundated this 'Ewa Plain karst sinkhole with groundwater. Nearly all the aquatic sediments beneath the pond formed within the water column, and three main general sediment types occur: amorphous aquatic organic matter, inorganic carbonate minerals, and diatom tests. The sediments are finely laminated (<1 mm) prior to Western human contact and alternate between being light and dark in color. This alternation is a function of the relative fraction of each sediment type present in the lamina. The time-series analyses of the modern pond biogeochemistry showed that light/dark laminae couplets are spring/summer – fall/winter varves.

Changes in Ordy Pond sediments record historic environmental conditions on O'ahu's 'Ewa Plain. Following the initial inundation, continued sea level rise created a deeper pond with different winter and summer depositional conditions. Sediments produced in the fall/winter seem to have retained their primary geochemical values, but sediments produced in the spring/summer appear to have been chemically altered before settling out of the water column. Evidence of significant changes in the water balance of the pond are found at 6.72 meters below the sediment surface (mbs), or ~ 1 kya. Coeval changes in carbonate mineralogy, carbonate stable isotopes, and the diatom species assemblage reveal an influx of meteoric water contemporaneous with replacement of the forest that once surrounded the pond with dry grassland fauna. These changes cannot be anthropogenic and may have resulted from a 2m drop in sea level around O'ahu. Sediments become sapropelic at the first appearance of pollen associated with Western human contact at 5.21 mbs (1830 AD), which possibly resulted from the introduction of phosphorus fertilizers. The most recent sediments indicate that the pond is returning to a state similar to its earliest period, perhaps the result of the reestablishment of a local forest and an end to large-scale agriculture on O'ahu.

Unlike Ordy Pond, the waters in Kahana Bay experience greater exchange with the surrounding environment. CTD profiles of the water column found the bay to hold a combination of water masses, including a surficial layer of fresh water runoff, a bottom layer of coastal ocean water, and an intermediate mixed layer. Total submarine groundwater discharge (SGD), is as significant as terrestrial surface water runoff to the bay, ~ 90 x 10^6 L d^{-1}. During the Kahana Bay study, benthic seepage meters were used to quantify, isolate, and sample SGD seeping from the seafloor sediments. Natural tracers (^{222}Rn, Si, Cl^-, and total alkalinity) were used to measure the terrestrial groundwater fraction in total SGD, ~16%. Nutrient fluxes into the bay via SGD were also measured, and estimated fluxes of total dissolved phosphorus and nitrogen by SGD to the bay were 500% and 200% greater than fluxes via surface runoff, respectively. Thus, SGD in Kahana Bay is a significant source of both fresh water and total nutrient input, and the Kahana Bay system includes not only the bay itself, but important contributions from terrestrial watersheds, the submarine aquifer, and the coastal ocean. Therefore, the sediments in Kahana Bay are affected by processes over a much broader physical and temporal scale than Ordy Pond.